

**Report to the Marine Monitoring  
and Research Technical Series,  
MMRTS-01-01**

Christian Krahforst  
Marine Monitoring and Research Program  
Massachusetts Coastal Zone Management  
251 Causeway Street  
Suite 900  
Boston, MA 02114

---

---

**Fate and Transport Modeling of Contaminants  
In Salem Sound**

ASA Report 00-031  
December 2001

Final Report

---

---

Hyun-Sook Kim  
J. Craig Swanson



*Applied Science Associates, Inc.  
70 Dean Knauss Drive  
Narragansett, Rhode Island 02882*

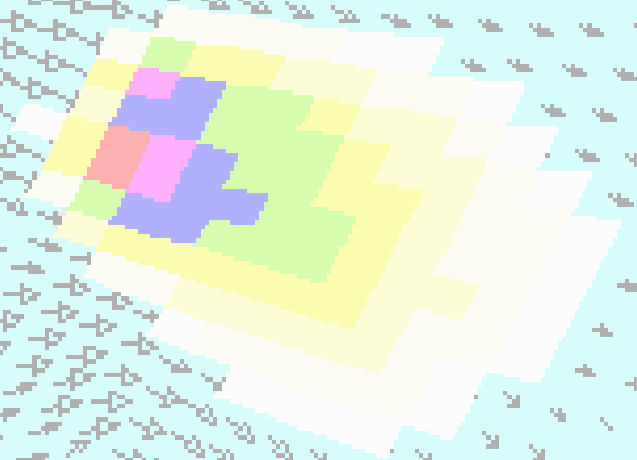


# Table of Contents

Executive Summary .....	iv
List of Figures .....	vi
List of Tables.....	viii
1. Introduction .....	1
1.1. Purpose of Study .....	1
1.2. Description of Study Area .....	1
2. Background .....	2
2.1. Physical Measurements.....	2
2.2. Water Quality Measurements .....	8
3. Model Descriptions .....	9
3.1. CORMIX Description.....	9
3.2. WQMAP Description.....	10
3.2.1. Hydrodynamic Model (BFHYDRO).....	11
3.2.2. Pollutant Transport Model (BFMASS) .....	12
4. Application of Models to Salem Sound .....	13
4.1. CORMIX Application.....	13
4.2. BFHYDRO Application.....	14
4.3. BFMASS Application.....	17
4.3.1. Loading Scenarios .....	17
5. Modeling Results.....	20
5.1. CORMIX.....	20
5.2. WQMAP .....	21
5.2.1. BFHYDRO Current Simulations.....	21
5.2.2. Comparison between 2-D and 3-D BFHYDRO Simulations.....	27
5.2.3. BFMASS Transport Simulations.....	29
5.2.4. 3-D Transport Simulations .....	40
5.2.5. Water Quality Comparisons .....	45
6. Field Monitoring Program Proposal.....	46
7. Conclusions .....	48
8. References .....	51

APPENDIX A. WQMAP Product Description

APPENDIX B. Muin and Spaulding 1977

APPENDIX C. CORMIX Output

## Executive Summary

This report presents results of hydrodynamic simulations of Salem Sound. The presentation also includes preliminary assessments of total residual chlorine (TRC) levels, because the discharge of TRC from the South Essex Sewage District (SESD) Waste Water Treatment Plant (WWTP) was thought to potentially impact the natural resources in the Sound. The hydrodynamics and pollutant transport simulations were performed using the ASA WQMAP BFHYDRO and BFMASS models, respectively. Both of the models were based on boundary fitted grids that can conform complex coastlines and covered the area west of a line between Marblehead and Cape Ann. In addition the CORMIX2 model was applied to the SESD outfall diffuser.

The two-dimensional, vertically averaged hydrodynamic model was calibrated with the tidal ellipses and mean speed and direction of total currents for a period from July to September 1985 during which observations were available. The 11-layer 3-D model was also applied to the study domain. The results with the 3-D model were similar to that with 2-D model.

A review of the data showed that the general circulation in the Sound was clockwise, which was a result of the prevailing southwesterly winds during the simulation period. There were substantial residual currents off the Marblehead and Manchester coastlines that were associated with asymmetry between the flood and ebb tides, and at the outer boundary that was caused by the combined influence of atmospheric winds and weak tides.

The hydrodynamic simulations indicated that the dynamics in the study area had two regimes in both space and time. In space, the currents inside the Sound were primarily governed by semi-diurnal  $M_2$  tides, and the speeds were 30 cm/s at maximum. Although there were local variations in currents due to bottom topography effects, especially conspicuous along the coastline, the flow was mainly in the direction of the Sound axis. The currents at the outer boundary of the Sound were driven by prevailing winds and the total current speed was generally large. In the time domain, the currents were differentiated to low and high frequency variations, in which the former was controlled by the atmospheric forcing and the latter was governed by tides.

The predicted tidal currents in most of the study area were of an elliptic shape whose major axis was in the same direction as the Sound axis. This prediction agreed with the observations, except at a location to the southwest (CM2). The observations suggested that the tides at that location were more circular and the tidal currents were the smallest among the three current meter sites. The simulation instead showed an elliptic rotation, being aligned to the northwest-southeast direction.

The preliminary near and far field simulations of the TRC fate and transport with CORMIX2 and WQMAP BFMASS indicated that for the SESD plant reported operating conditions (flow-rate of  $1.98 \text{ m}^3/\text{s}$  and TRC concentration of  $0.034 \text{ mg/L}$ ) in April 2000, the maximum TRC levels predicted at the release site were lower than the USEPA water

quality criteria. It should be emphasized that BFMASS was not calibrated and that these results should be considered preliminary.

Based on the result of the BFMASS simulation, the fate of TRC was found to be sensitive to dispersion and more sensitive to decay, but not sensitive to source type. The TRC response in both the near and far fields was linear with respect to the load. The TRC concentration level decayed rapidly away from the release site in an elongated shape whose axis was parallel to the Sound axial direction. The TRC transport was primarily due to advection by currents, as the TRC plume moved at the same frequency as the tides.

## List of Figures

Figure 1-1. Location of Salem Sound and the SESD outfall site.....	2
Figure 1-2. Bathymetry in the study domain.....	3
Figure 2-1. Physical measurement locations during the SESD 1985 field observations: a) hydrographic stations, b) current meter mooring locations and c) drogue release sites. ....	4
Figure 2-2. Hydrographic section stations during the SESD 1985 field observation. ....	5
Figure 3-1. Flow classes for CORMIX2 (reproduced from Jirka et al., 1996). ....	10
Figure 4-1a. Plan view of diffuser with input parameters (reproduced from Jirka et al., 1996).....	13
Figure 4-1b. Section view of diffuser with input parameters (reproduced from Jirka et al., 1996).....	14
Figure 4-2. Model domain in Salem Sound. ....	16
Figure 4-3. Time series of tidal elevation used at the open boundary. ....	16
Figure 4-4. Time series of hourly wind vectors (meteorological convention) from Logan Airport, Boston, MA, used to drive the model. ....	17
Figure 4-5. Time series of effluent total residual chlorine (TRC) concentration and flow-rate observed at the SESD Waste Water Treatment Plant (WWTP).....	18
Figure 5-1a. Predicted (solid circle) and observed (thick line) aspect ratio of tidal ellipse at CM1.....	23
Figure 5-1b. Predicted (solid circle) and observed (thick line) aspect ratio of tidal ellipse at CM2.....	23
Figure 5-1c. Predicted (solid circle) and observed (thick line) aspect ratio of tidal ellipse at CM3.....	24
Figure 5-2. Tidal ellipses of the observed data and 2-D model predictions at stations CM1 (a), CM2 (b) and CM3 (c).. ....	25
Figure 5-3. Predicted circulation in Salem Harbor on 31 August 1985.....	27

Figure 5-4. Typical maximum flood (a) and maximum ebb (b) currents in Salem Sound. .....	30
Figure 5-5. Time series of model predicted velocity currents at station CM1.....	32
Figure 5-6. Time series of wind speed, and the predicted east and north component speeds at stations CM1, CM2 and CM3.....	33
Figure 5-7. Load location (star): a) single source, b) distributed source (three cells), with insert of the detail around the outfall.....	34
Figure 5-8. Seven model time series locations used to monitor TRC concentration.....	35
Figure 5-9. Comparison of predicted TRC concentration with single load (blue) and distributed load (black) for Run#1. ....	37
Figure 5-10. Comparison of the effluent contaminant field (mid-night 14 July 1985) between two different dispersion coefficients.....	38
Figure 5-11. Time series of TRC concentration in the near field for different dispersion coefficients .....	39
Figure 5-12. Simulated TRC concentration distribution at maximum flood (a) and maximum ebb (b) for scenario 1. ....	41
Figure 5-13. Simulated TRC concentration distribution at maximum flood (a) and maximum ebb (b) for scenario 2. ....	42
Figure 5-14. Simulated TRC concentration distribution at maximum flood (a) and maximum ebb (b) for scenario 3. ....	43
Figure 5-15. Simulated TRC concentration distribution during slack tide for Scenario 1 (a), Scenario 2 (b) and Scenario 3 (c).....	44
Figure 6-1. Proposed stations and transects for velocity, physical property and water quality measurements .....	48

## List of Tables

Table 2-1. Oceanographic Station Locations during Physical Oceanography Study as part of the SESD Revised 301(h) Waiver Application in 1985 (by OSI).....	7
Table 2-2. Mean speed and direction of total current observed at current meter site inside the Sound. ....	8
Table 4-1. CORMIX2 input parameter description and values used in the application to the SESD discharge. ....	15
Table 4-2 CORMIX2 input parameters for different tide stages. ....	15
Table 4-3. Specifications for the SESD WWTP outfall pipe line (CDM, 1991). ....	18
Table 4-4. Estimates of TRC load at diffuser. The C and U represents the concentration and mean velocity at the end of pipe.. ....	19
Table 5-1. Predicted semi-diurnal $M_2$ tidal ellipses and total currents from linear 2-D and 3-D BFHYDRO modes, and the observations (shaded cells in the linear 2-D columns).. ....	20
Table 5-2. CORMIX2 results for different historical operating conditions.....	21
Table 5-3. Predicted semi-diurnal $M_2$ tidal ellipses and total currents from linear 2-D and 3-D BFHYDRO model simulations. . ....	28
Table 5-4. Sensitivity study for load, dispersion and decay rate for 2-D model.....	36
Table 5-5. Sensitivity study for vertical diffusivity. ....	40
Table 5-6. Horizontal areal coverage of TRC (greater the 0.1 $\mu\text{g/L}$ ) and maximum TRC value during maximum flood and maximum ebb currents.....	45
Table 5-7. CORMIX2 and WQMAP predictions of maximum TRC Concentrations and coverage areas greater then water quality criteriafor various plant operating conditions. . ....	46

# 1. Introduction

The Executive Office of Environmental Affairs through Massachusetts Coastal Zone Management (MCZM) sought a computer model of the fate and transport of wastewater effluent and contaminants from the South Essex Sewage District (SESD) in Salem Sound. They contracted with Applied Science Associates, Inc. (ASA) to develop and apply a hydrodynamic and pollutant transport model for this purpose.

The sections below outline the development of the model system for Salem Sound. Section 2 describes background information including historical physical and water quality measurements. Section 3 presents a description of the USEPA CORMIX plume model, and WQMAP, ASA's hydrodynamic, pollutant transport and water quality model system, followed by the model applications to Salem Sound in Section 4. Section 5 presents the near field and far field modeling results. A field monitoring program proposal is presented in Section 6. Conclusions are in Section 7.

## 1.1. Purpose of Study

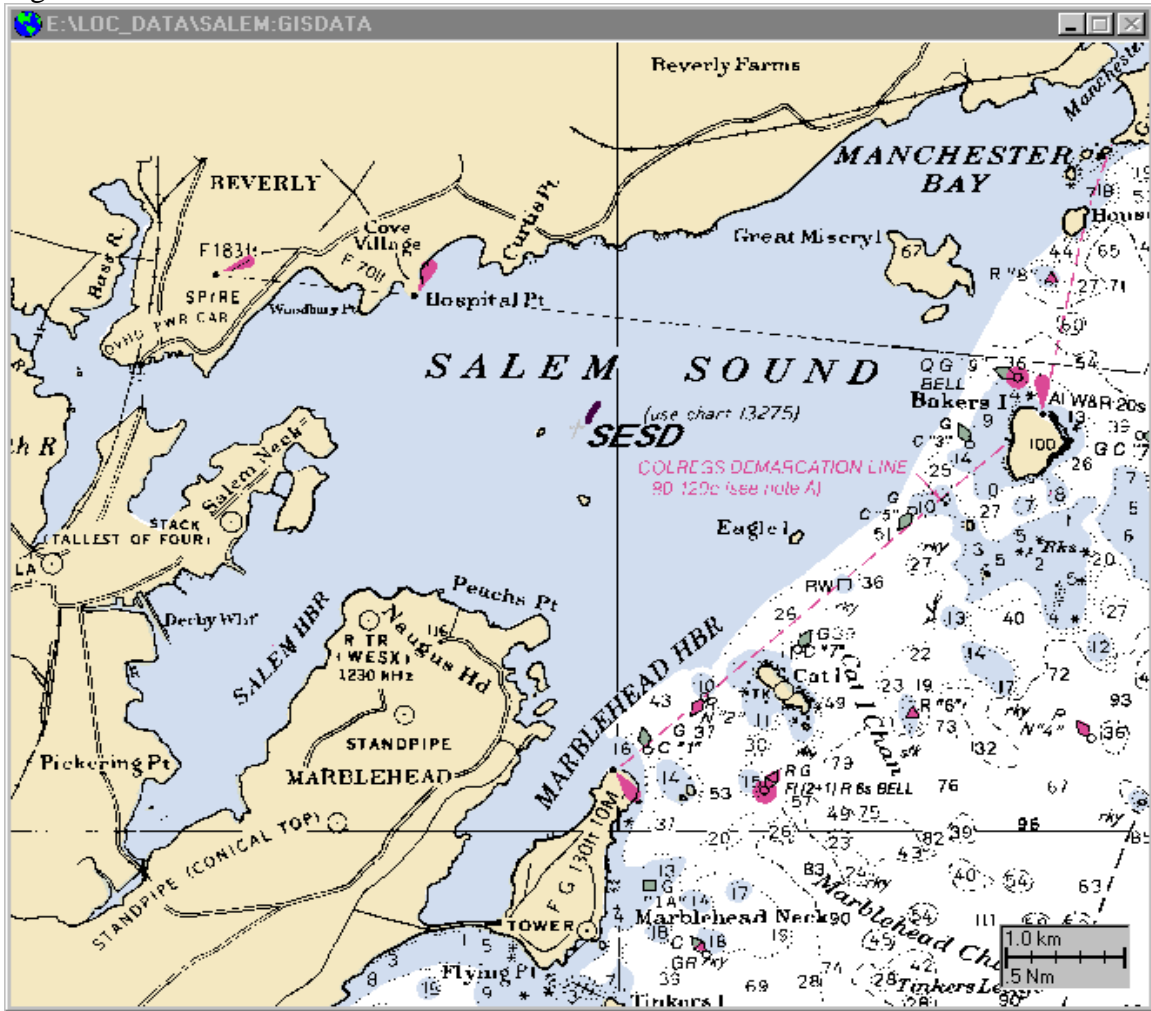
The objective of this study is to simulate the fate and transport of effluent residual chlorine in Salem Sound. This action was driven, in part, in response to issues raised by local officials and lobstermen. The specific issue raised with MCZM is the effect of residual chlorine in the SESD effluent and its impact on natural resources in the sound. The ultimate goal of MCZM is to identify relationships, if any, between the impacts from the discharge and the perceived decline in the lobster fishery. The purpose of the present effort is the development and application of hydrodynamic and pollutant transport models for Salem Sound. One specific future use of the model system will be to explore the effects of historical, present and future loadings from the SESD in terms of residual chlorine concentration levels in the sound.

## 1.2. Description of Study Area

Salem sound is located in northwestern Massachusetts Bay, between Marblehead and Cape Ann with a total area of approximately  $38 \text{ km}^2$  ( $14.6 \text{ mi}^2$ ) (Figure 1-1). Mean depth of the Sound is about 9.8 m with deepest areas of about 45.4 m in the head of Salem Sound Channel, between Baker's Island and Great Misery Island (Figure 1-2). The SESD outfall site is located about 2 km (1.24 mi) north of Marblehead (see Figures 1-1 and 1-2).

The hydrodynamics in the Sound is dominated by tides. According to the observations during a field program supported by SESD in July – September 1985, currents in the area are governed by semi-diurnal tides of low velocity (5 cm/s), with residual currents in order of 2 cm/s (CDM, 1986a and 1986b). The magnitudes of the tidal and non-tidal currents increase towards offshore by a factor of 1.6 and 2, respectively. Water inside the

Figure 1-1. Location of Salem Sound and the SESD outfall site.



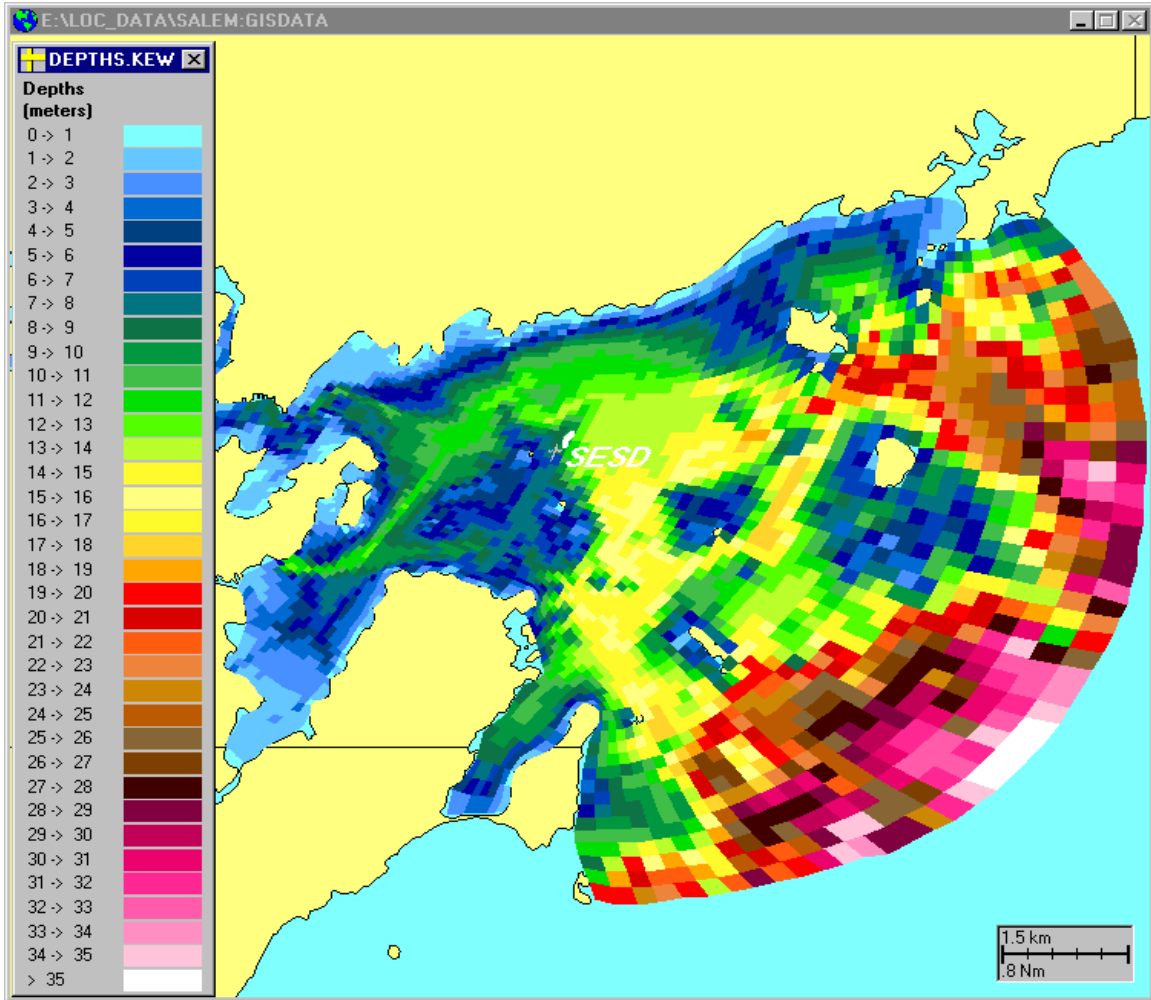
sound is relatively well mixed due to tides, with density differences in the vertical ranging between  $0.5$  and  $1\sigma_t$ . However, the density difference increases offshore, resulting in a two-layer system with a thermocline at approximately 20 m below the surface. One study (CDM, 1991) indicated that there is an occasional freshwater intrusion event from the Merrimack River. However, a careful examination of the 1985 hydrographic data suggested that the influence mainly occurred offshore, not affecting the salinity of the sound, during that year.

## 2. Background

### 2.1. Physical Measurements

The most extensive physical measurements in Salem Sound were performed over a three-month period July –September 1985 in support of the SESD Revised 301(h) Waiver Application. The primary measurements were *in-situ* temperature, salinity and density

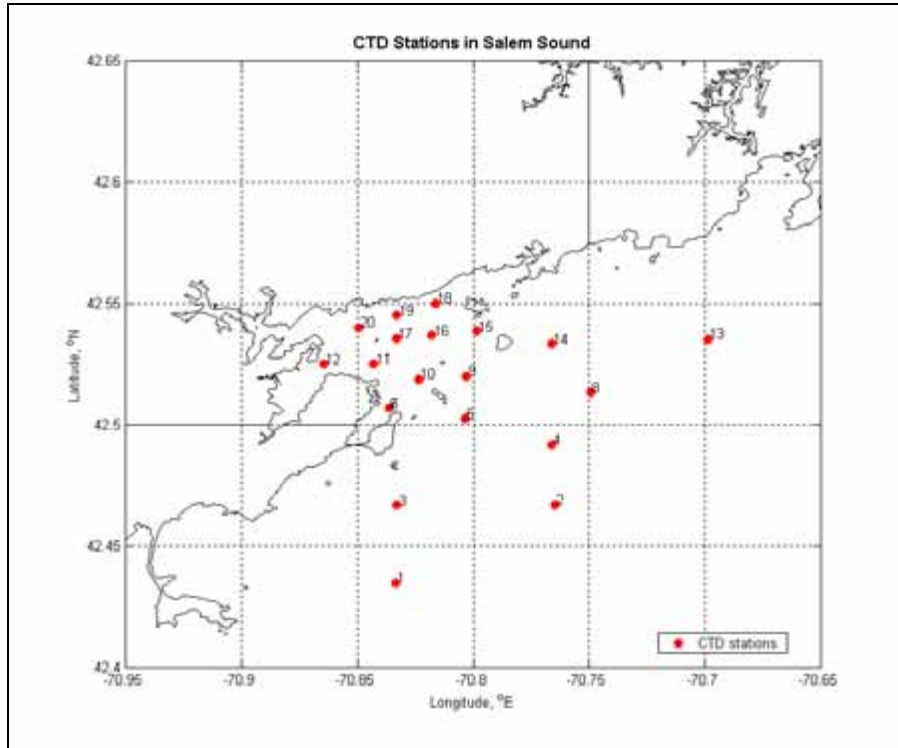
Figure 1-2. Bathymetry in the study domain.



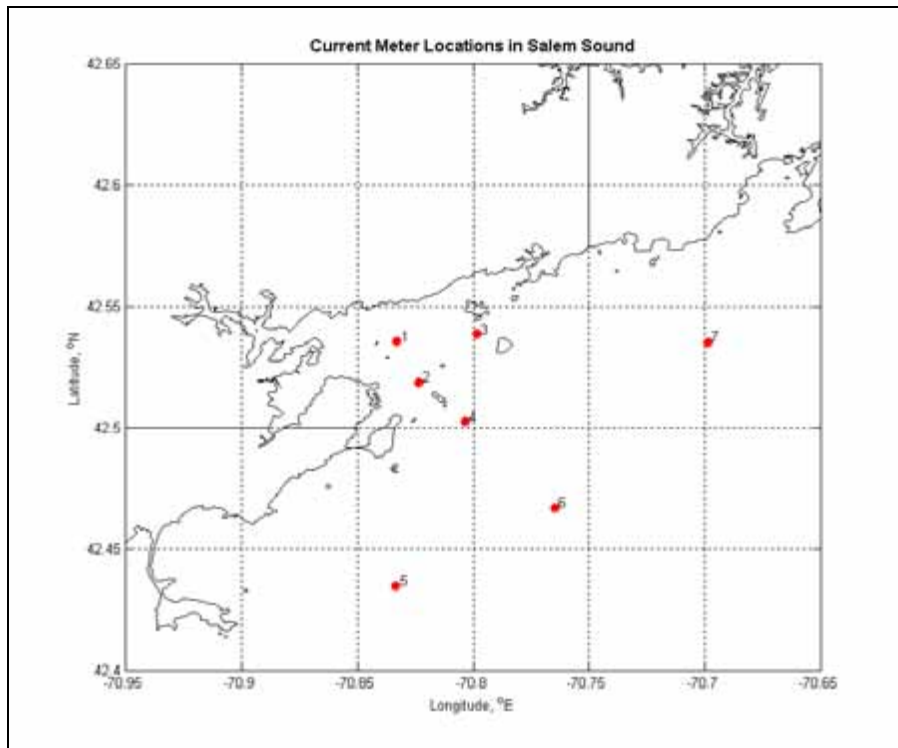
(CTD), time series of waves and tides, surface/bottom velocities, winds, and trajectory measurements. Figure 2-1 shows the locations of 20 CTD stations (a), 7 current meter moorings (b), and 7 drogue releases (c), respectively. Measurements took place both inside and outside the Sound. Table 2-1 lists the latitude and longitude positions of the stations, with the observations inside the Sound marked by a star symbol (\*). Numbers in the table correspond to those in Figure 2-1. Additional *in-situ* temperature and salinity data were collected at the beginning of October 1985 during a hydrographic survey conducted by the University of Massachusetts/Boston (CDM, 1986a). The locations are shown in Figure 2-2, except Station 8 that is located outside the map area.

Figure 2-1. Physical measurement locations during the SEDS 1985 field observations: a) hydrographic stations, b) current meter mooring locations and c) drogue release sites.

a)



b)



c)

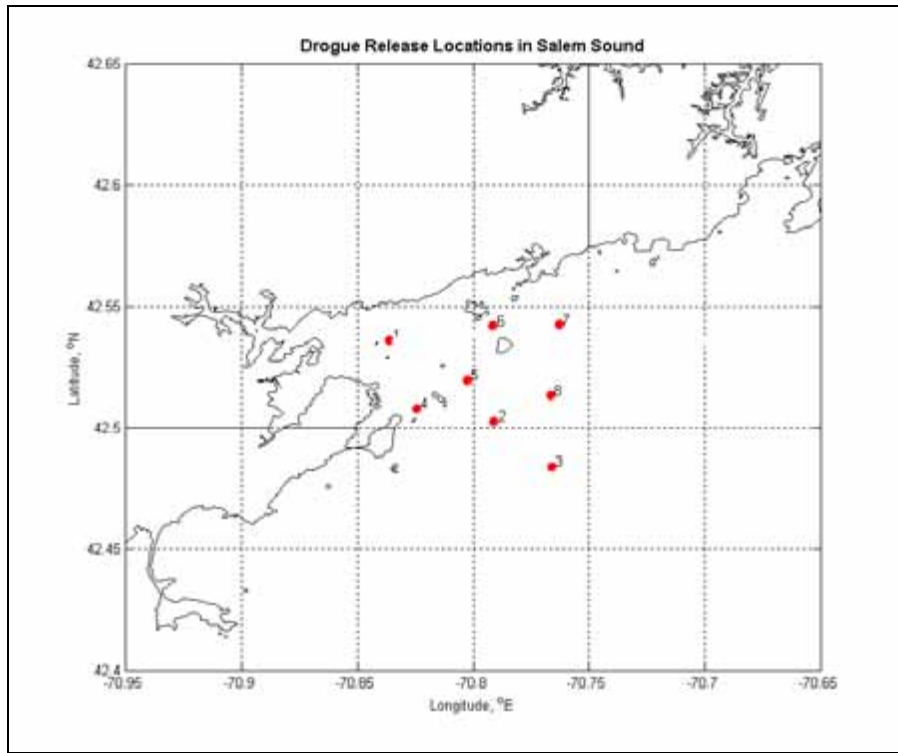
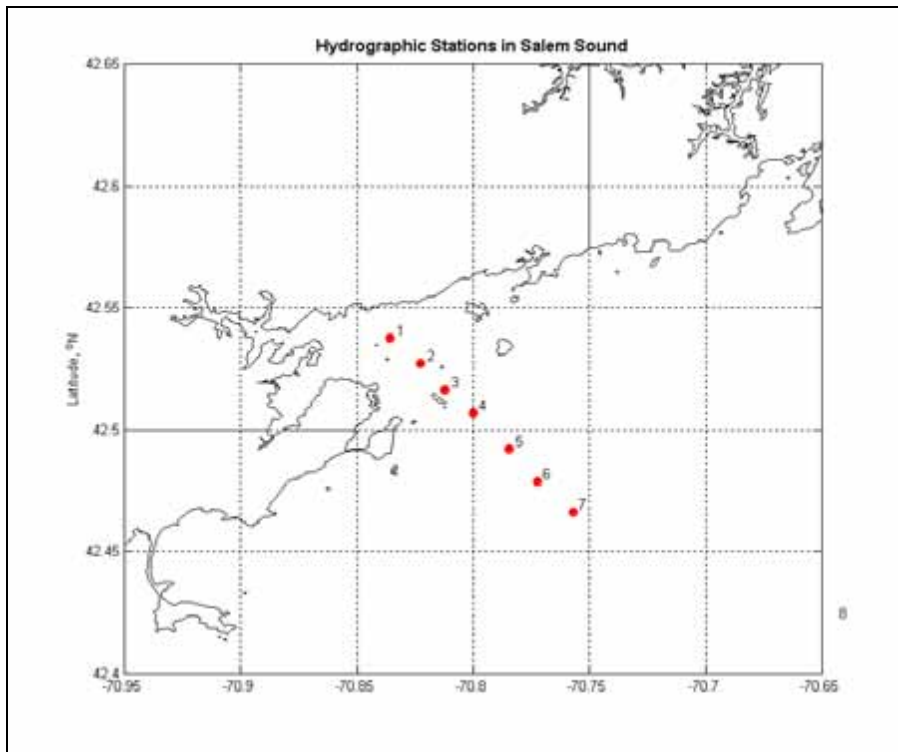


Figure 2-2. Hydrographic section stations during the SESD 1985 field observations.



Like other shallower water in this area, the temperature in the Sound during summer promptly responds to the solar heating by showing higher temperature at the surface than in the deep water. The surface water temperature over the three-month period in the Sound ranged from 13.4 to 19.6°C and the vertical temperature difference varied between 0 and 4°C. The vertical temperature difference increased towards offshore. The spatial and temporal variability of salinity was in a range between 31.3 and 33.3 ppt, in which the lowest salinity was observed during the September 23 survey, presumably associated with the precipitation before Hurricane Gloria (which passed by New England on September 27). The water density changed from 21 to 26  $\sigma_t$  in time, in which the lowest density, 21 $\sigma_t$ , was found four days before Hurricane Gloria. The average vertical density difference in the vertical inside the Sound was approximately 3 $\sigma_t$ . The maximum density difference offshore was 5 $\sigma_t$  and was observed at hydrographic station 4 on 3 September 1985. Dissolved oxygen varied between 5.25 and 10.5 ppm (parts per million) during the 3-month study.

Among seven current meter (CM) moorings deployed in the field study area, three moorings were located within or near Salem Sound (see Figure 2-1b). The observations from the three locations indicated that the total currents at the existing site were steady, simply responding to tidal forcing. The currents at CM2 showed a net flow out of the Sound, whereas the currents at CM3 indicated periods of steady flow south into the Sound and periods of no residual flow. Tidal currents at each location were between 60 and 90% of the total currents, with mean speeds and directions during the observation period shown in Table 2-2. The directions are in degree relative to true north ( $^{\circ}$ T). The lowest speed was found at the south (CM2) station while the highest speed was observed at the north (CM3) station.

A tidal gauge located at Newcomb Ledge (42°30'48"N, 70°44'57"W) along with a wave gauge indicated that an average range of  $M_2$  tidal elevation was 2.7 m and with  $M_2$  and  $S_2$  together was 3.1 m. Waves at the location showed a height of 35 cm on average and 140 cm at maximum, with a period of about 8.8 seconds on average and ranging between 5.2 and 12.3 seconds. According to the drogoue study, the surface drogoue speed appeared to be equal to 1 to 5% of the wind speed. Surface currents seemed to be highly correlated to the wind, especially within the Sound. However, the currents in the deep layer appeared to follow the counterclockwise gyre along the coast of Mass Bay (CDM, 1986a).

Over the three-month period, winds were dominantly southwesterly, northerly, northeasterly and northwesterly. According to the meteorological data collected at the Boston Harbor NDBC buoy (42°21'14"N, 70°41'29"W) (since the time series of the wind data collected at Cat Island was not available), average wind speed and direction during the period were 2.5 m/s and 183° T (southerly), respectively.

The separate hydrographic survey between October 8 and 10, 1985, along a transect (Figure 2-2) showed that the water inside the sound was uniform but became stratified towards the offshore. The thermocline was located at about 20 m below the surface.

Table 2-1. Oceanographic station locations during physical oceanography study as part of the SEDS Revised 301(h) Waiver Application in 1985 (by OSI). Stations marked by a symbol (\*) are either within or near Salem Sound. (CDM, 1986a)

Station Designation	Latitude (°N)	Longitude (°W)	Instrument
CM1*	42.5355	70.8329	CM Mooring
CM2*	42.5187	70.8236	“
CM3*	42.5385	70.7984	“
CM4*	42.5025	70.8036	“
CM5	42.4348	70.8334	“
CM6	42.4670	70.7648	“
CM7	42.5354	70.6987	“
TG/WG	42.5134	70.7492	Tide/Wave Gauge
D1*	42.5361	70.8363	Drogue
D2*	42.5026	70.7910	“
D3	42.4840	70.7662	“
D4*	42.5078	70.8244	“
D5*	42.5196	70.8027	“
D6*	42.5421	70.7915	“
D7	42.5424	70.7630	“
D8	42.5134	70.7665	“
W1	42.4348	70.8334	CTD(+DO) profile
W2	42.4670	70.7648	“
W3	42.4668	70.8328	“
W4	42.4918	70.7662	“
W5*	42.5025	70.8036	“
W6*	42.5033	70.8167	“
W7*	42.5068	70.8362	“
W8	42.5134	70.7492	“
W9*	42.5201	70.8028	“
W10*	42.5187	70.8236	“
W11*	42.5251	70.8428	“
W12*	42.5251	70.8645	“
W13	42.5354	70.6987	“
W14	42.5334	70.7662	“
W15*	42.5385	70.7984	“
W16*	42.5368	70.8178	“
W17*	42.5355	70.8329	“
W18*	42.5501	70.8162	“
W19*	42.5451	70.8328	“
W20*	42.5401	70.8495	“

Table 2-2. Mean speed and direction of total currents observed at current meter sites inside the Sound.

Station	Mean speed (cm/s)	Mean direction (°T)
CM1	5.0	365.5
CM2	4.5	156.5
CM3	9.5	186.5
CM4	6.5	348.5

## 2.2. Water Quality Measurements

A major field observation program for water quality took place 8-10 October 1985, along with hydrographic survey, as a baseline assessment of Salem Harbor-Salem Sound and adjacent waters (CDM, 1986a). Additional water quality measurements took place at six stations over the period April-September 1986, on a monthly basis, as part of a biological field study (CDM, 1986b).

From oxygen measurements in October 1985, the water column DO ranged between 5.8 and 7.0 mg/L in the Sound, within 80% of saturation values, and between 5.3 and 6.7 mg/L outside the Sound, except station 4 (Figure 2-2). The deep sample at station 4 (in Marblehead channel) was lower (less than 5.0 mg/L), at about 67% of saturation. The DO level observed during this period was relatively lower than the monthly data collected in 1986 (CDM, 1986b), which ranged between 6.2 and 9.5 mg/L. As bottom waters get warmer and the water column stratifies, the DO level generally drops due to SOD (sediment-oxygen demand) and water column BOD (biochemical-oxygen demand). During this time, the near-bottom DO gradient (in the bottom 1 to 3 m) in Salem Sound peaked, reaching as high as 1 mg/L/m. The historical observations suggest that major depletion of DO in the Sound is rare.

Highest concentrations of Chlorophyll were observed inside the Sound (stations 1 and 2). Similar observations were found for ammonia (NH<sub>4</sub>). This indicated that a benthic source may be important. Within Salem Sound, and at the nearshore locations, the nutrient vertical gradient in the summer months was not consistent. The 1986 data indicated that NH<sub>4</sub> and NO<sub>3</sub>/NO<sub>2</sub> were sometimes uniform between the surface and bottom layers, which is probably a result of both mixing and the extended photic zone during the season.

The highest suspended matter concentration (1.30 mg/L) was found in the surface water near the SESD outfall site. Inside the Sound (at stations 1 and 2), the suspended matter concentration was higher at the surface than the deep water. At offshore stations (4-6), the vertical structure of the concentration formed a bi-modal distribution, having a lower value at an intermediate layer. Overall, less suspended materials was observed offshore than inside the Sound. The suspended concentration observed during this period ranged from about 0.15 to 1.3 mg/L.

### **3. Model Descriptions**

Two models have been applied to Salem Sound and the SESD discharge: CORMIX and WQMAP. Each is appropriate for a different domain. CORMIX predicts the concentration of pollutants in the vicinity of the discharge in an area known as the near field where the discharge plume has its own momentum. WQMAP predicts the circulation and pollutant transport in the area away from the discharge known as the far field where the plume momentum has dissipated and the pollutants are affected only by the ambient currents. Each model will be described in the following sections.

#### **3.1. CORMIX Description**

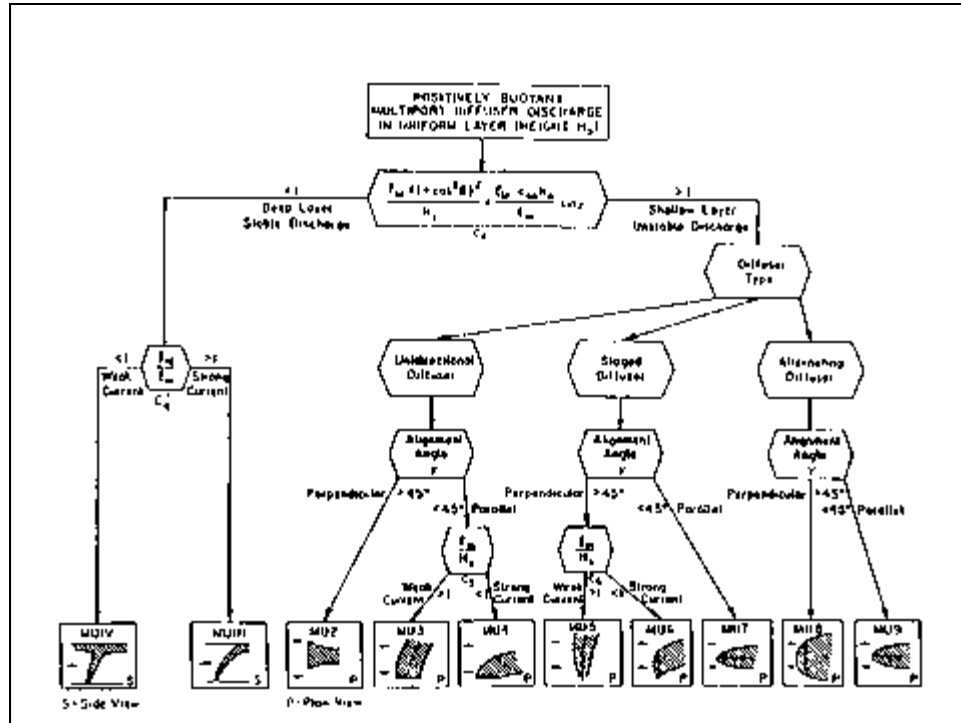
CORMIX models the near field dynamics of discharge plumes. CORMIX, the Cornell Mixing Zone Expert System (Jirka et al., 1996), was developed at Cornell from 1985 to 1995 under EPA funding to simulate plume characteristics and dilution from discharge systems. The software is now supported by the Department of Environmental Science and Engineering at the Oregon Graduate Institute. The discharge systems that can be simulated by CORMIX include submerged single port diffusers (CORMIX1), submerged multiple port diffusers (CORMIX2), and surface releases (CORMIX3). CORMIX2 is the component that was used for the SESD discharge.

CORMIX employs empirically based algorithms that are dependent on various non-dimensional parameters to classify the flow and then applies appropriate equations to estimate effluent plume centerline location, width and dilution as the plume moves through various regimes in the receiving water. Figure 3.1 shows the flow classes for positively buoyant plumes in CORMIX2. The flow class for the SESD discharge is MU1V which applies to a stable buoyant plume in relatively deep water and has relatively weak momentum flux.

CORMIX requires six types of input data:

- Project description – general description of the specific model run and project information
- Ambient information - water body width, depth and extent; currents and density structure; bottom friction
- Effluent specification – volume flow rate and density; pollutant type and initial concentration
- Discharge geometry – diffuser length and orientation relative to shore, port arrangement; port number, height, and diameter
- Mixing zone specification – effluent type and water quality criteria, size of mixing zone
- Output control – control of model results to be printed or plotted

Figure 3-1. Flow classes for CORMIX2 (reproduced from Jirka et al., 1996).



The model interface allows straightforward entry of data and automatically checks values for consistency. Additional specific information in model input and use of the model can be found in Jirka et al. (1996).

Although CORMIX has the capability to model both the near field and far field, many U.S. regulatory agencies recommend using the near field component of CORMIX and a separate far field model, such as WQMAP. One principal shortcoming of using the far field component of CORMIX is that it does not account for the far field buildup of pollutant where remnants of previously released constituent can impact the present pollutant field. Another shortcoming is its inability to incorporate spatially varying currents or complex shorelines. The CORMIX model output specifies when the plume dynamics change from near to far field regions so determining near field results is straightforward.

### 3.2. WQMAP Description

WQMAP is a PC-based system that integrates geographic information (coastlines, land use, watersheds, etc.) and models (analytical and numerical, hydrodynamic, pollutant transport, etc.) to provide the user with a tool to analyze (with a graphical user interface) many alternatives to determine the optimum solution to a particular problem. It has been applied, with different models, as appropriate, to Total Maximum Daily Load (TMDL) analysis of Greenwich Bay, RI; to wastewater treatment facility effluent impacts to Cohasset Harbor, MA; to fecal coliform impacts from combined sewer overflows to the

Providence River and upper Narragansett Bay, RI; to flushing estimates for alternative development configurations for Enighed Pond located on St. John, USVI; to circulation and flushing estimates for Nantucket Harbor, MA; and to dredging and disposal operations in Boston, MA and Providence, RI; among other applications.

The geographic information component of WQMAP holds user-specified layers of data appropriate for the task. Such layers might include shorelines, land use, pollutant point source locations, sampling locations, shellfishing closure areas, habitat maps, etc. Each data layer can be easily input, either directly into WQMAP with a mouse and screen forms or through import from existing geographic information systems such as ArcInfo. Data can be exported as well. Each layer can be displayed separately or in any combination. Graphics can be generated and sent directly to a printer (color or black and white) or stored for later use in a computer driven slide show.

The modeling component of WQMAP is uniquely versatile with its ability to link one or more of a suite of models of varying complexity into the system. These range from simple analytic calculations of flushing time in a single basin to full three dimensional, time dependent, boundary fitted numerical models of hydrodynamics and water quality. For the Salem Sound project we used a boundary fitted, three-dimensional hydrodynamic model to generate tidal elevations and velocities. A constituent transport calculation used the hydrodynamic model output and estimates of chlorine load to estimate residual chlorine distribution.

WQMAP has full featured display capabilities. Color or black and white hard copies of any geographic, environmental, or model data screen display can be made. In addition it has been our experience that WQMAP is an excellent tool to inform audiences, both general and technical, about project goals, methodology, and results. WQMAP can be installed on Pentium class PCs and can be used to drive large screen monitors (for small audiences) or projector displays (for larger audiences). The WQMAP product description is attached as Appendix A.

### **3.2.1. Hydrodynamic Model (BFHYDRO)**

The hydrodynamic model included in WQMAP solves the three dimensional, conservation of water mass, momentum, salt and energy equations on a spherical, non-orthogonal, boundary conforming grid system and is applicable for estuarine and coastal areas (Muin, 1993; Muin and Spaulding, 1996, 1997a,b).

The velocities are represented in their contra-variant form. A sigma stretching system is used to map the free surface and bottom to resolve bathymetric variations. The model employs a split mode solution methodology (Madala and Piaseck, 1977). In the exterior (vertically averaged) mode the Helmholtz equation, given in terms of the sea surface elevation, is solved by a semi-implicit algorithm to ease the time step restrictions normally imposed by gravity wave propagation. In the interior (vertical structure) mode the flow is predicted by an explicit finite difference method, except that the vertical

diffusion term is treated implicitly. The time step generally remains the same for both exterior and interior modes. Computations are performed on a space staggered grid system in the horizontal and a non-staggered system in the vertical. Time is discretized using a three level scheme. Muin and Spaulding (1996, 1997a) provide a detailed description of the governing equations, numerical solution methodology, and in depth testing against analytic solutions for two and three dimensional flow problems. A copy of Muin and Spaulding (1997a) is included as Appendix B to provide additional details on the model. Additional applications are given in Swanson and Mendelsohn (1993, 1996) and Mendelsohn et al. (1995).

### **3.2.2 Pollutant Transport Model (BFMASS)**

There are three separate models within the WQMAP pollutant transport model system. The first is a single constituent transport model, which includes first order reaction terms. This model is suitable for a single constituent contaminant that is conservative, settles, decays, or grows. This model can be used to predict the temporally and spatially varying concentrations associated with treatment of sewage effluent or other contaminants (e.g. fecal coliforms, residual chlorine). The second is a multi-constituent transport and fate model with a reaction matrix that can be specified by the user. This model can be used to custom design a multi-component water quality model system (e.g. dissolved oxygen and biochemical oxygen demand). The third is a multi-constituent eutrophication model (e.g. nitrogen, phosphorous, dissolved oxygen) which incorporates EPA WASP5 kinetic rate equations (Ambrose et al., 1994). The user can set the parameters of the rate equations via the user interface or select default values. The suite of models allows the system to be used for a wide range of pollutant transport and fate studies, extending from simple single parameter systems to complex multi-constituent problems with interacting components.

In each model the three-dimensional advective diffusion equation is solved on a boundary conforming grid for each constituent of interest. The model employs the same grid system and obtains the face-centered, contra-variant velocity vector components from the hydrodynamic model. This procedure eliminates the need for aggregation or spatial interpolation of the flows from the hydrodynamic model and assures mass conservation. The transport model is solved using a simple explicit finite difference technique on the boundary conforming grid (ASA, 1997). The vertical diffusion, however, is represented implicitly to ease the time step restriction caused by the normally small vertical length scale that characterizes many coastal applications. The horizontal diffusion term is solved by a centered-in-space, explicit technique. The solution to the advective diffusion equation has been validated by comparison to one and two dimensional analytic solutions for a constant plane and line source loads in a uniform flow field and for a constant step function at the upstream boundary. The model has also been tested for salinity intrusion in a channel (Muin, 1993).

## 4. Application of Models to Salem Sound

### 4.1. CORMIX Application

The CORMIX2 model was applied to the SESD discharge in Salem Sound. The SESD discharge pipe extends from Salem Neck in a generally west-northwest direction to the diffuser location approximately 2.1 km north-northeast of Marblehead in 9.8 m of water. The diffuser lies along an axis approximately  $60^\circ$  west of north and consists of a 1.37 m diameter manifold 200 m long with a series of 66-10.8 cm diameter ports oriented vertically every 3 m.

Figure 4-1a and b show some of the input diffuser geometry and ambient condition parameters necessary to run the model. Table 4-1 provides a listing of input parameters used to run CORMIX2 for the SESD simulations with arbitrary flow-rate and loading. Additional details can be found in Jirka et al. (1996).

The model was applied for four stages of the tidal cycle to determine the extent of the plume: high slack water, maximum ebb, low slack water and maximum flood. These conditions span the range of ambient conditions reasonably expected to occur at the discharge. The different ambient conditions are shown in Table 4.2. The tide range is 2.6 m as indicated by the difference of the high and low slack water depths. CORMIX2 recommends a minimum current speed always be used so 0.01 m/s was selected to represent slack water conditions. The maximum velocities near the site are relatively small. The current directions indicate a rectilinear tide with maximum ebb toward the east and maximum flood toward the west. Gamma is the relative angle between the ambient current and the diffuser.

Figure 4-1a. Plan view of diffuser with input parameters (reproduced from Jirka et al., 1996).

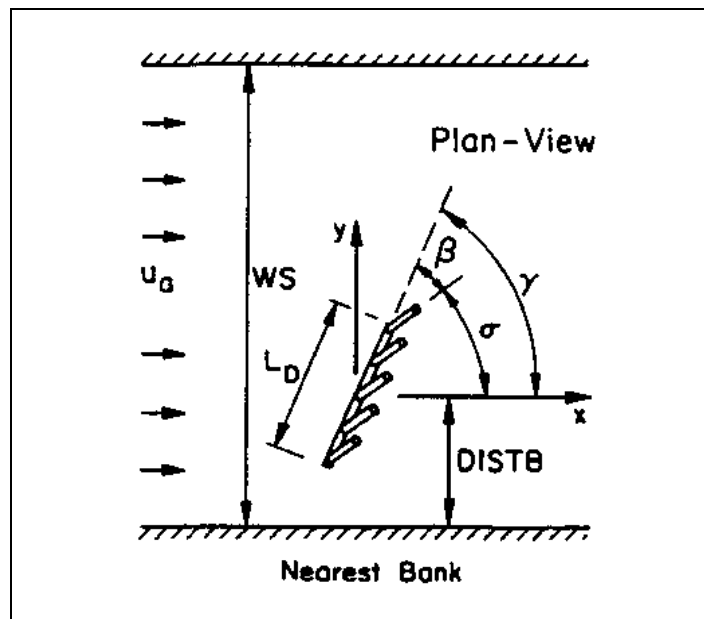
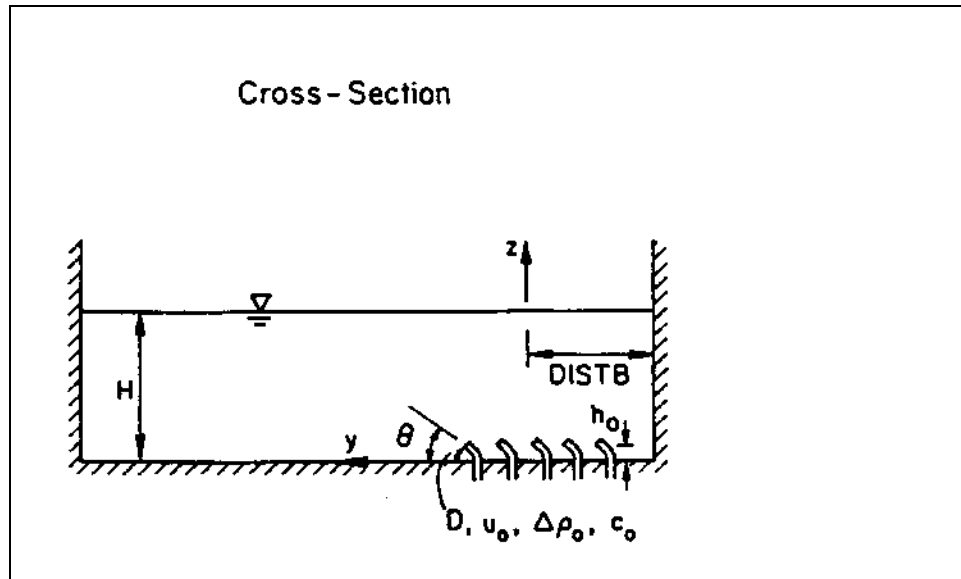


Figure 4-1b. Section view of diffuser with input parameters (reproduced from Jirka et al., 1996).



## 4.2. BFHYDRO Application

The model applied to Salem Sound includes the area west of a line from Manchester Harbor through Baker Island to Marblehead Neck (see Figure 1-1). The modeling domain was extended further offshore, including part of three channels, Salem Sound, Cat Island and Marblehead Channels (Figure 4-2). The model grid conforms to the boundaries, *i.e.*, a boundary fitted grid, where each cell is not necessarily rectangular, square, or even orthogonal. The grid consists of 4552 cells, covering an area of approximately 39.25 km<sup>2</sup> (15.15 mi<sup>2</sup>). The hydrodynamic simulation period chosen was a three-month period from 1 July to 30 September 1985, corresponding to the available field data. The hydrodynamic model (BFHYDRO) was driven by a time varying tidal elevation (Figure 4-3) at the open boundary, and predicted the surface elevation and currents in the area. Forcing used besides the tidal elevation was the time varying wind (Figure 4-4). BFHYDRO simulated the Sound circulation in both 2-dimensional, vertically averaged, and 3-dimensional modes. The 3-D model used a total of 11 layers in the vertical, to resolve vertical mixing and shear due to wind forcing. Both the 2-D and 3-D models included the surface and bottom frictional stresses.

During the simulation period, the tidal elevation (Figure 4-3) ranged between -1.8 and 1.8 m, varying at periods of semi-diurnal ( $M_2$  and  $S_2$ ) and fortnight. The simulation period was chosen for the period 1 July – 1 October 1985, which coincided with the SESD 1985 field program. During this period, there were occasional anomalous events whose wind speed (Figure 4-4) was greater than 8 m/s, for example, 2 August, 1 September, and 28 September. The event at the end of September (speed of about 23 m/s)

was influenced by the Hurricane Gloria. Average wind direction during the simulation period was southwesterly, and the speed was about 4 m/s (8 kt).

Table 4-1. CORMIX2 input parameter description and values used in the application to the SESD discharge.

Parameter	Parameter Description	Value
	Cross section	Unbounded
HA	Average depth	9.8 m
HD	Depth at discharge	9.8 m
UA	Ambient velocity	0.05 m/s
	Manning's coefficient	0.03
UW	Wind velocity	1 m/s
	Stratification	Unstratified
RHOAS	Water density	1030 kg/m <sup>3</sup>
	Diffuser type	Alternating
LD	Diffuser length	198 m
	Nearest bank	Right
YB1 / YB2	Diffuser endpoints	1000 m / 1186 m
NOPEN	Number of openings	66
SPAC	Spacing between ports	3.05
D0	Port diameter	0.108 m
	Port contraction ratio	1
Q0	Discharge flowrate	1.31 m <sup>3</sup> /s
H0	Port height	1.2 m
GAMMA	Diffuser alignment angle	70
THETA	Vertical discharge angle	90
SIGMA	Horizontal discharge angle	0
BETA	Relative orientation angle	90
RHO0	Discharge density	1000 kg/m <sup>3</sup>
C0	Discharge concentration	1.4 mg/L
KD	Decay coefficient	0.000231 /s

Table 4-2. CORMIX2 input parameters for different tide stages.

Tide Stage	Water depth	Current Speed	Current Direction	Gamma
	(m)	(m/s)	(°T)	(°)
High slack water	11.1	0.01	15	165
Maximum ebb	9.8	0.05	95	160
Low slack water	8.5	0.01	190	165
Maximum flood	9.8	0.05	280	70

Figure 4-2. Model domain in Salem Sound.

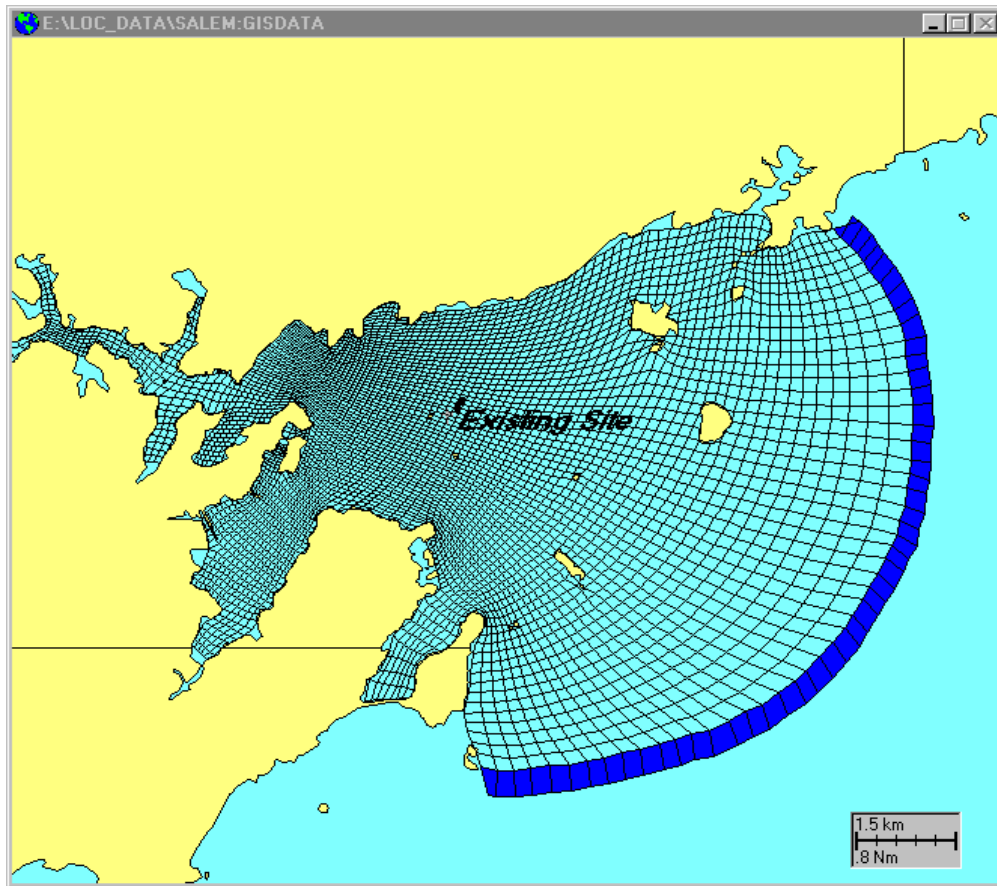


Figure 4-3. Time series of tidal elevation used at the open boundary.

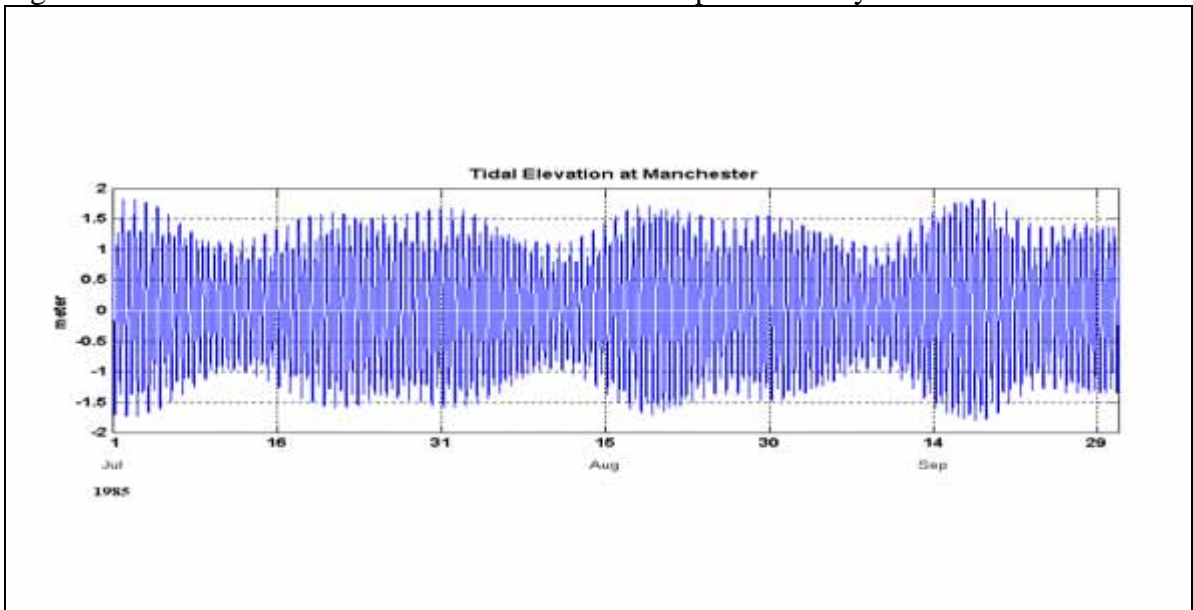
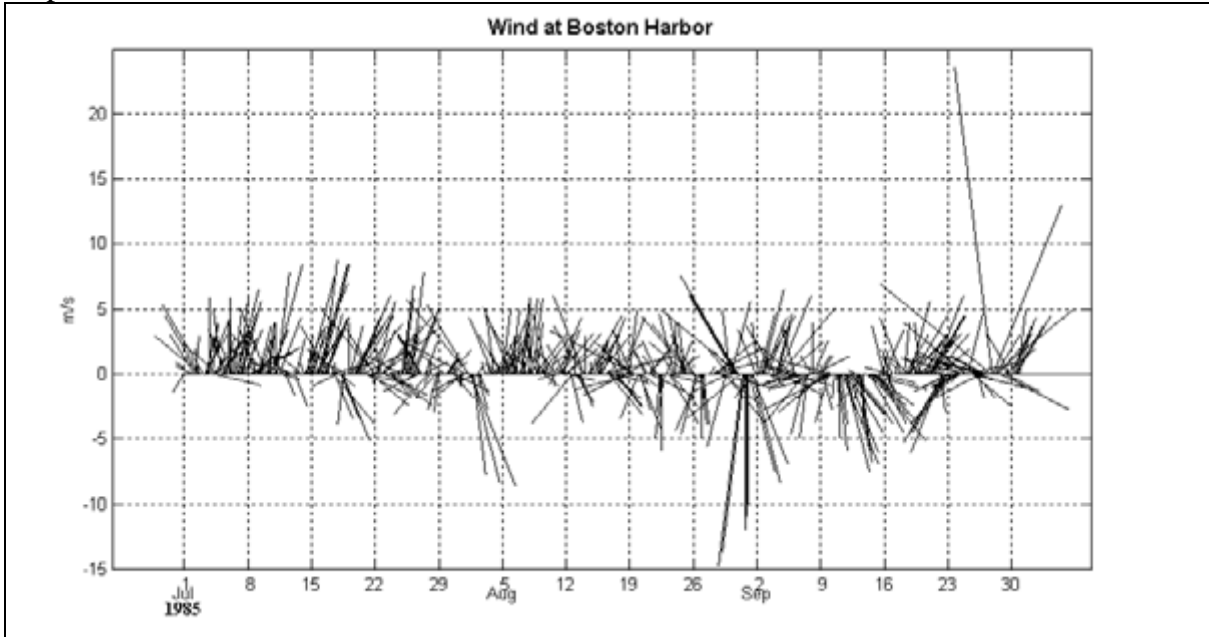


Figure 4-4. Time series of hourly wind vectors (meteorological convention) from Logan Airport, Boston, MA, used to drive the model.



### 4.3. BFMASS Application

The distribution of residual chlorine was preliminary simulated using the constituent mass transport (BFMASS) model. This calculation solved the conservation of a constituent on the same grid as the BFHYDRO. A set of three source strengths of residual chlorine was chosen from a 26-month long discharge record of the SESD.

The objective of this work was to assess the general transport of residual chlorine from the SESD outfall and estimate potential concentrations. Chlorine is a passive decaying tracer and was advected by ambient currents that were generated in 2- and 3-dimensional BFHYDRO applications.

#### 4.3.1 Loading Scenarios

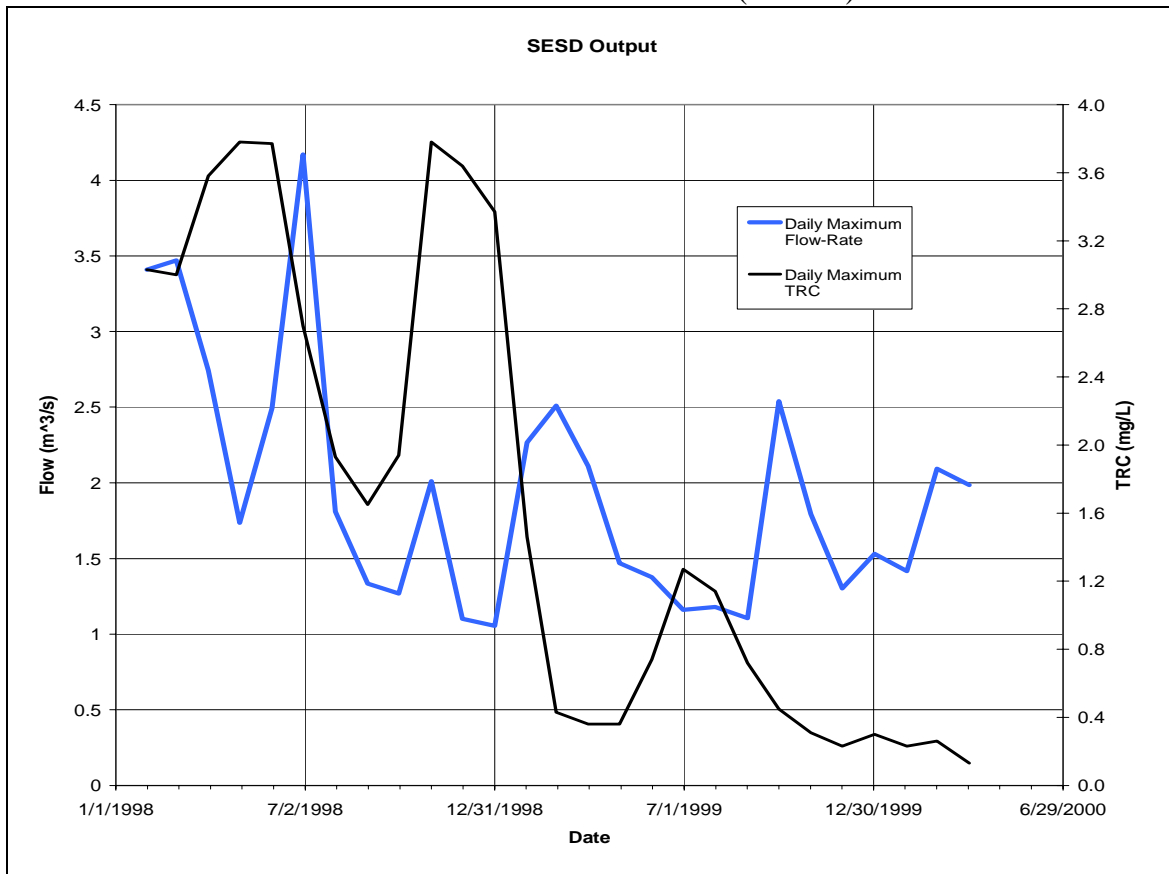
The terminus of the SESD outfall is located at (42°32'09"N,70°50'13"W), about 2.5 km offshore, and at 9.8 meter below the surface. The pipeline from the SESD WWTP to the diffuser is 349 m long and is made of two sections (Table 4-3).

Based on monthly reports during the period from February 1998 to March 2000, daily-maximum concentration of total residual chlorine (TRC) varied from 0.13 mg/L to 3.8 mg/L, while daily-maximum of flow ranged from approximately 1.0 and 4.1 m<sup>3</sup>/s. Figure 4-5 shows a time series of effluent TRC and flow at the SESD WWTP for the 26 month period. Overall both TRC (black) and flow rate (blue) decreased, with a dramatic

Table 4-3. Specifications for the SESD WWTP outfall pipe line (CDM, 1991).

	On Land (pipe 1)	In Water (pipe 2)
Material	Cast-iron	Cast-iron
Diameter, m	1.68	1.37
Cross-section area, m <sup>2</sup>	4.43	2.95
Length, m	980	2,510
Volume, m <sup>3</sup>	4,341.4	7,491.85

Figure 4-5. Time series of effluent total residual chlorine (TRC) concentration and flow rate observed at the SESD Waste Water Treatment Plant (WWTP).



reduction for TRC. The period maximum daily-maximum flow-rate of 4.1 m<sup>3</sup>/s occurred in July 1998 with a corresponding 2.6 mg/L TRC. The period maximum daily-maximum TRC (3.8 mg/L) was observed in June and November 1998. We chose three representative cases for analysis: 1., maximum flow-rate (July 1998 condition), 2., maximum TRC concentration (November 1998 condition), and 3., Recent condition (April 2000). These cases are summarized in Table 4-4.

The TRC reported by SESD is the concentration occurring at the WWTP before discharge and not at the diffuser. This is important because TRC decays over time. The

Table 4-4. Estimates of TRC load at diffuser. The C and U represent the concentration and mean velocity at the end of the pipe. Numbers 1 and 2 denote the pipe on land and in water, respectively. The Co and C2 are the TRC concentrations at the plant and diffuser, respectively.

Scenario	Date	Flow-rate (m <sup>3</sup> /s)	Co (mg/L)	U1 (m/s)	C1 (mg/L)	U2 (m/s)	C2 (mg/L)	Load (mg/s)
1	Jul-98	4.17	2.6	0.9515	2.055	1.4158	1.377	5747.873
2	Nov-98	1.98	3.8	0.4462	2.313	0.6706	0.993	1963.161
3	Apr-00	1.98	0.13	0.446	0.079	0.6706	0.034	67.218

TRC at the diffuser can be estimated, however, using a mass conservation equation (Huang et al, 1997). Assuming the flow is steady state, the equation is as follows

$$(1) \quad u \frac{\partial C}{\partial x} = -KC,$$

where  $x$  is the distance along the outfall pipe,  $C$  is total residual concentration,  $u$  is the mean flow velocity in the pipe, and  $K$  is the overall decay constant. This constant  $K$  consists of two components ( $K = K_s + K_d$ ; Huang et al, 1997): static decay  $K_s$  which is associated with chlorine decay in the bulk flow and dynamic decay  $K_d$  that is related to the chlorine consumption by the biofilm at the pipe wall (Milne et al, 1993). The latter depends on both the hydraulics of the pipe flow and the interaction with biofilm. For the mean velocity estimate  $u$ , the following was used:

$$(2) \quad u = \frac{Q}{A},$$

where  $Q$  and  $A$  are flow rate (m<sup>3</sup>/s) and cross-sectional area of the pipe (m<sup>2</sup>), respectively.

The CDM report (1991a) states that there were slimy deposits built up on the inside surface of the pipe about 3 mm thick. However, the biological component of the deposit and its interaction with chlorine are not known, therefore the dynamic decay constant  $K_d$  can not be determined. For this study,  $K_d$  was ignored and only  $K_s$  was used. A value of 19.5/d (Huang et al, 1997), representative of TRC decay, was used for the decay parameter  $K$ .

The estimates of TRC concentration at the plant (Co) and the end of the on-land pipe (C1) and in-water pipe (C2) are listed in Table 4-4. There is a 47% reduction in TRC concentration at the higher flow rate and a 74% reduction at the lower flow rate. The TRC loads used for the BFMAS simulations were calculated as 6000 mg/s, 2000 mg/s and 60 mg/s, representing the three cases. The release is modeled at one or three grid cells that represent multi-ports along the diffuser. With three release cells, the load was equally distributed among the cells.

## 5. Modeling Results

### 5.1. CORMIX

The CORMIX2 model was applied to the SESD outfall to obtain near field dilution predictions for various stages of the tide and for different operating conditions described in Table 4-4. The prediction files (.prd) for model output with the four cases at different stages of the tide are included as Appendix C. The first section of the prediction file summarizes the data input and the variables used to classify the flow. Next, the output from a series of calculation modules describes the location, geometry and dilution of the plume. The near field region module provides a series of outputs along the plume centerline describing the dilution and plume size between the discharge ports and the water surface.

The results for the four tide stages are summarized in Table 5-1. The plume rises quickly to the surface taking between 9 and 14 s. This range of times is a function of the water depth; shallower depths take less time to surface. See Table 4-1 for the list of CORMIX2 input parameters. The downstream distances traveled by the plume are very small due to the short time that the plume takes to surface and the low ambient velocities that would transport the plume downstream. The plume widths are also low since there is little time for the plume to entrain ambient water. The dilution is significant, however, showing a range from 20.8 to 33.6, depending on the variation of water depth over the tide cycle.

Table 5-1. CORMIX2 predictions for different tide stages.

Tide Stage	Time to Surface	Downstream Distance	Plume Width	Dilution
	(s)	(m)	(m)	
High slack water	14	0.27	1.84	33.6
Maximum ebb	12	1.39	1.78	31.2
Low slack water	9	0.17	1.36	20.8
Maximum flood	12	1.40	1.78	31.2

The CORMIX2 model was also used to estimate the dilution and ultimate near field concentration based on different operating conditions of the plant. A series of runs were made based on historical reported discharge flow-rates and concentrations that have previously been summarized in Table 4-4. Table 5-2 summarizes the CORMIX2 results for the maximum ebb tidal condition. The dilution and ultimate concentration are reported where the plume reaches the water surface.

With a lower flow-rate there is more time to reach the surface and so there is more time for dilution. Thus the dilution is shown to increase by 45% when the flow is reduced from 4.2 to 2.0 m<sup>3</sup>/s. The ultimate concentration is seen to directly scale with the change in diffuser residual chlorine levels at constant flow-rate, i.e., a reduction of a factor of 29 in diffuser chlorine (0.99 to 0.034 mg/L) results in an ultimate concentration reduction of 29 (0.041 to 0.014 mg/L).

Table 5-2. CORMIX2 results for different historical operating conditions.

Time Period	Flowrate	Diffuser Chlorine Concentration	Dilution	Ultimate Concentration
	(m <sup>3</sup> /s)	(mg/L)		(mg/L)
July 1998	4.2	1.4	16.5	0.085
November 1998	2.0	0.99	23.9	0.041
April 2000	2.0	0.034	23.9	.0014

## 5.2. WQMAP

### 5.2.1 BFHYDRO Current Simulations

As part of the initial phase of the simulation of currents in Salem Sound, a sensitivity test was performed on forcing functions (tidal elevation and wind) to test the BFHYDRO model. Sensitivity is a measure of the model response to change in the forcing function. The sensitivity testing results can be compared via the predicted  $M_2$  tidal ellipses and their observations (there were no time series of current data available to use for comparison). However, we can use tidal ellipse parameters observations at the three current meter sites, reported in Zhang and Adams (1991), and the mean speed and direction of total currents presented in CDM (1986a; 1991).

The observed tidal currents at CM1 and CM2 were clockwise-rotating ellipses whose the major axis was oriented in northwest-southeast direction. However, the currents at CM2 were more circular having the minor axis almost 60% of the magnitude of the principal axis. The tidal ellipse at CM3 rotated opposite to the other locations and the major axis orientation was in a north-northeast direction. The total currents at site CM1 had a mean speed of 5.2 cm/s and 356.5°T mean direction, while the mean speeds and directions at CM2 and CM3 were 4.7 cm/s and 9.7 cm/s and 156.5°T and 186.5°T, respectively.

The tidal elevation used for the BFHYDRO simulation was the time varying observations taken at Manchester station at the northeast corner of Salem Sound. A focus of the sensitivity test for the tides was on the slope at the open boundary. In Massachusetts Bay, currents flow in from the northeast to the south of Cape Ann and flow out into the Gulf of Maine north of Cape Cod, although they often alter direction due to occasional wind and freshwater discharge events. The current flow in the Bay forms a cyclonic circulation and sets up higher elevation to the north than to the south. During the MWRA outfall study (1988), field measurements showed the latitudinal sea level difference was 5 cm. Accordingly, options chosen for sensitivity test were as follows: 1. zero slope, 2. a linearly decreasing to south (positive) slope and 3. a linearly decreasing amplitude to north (negative) slope along the open boundary. With the zero slope applied, the predicted rotation of tidal currents was the same as the observations at all three locations. However, the simulated major axes of tidal ellipse at CM1 and CM3 were underestimated, while the minor axes were overestimated at CM1 and underestimated at

CM3. The predicted major axis at CM2 was overestimated but the minor axis was underestimated at CM2.

One result of the sensitivity study found was that the circulation and tidal ellipse behave oppositely to positive and negative slopes. While the positive slope produced counter-clockwise rotating tides at all three locations, the negative slope produced clockwise rotation at CM1 and counter-clockwise ellipse at CM2 and CM3. The positive slope resulted in currents flowing in a counter-clockwise direction, whereas the negative slope produced a clockwise circulation. Compared to the results with a constant slope, the positive slope produced a larger principal axis at CM1 and larger minor axes at both CM2 and CM3, with the minor axis at CM1 and major axis at CM2 almost same. The sensitivity study was also performed for different slopes. When a larger slope was used, a larger total current speed was simulated. Also, the  $M_2$  tide principal axis was further oriented counter-clockwise for the positive slope and clockwise for the negative slope. The best agreement to the observed tidal ellipses and the circulation was found with a zero slope.

A sensitivity study for the atmospheric wind indicated that the forcing with tidal elevation applied amplified the Sound total currents by between 1% and 12% on average, of which the smaller influence occurred inside the Sound and the larger effect occurred near the outer boundary of the Sound. The most conspicuous response to the wind was found in the total current direction in a way that altered the currents to align with the same direction as the wind. Therefore, the currents in the Sound formed a clockwise circulation. However, this manifestation was a low-frequency variation of the currents. The current response was more conspicuous at the outer boundary of the Sound, for example, at CM3, than inside the Sound (see details later). By having the negative sea slope at the open boundary, the clockwise circulation was enhanced by the southwesterly wind. On the other hand, the wind diminished the counter-clockwise circulation resulting from the positive slope.

An important parameter in any hydrodynamic simulation is friction, especially at the bottom layer. Depths in the Sound range from 0.1 m to 45.4 m, with average of 9.8 m. Although the topography varies smoothly in most of the western area, there is an area where the topography varies abruptly. For example, north of Marblehead depths change in 14 m over a 400 m distance. Accordingly, the Chezy depth-dependent formula for the bottom frictional dynamics was more relevant to this area than the quadratic drag coefficient formulation. In order to simulate as closely as possible the actual hydrodynamics in the Sound, calibration was performed to tune the bottom friction parameter.

Figures 5-1a through 5-1c show the predicted tidal ellipse aspect ratio, defined as the ratio of major to minor tidal axes, as a function of Manning number, which is part of the Chezy formula. Also shown is the ellipse aspect ratio from observations. The ellipse data was obtained from the 2-D simulations with both tide and wind forcing. The figures suggested that, at sites CM1 and CM3, the optimal friction coefficient lay between 0.3 and 0.4, and between 0.7 and 0.8, respectively. However, the predicted aspect ratio at

Figure 5-1a. Predicted (solid circle) and observed (thick line) aspect ratio of tidal ellipse at CM1.

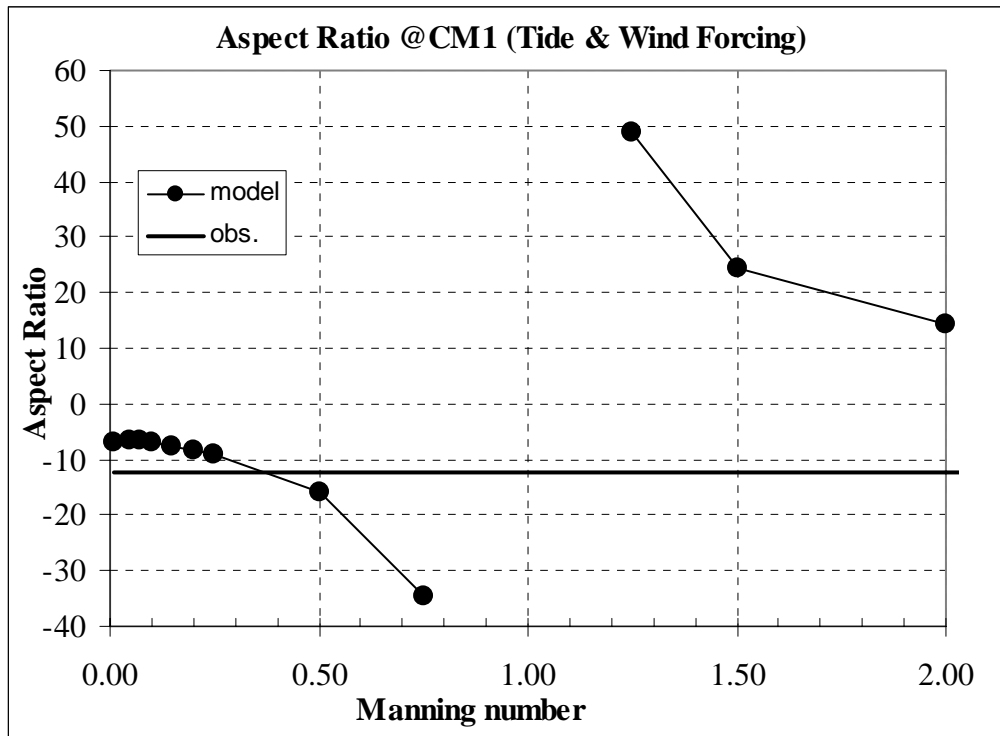


Figure 5-1b. Predicted (solid circle) and observed (thick line) aspect ratio of tidal ellipse at CM2.

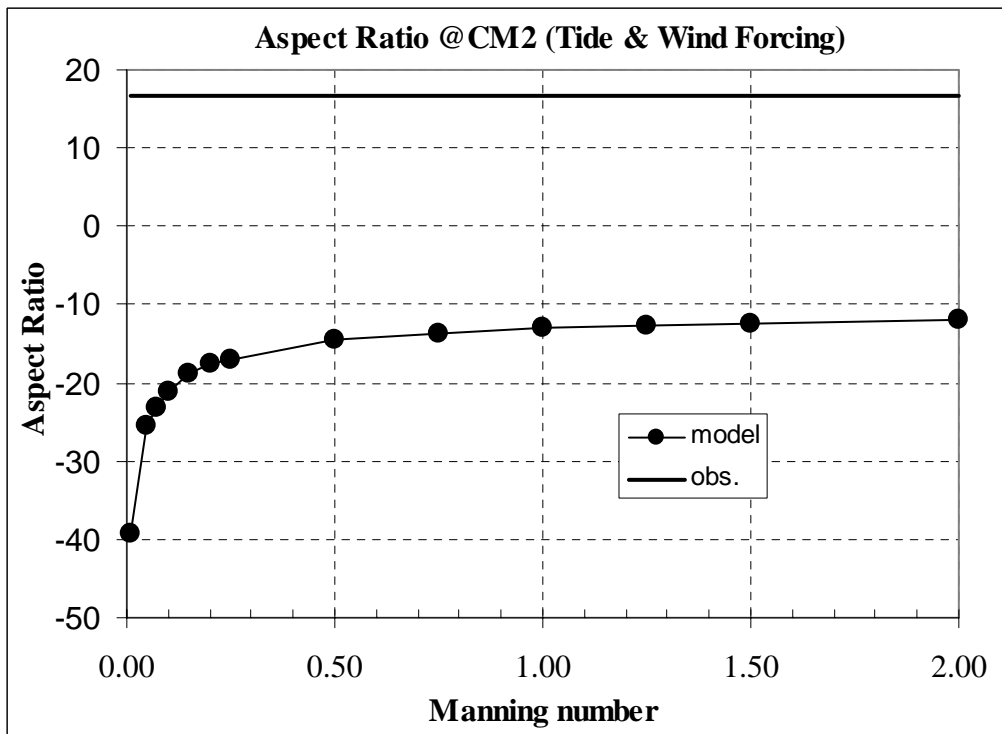
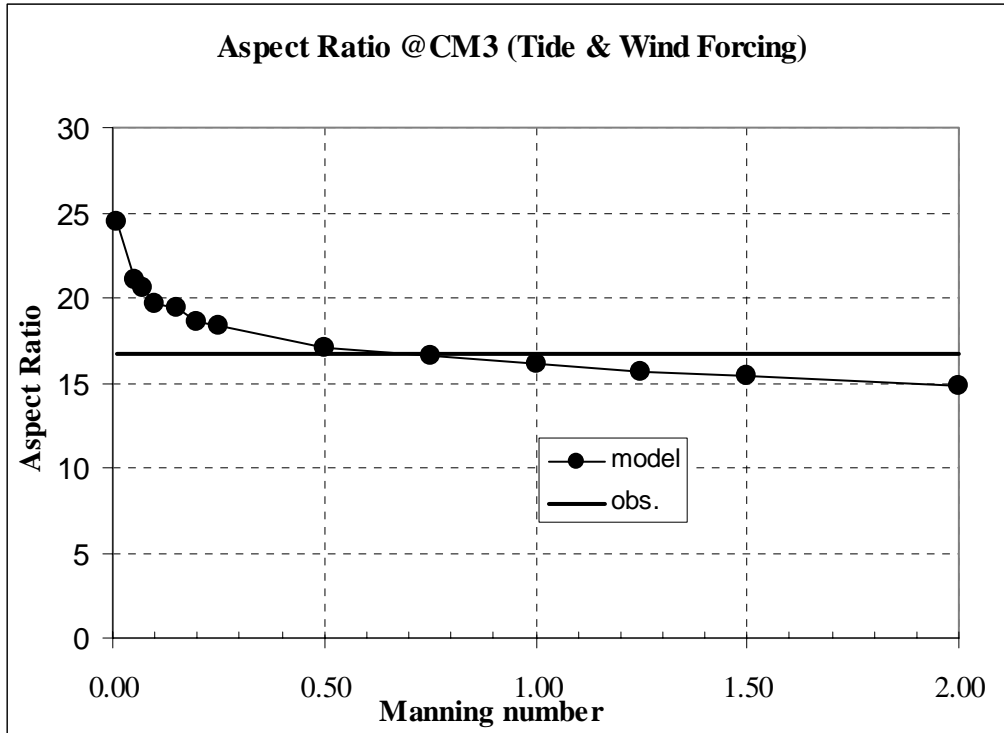


Figure 5-1c. Predicted (solid circle) and observed (thick line) aspect ratio of tidal ellipse at CM3.



CM2 did not cross the observed line anywhere within the range of the Manning numbers used.

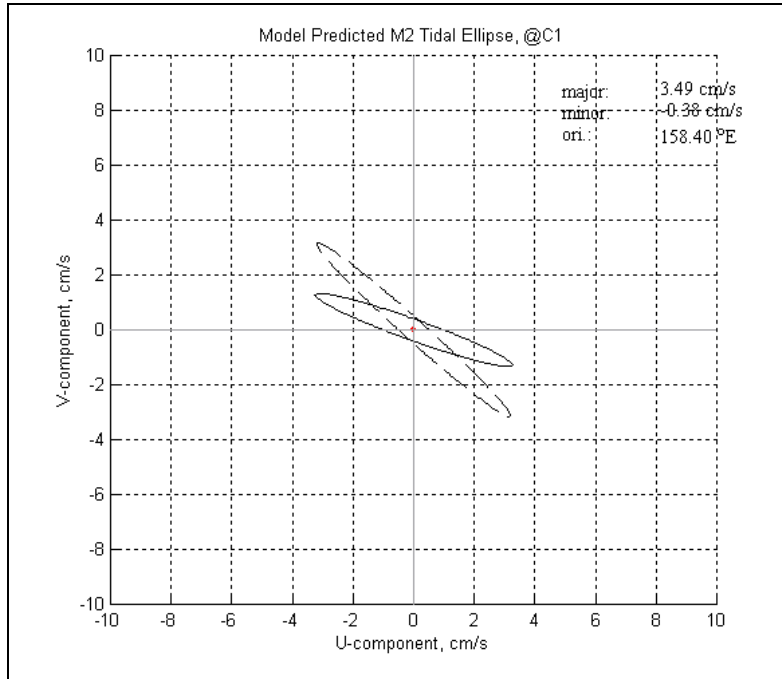
For a Manning numbers greater than 1, the tidal ellipse rotation at CM1 switched from clockwise (negative) to counter-clockwise (positive). The rotation switch for CM3 occurred at a Manning number less than 0.75. Similar results were found at sites CM1 and CM2 for tidal forcing only, except that the optimal friction coefficient fell between 0.2 and 0.3 for CM1 and between 0.75 and 1.0 for CM3.

Overall, the results of the sensitivity study to forcing functions showed that applying both tidal elevation and wind together provided a better simulation. This is because the tides govern high-frequency variations of the currents, while the atmospheric forcing controls the low-frequency fluctuations. The open boundary with a non-constant water slope resulted in a substantial increase of the total current speed and a substantial change in the general direction. According to the calibration study for bottom friction, the depth-dependent formula was most appropriate for this application and the best friction coefficient was a Manning number of 0.25.

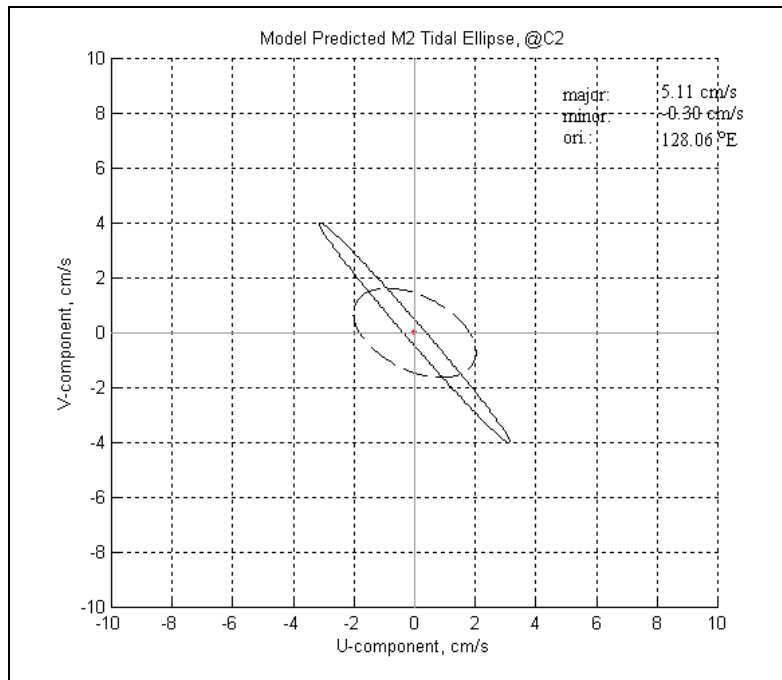
Figures 5-2a to 5-2c exhibit 2-D model predicted tidal ellipses at three stations, CM1 to CM3, with zero tidal slope at the open boundary and 0.25 Manning number for the bottom friction, and are compared with the observations. In general, the predicted parameters agreed with the observations, except at station CM2. The tidal ellipse analysis

Figure 5-2. Tidal ellipses of the observed data (dashed) and 2-D model predictions (solid) at stations CM1 (a), CM2 (b) and CM3 (c).

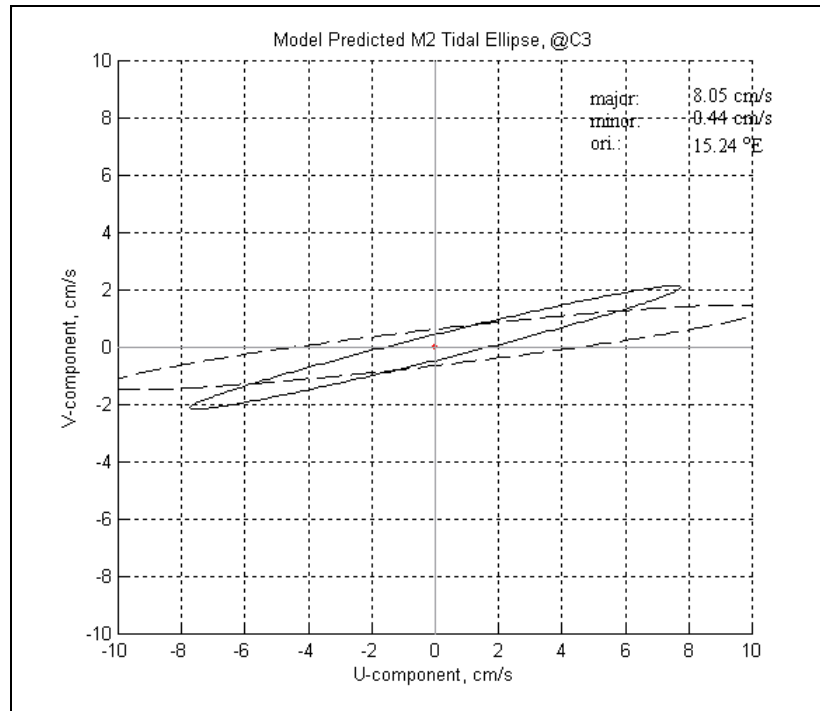
(a)



(b)



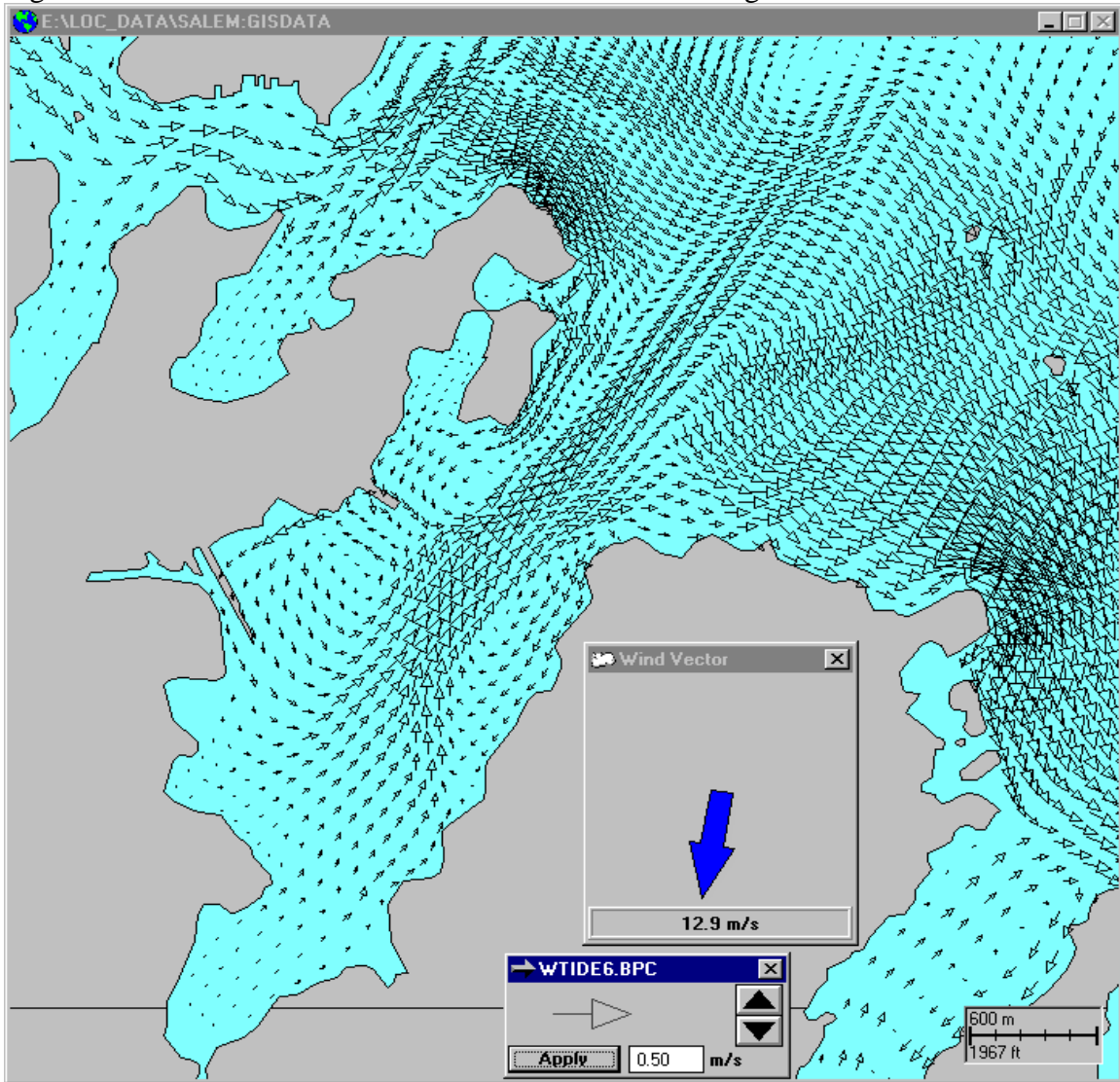
(c)



was performed with only the semi-diurnal  $M_2$  constituent. Major and minor axes of the predicted and observed tidal currents at CM1 and CM3 were of a similar order of magnitude, and the predicted ellipse orientations showed a  $23^\circ$  and  $8^\circ$  difference towards north at CM1 and CM3, respectively. The predicted  $M_2$  tidal currents in the southwestern area rotated in an elliptic rather than circular motion as observed in the measurements (Figure 5-2b), both of which were aligned to the northwest-southeast direction. The tidal rotations from the models were consistent with the observations, which were clockwise at CM1 and CM2 and counterclockwise at CM3.

Of interest is the hydrodynamic response that occurs at Salem Harbor. During the simulation period, there were occasional northerly wind events. When the tides were ebbing and the northerly wind prevailed, the circulation in the Harbor consisted of three distinctive gyres. Figure 5-3 shows the currents in Salem Harbor for the 31 August 1985 event. While most of the water in the Harbor drained out into the Sound, there was an opposing flow forming a strong horizontal shear east of Salem Neck. Inside the Harbor, there were three re-circulation gyres: two were cyclonic circulations at diameters of 400 m and 800 m in the western Harbor, and one was an elongated shape at the eastern Harbor. The highest speed existed along the dredge channel at the order of 25 cm/s,  $O(25$  cm/s), and the current speed in the rest of the Harbor were significantly weaker.

Figure 5-3. Predicted circulation in Salem Harbor on 31 August 1985.



### 5.2.2 Comparison between 2-D and 3-D BFHYDRO Simulations

Both the 2-D and 3-D simulations were driven by a time varying tidal elevation at the open boundary and winds at the surface. A Manning number of 0.25 was used for the bottom friction coefficient. A total of 11 layers were used in the 3-D simulations to resolve the vertical structure of the horizontal currents. In the 3-D simulation, the non-linear, advection processes were also considered that required longer computational times than for similar results with 2-D and 3-D linear simulations.

Table 5-3 presents a comparison among linear 2-D and 3-D simulations and the observations (numbers in the shaded cells) of tidal ellipses and the total currents at the three current meter mooring locations. The total currents from 2-D model were underestimated at CM1 and CM2 but overestimated at CM3, compared to the measured

speed. However, the 3-D model computed relatively larger speeds everywhere except at the bottom layer of CM1 and CM2. For the mean direction of total currents, a consistency was found between the two models, but not between observations and the models. The measured directions were north-northeastward at CM1, south-southeastward at CM2, and south-southwestward at CM3, whereas the model calculations were north-northeastward at CM1 and CM2, and east-northeastward at CM3.

Compared to the 2-D ellipses at the individual locations, the 3-D simulated  $M_2$  tidal ellipses were fatter and longer at CM1, and thinner and shorter at CM2 and CM3. The difference in ellipse orientation between the 2-D and 3-D simulations was very minor, on the order of a half degree.

Table 5-3. Predicted semi-diurnal  $M_2$  tidal ellipses and total currents from linear 2-D and 3-D BFHYDRO model simulations. Observations are shown as shaded cells. Mean values in the linear 3-D columns are averages over the 11-layers. Orientation is in degrees counter clockwise from east (E), and mean direction is degree clockwise from true north (T).

station	Linear 2-D						Linear 3-D						
	tidal ellipse				total current		level	tidal ellipse				total current	
	major cm/s	minor cm/s	a-ratio	orientation E	speed cm/s	direction T		major cm/s	minor cm/s	a-ratio	orientation E	speed cm/s	direction T
CM1	3.49	-0.38	-0.109	158.40	4.71	293.03	top	3.85	-0.65	-0.169	158.90	5.93	22.86
							mid	3.73	-0.58	-0.155	158.90	5.42	22.67
							bottom	3.41	-0.50	-0.147	158.94	4.88	22.40
	4.47	-0.36	-0.081	135.20	5.20	356.50	mean	3.66	-0.58	-0.157	158.91	5.41	22.64
CM2	5.11	-0.30	-0.059	128.06	4.47	286.80	top	5.33	-0.31	-0.058	128.25	5.66	18.50
							mid	5.20	-0.23	-0.044	128.31	4.96	16.88
							bottom	4.74	-0.18	-0.038	128.79	4.40	16.48
	2.23	-1.32	-0.592	148.30	4.90	156.50	mean	5.09	-0.24	-0.047	128.45	5.01	17.29
CM3	8.05	0.44	0.055	15.24	9.96	53.85	top	8.56	0.45	0.053	15.51	13.51	54.17
							mid	8.14	0.41	0.050	15.13	12.21	56.18
							bottom	6.52	0.31	0.048	13.33	9.99	56.75
	10.52	0.63	0.060	7.30	9.70	186.50	mean	7.74	0.39	0.050	14.66	11.90	55.70

Another result of the non-linear 3-D simulations was that the tidal ellipse direction in the non-linear 3-D simulations were counter-clockwise at CM1 and clockwise at CM3, both of which were opposite to the observations. While the non-linear 3-D predicted tidal ellipses were fatter at CM1 and CM3 and thinner at CM2 compared to the linear 2-D simulation and the observations, the major axes were shorter at CM1 and CM3 but longer at CM2 for the 3-D. The average of the total current speeds predicted from the 3-D model was smaller at all locations than the 2-D by about 3.8 cm/s at CM3 and smaller than the observations by about 3.6 cm/s at CM3. The mean direction at CM1 from the non-linear 3-D model was north-northwestward compared to north-northeastward with the 2-D, however it was very close to the observed direction. The mean direction at the rest of the locations CM2 and CM3, were similar to the 2-D results, but they were still oriented towards different directions.

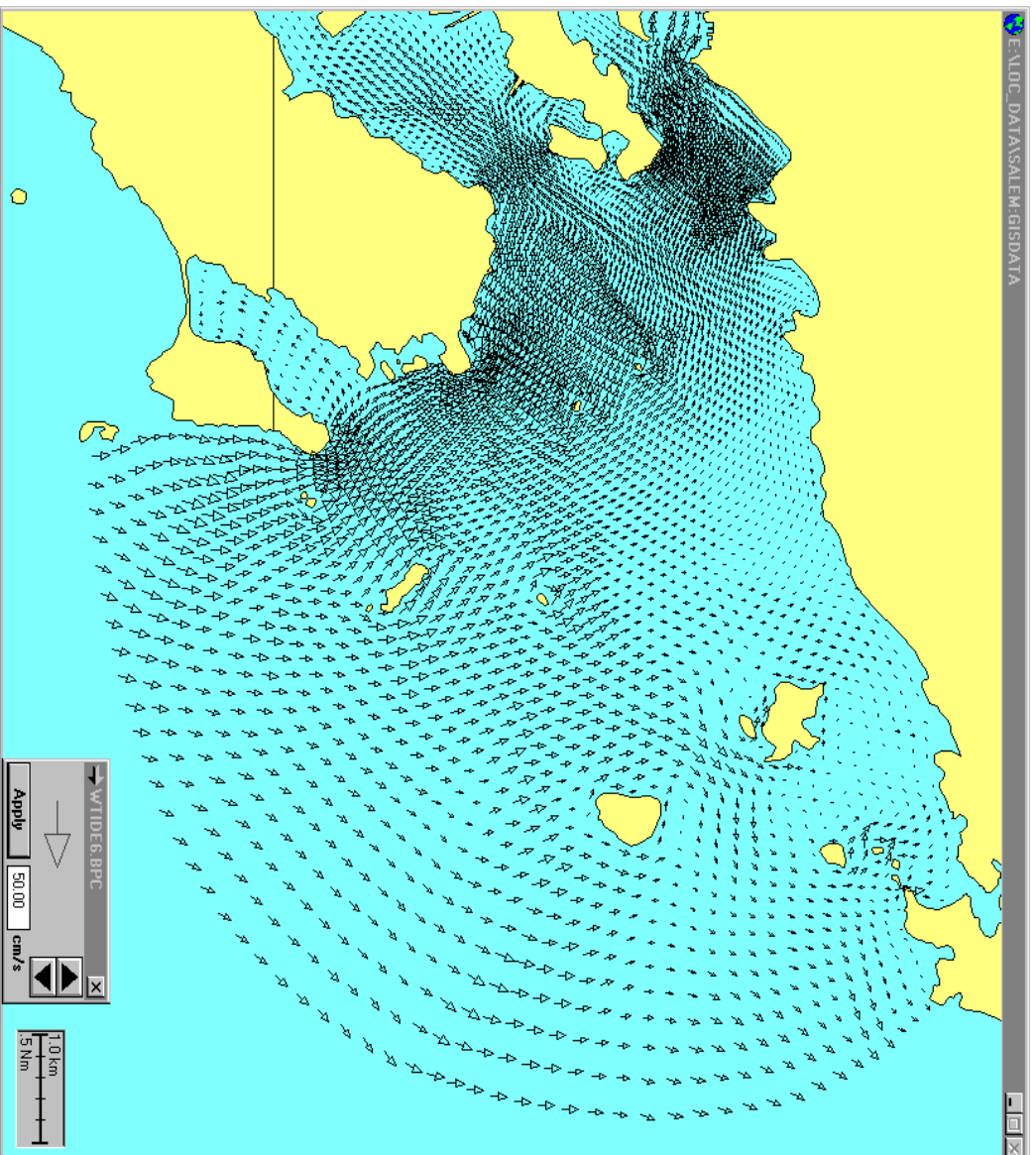
Figure 5-4 shows typical maximum flood (a) and maximum ebb (b) currents in Salem Sound. Both current fields were selected from the 2-D simulation, although the fields were very similar for the 3-D results. The current fields in the Sound consisted of two dynamic regimes. In the area east of a line between Marblehead Harbor and Manchester Bay, the simulated currents flew northward most of time and showed less tidal variations. This was because of the southwesterly prevailing winds. On the other hand, the interior currents changed direction during the tidal cycle and the variations were more frequent than the currents at the outer boundary. The hydrodynamic simulations inside the Sound showed that during flood a strong inflow existed north of the Marblehead coastline with maximum speed of about 30 cm/s, while currents south of Manchester, were much smaller and their direction was generally eastward. However, when the winds were northerly the currents in the area south of Manchester were also towards the Sound. During ebb, the flow south of Manchester became stronger at a maximum speed of 30 cm/s, and the currents north of Marblehead were weak.

The variation of currents inside the Sound was dominated by tides, in the direction of east during ebb and west during flood. For instance, the currents at the SESD site (CM1) were primarily east-west as shown in Figure 5-5, with a strong response to tidal elevation (Figure 4-3), except occasional perturbations (1 and 28 September 1985). These anomalous events were associated with the prevailing wind during the period. Currents at a location to the southwest (CM2) were weaker than at site CM1, but they showed larger variation in the north component than the east component, which was opposite to the currents predicted at CM1. The current speeds at CM3 were larger by a factor of almost 2, as seen in the total current comparison (Table 5-3). There was a high-frequency energy that was driven by tides. However, most of variations in the currents at CM3 was governed by the atmospheric forcing. Figure 5-6 shows time series of low-pass filtered speeds vs. wind speed. As seen in the figure, correlation between the currents at CM3 and the wind speed was high. Instantly, the low-frequency variations predicted at the other locations (CM1 and CM2) also seemed to coincide with the wind fluctuations. The correlation was more significant for the north components than the east components.

### 5.2.3 BFMASS Transport Simulations

The sensitivity study of BFMASS transport model used the 2-dimensional version of model and varied the size of the load (6000, 2000, 100 and 60 mg/s), types of sources (single or distributed), dispersion coefficient (1, 5 and 10 m<sup>2</sup>/s), and decay rate (0.1, 1, 10, 20 and 100/d). Figure 5-7 shows locations of the loads: a) single source, and b) distributed source (represented by three cells). The cells were located at the center and both ends of the diffuser (details shown in insert of Fig. 5-7b). The figure also shows four model time series locations used to monitor mass concentration around the diffuser in time. They were located at (42.5411°N, 70.8391°W) approximately 550 m north, (42.5355°N, 70.8304°W) about 450 m east, (42.5301°N, 70.8437°W) about 1,100 m south, and (42.5360°N, 70.8508°W) approximately 1,150 m west of the outfall. There were three more locations offshore, shown in Figure 5-8, at the Salem Sound channel, the

Figure 5-4. Typical maximum flood (a) and maximum ebb (b) currents in Salem Sound.



(b)

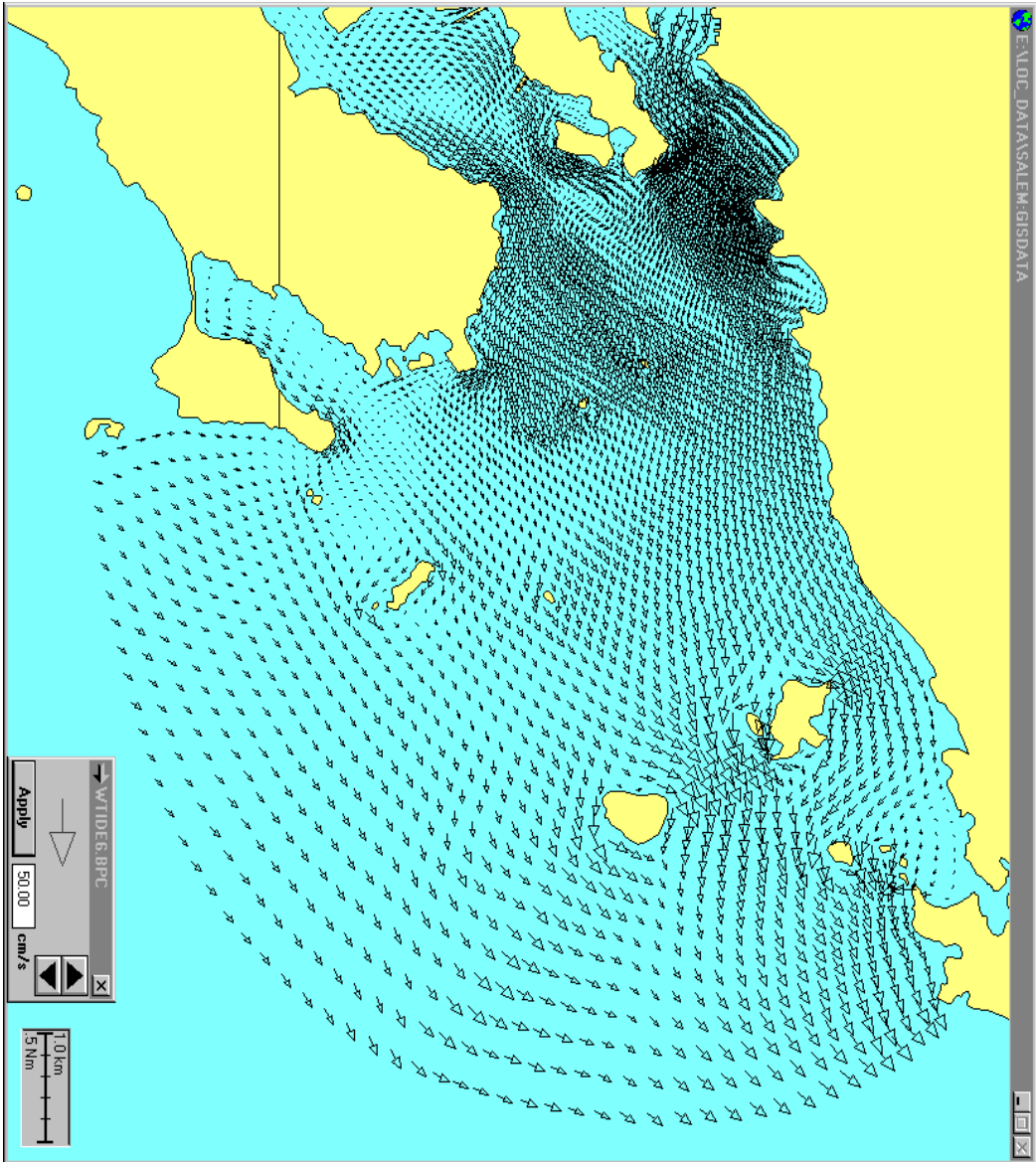


Figure 5-5. Time series of model predicted velocity currents at station CM1.

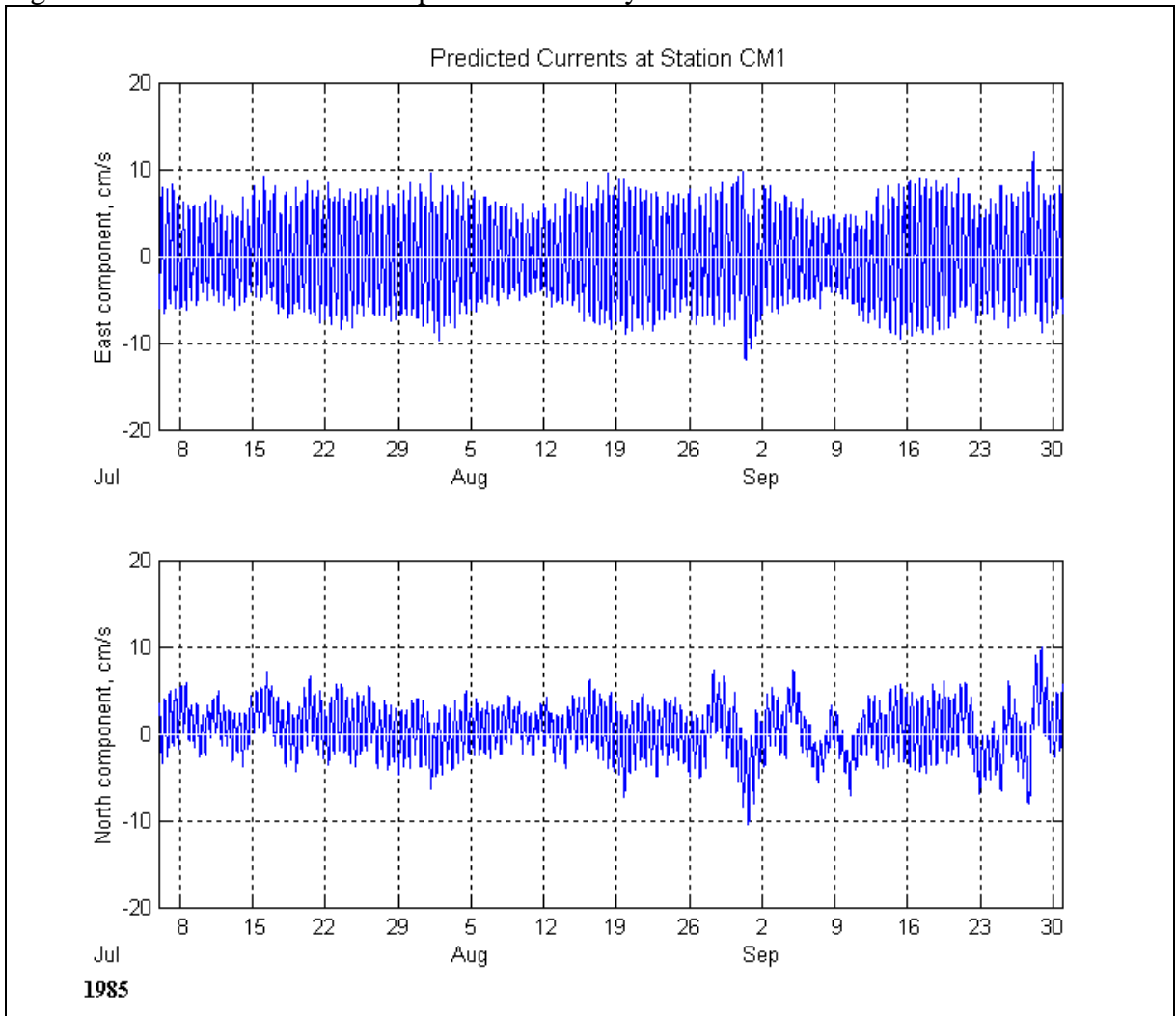


Figure 5-6 Time series of wind speed, and the predicted east and north component speeds at stations CM1, CM2 and CM3. All the speeds are filtered with 2-day running average.

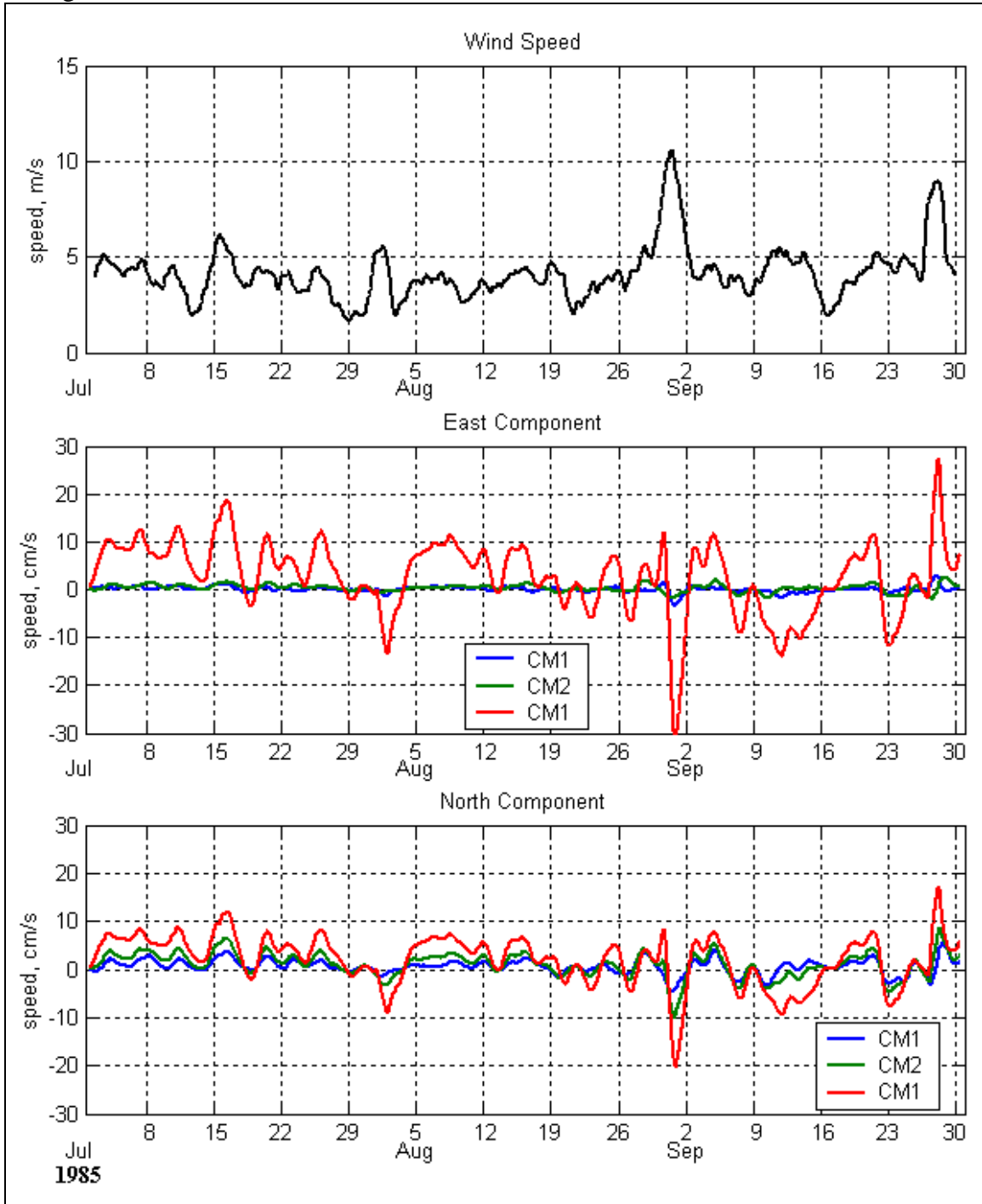
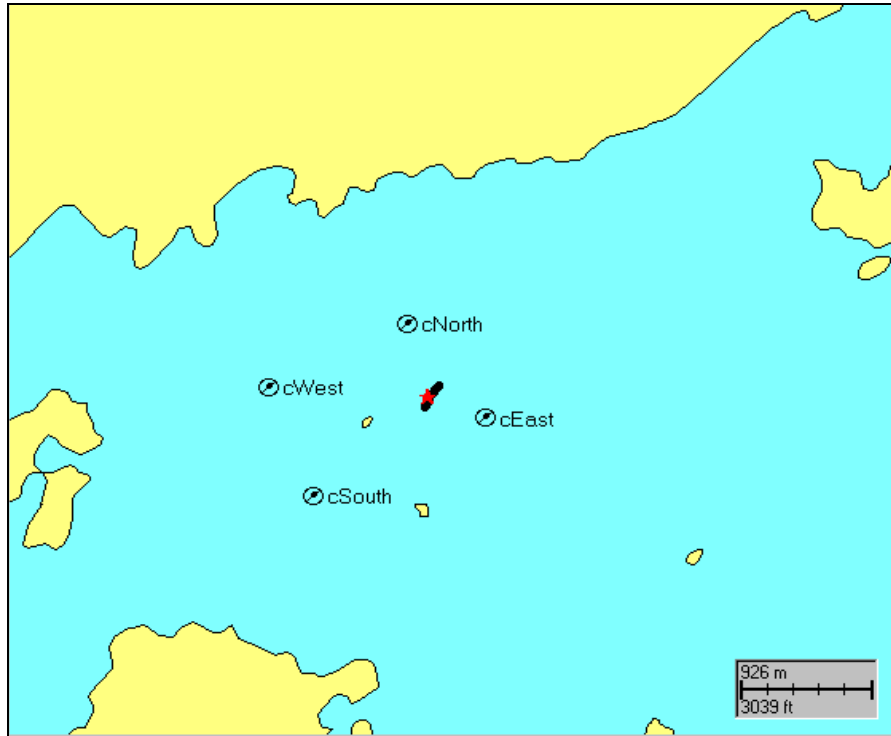


Figure 5-7. Load location (star): a) single source, b) distributed source (three cells), with insert of the detail around the outfall.

a)



b)

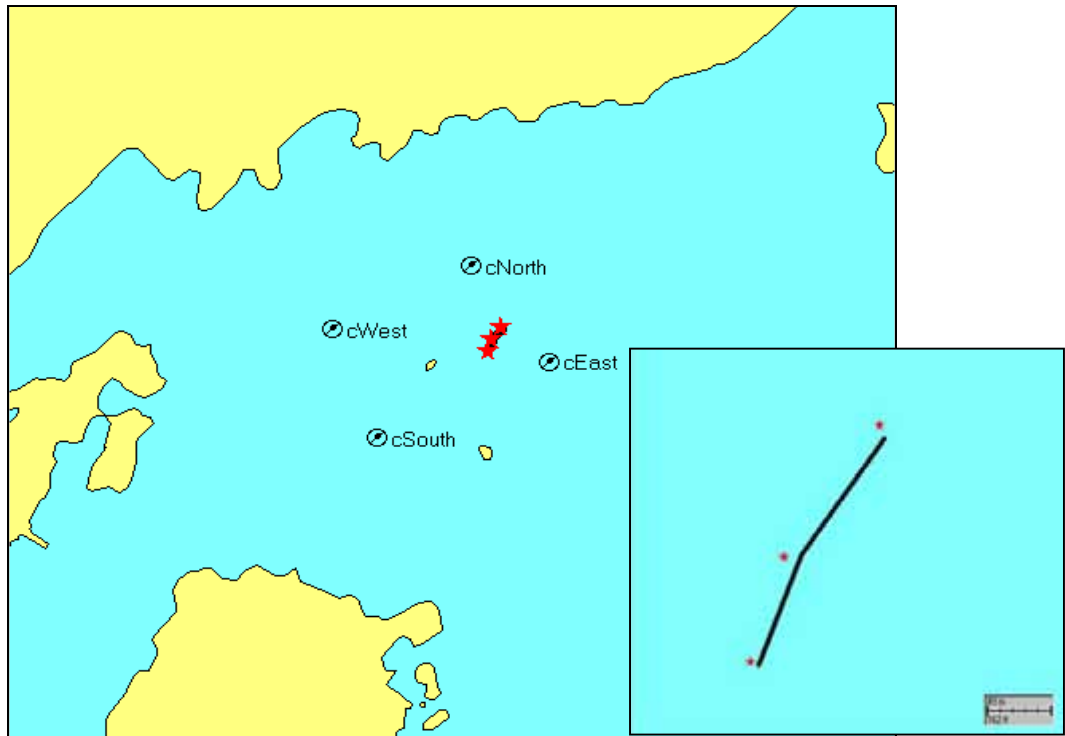
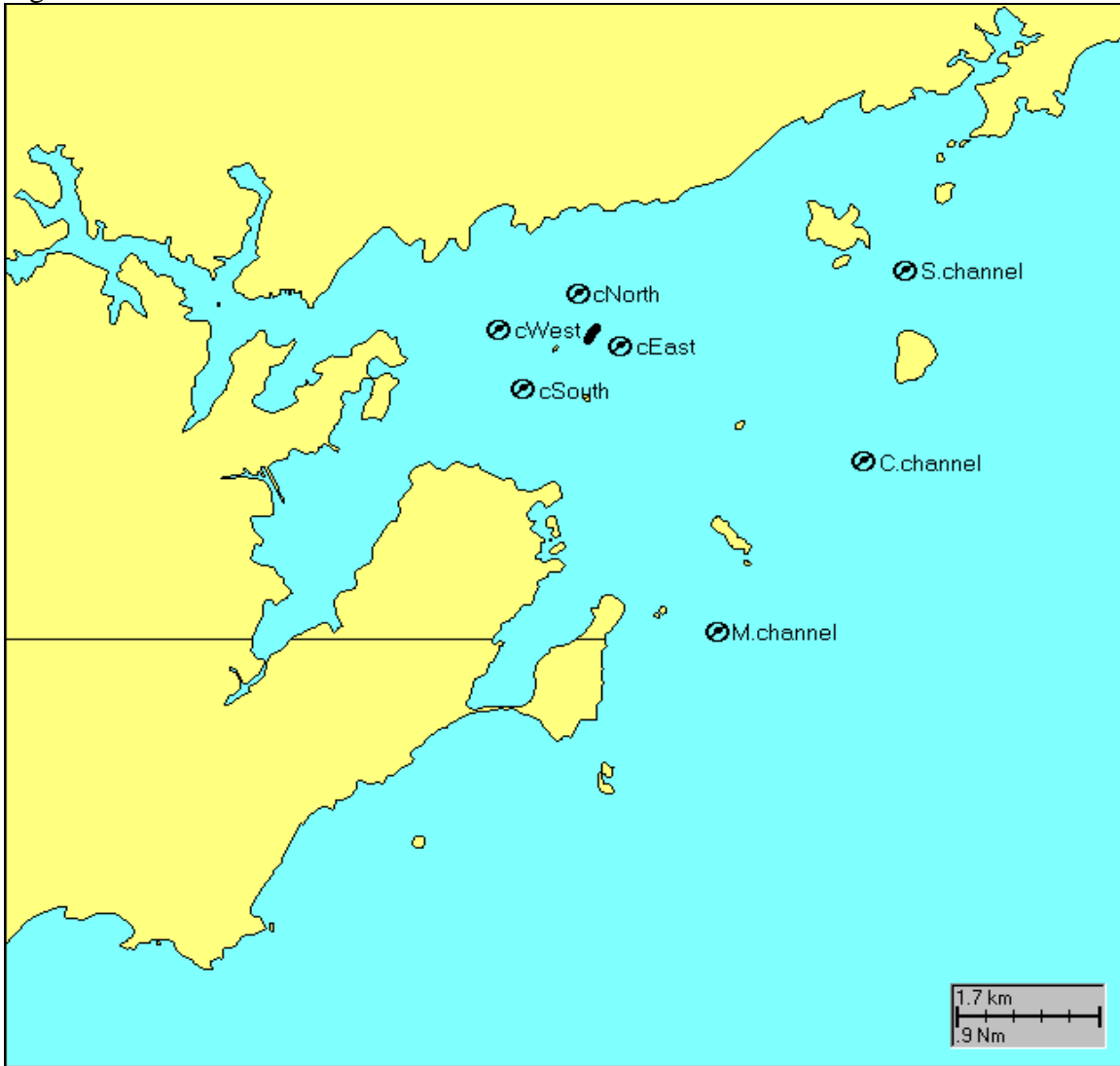


Figure 5-8. Seven model time series locations used to monitor TRC concentration.



Cat Island channel, and the Marblehead channel, which are about 4.0 km, 3.9 km and 4.2 km east of the outfall, respectively.

Based on previous studies (Newman et al., 1990; Zhang and Adams, 1991), the dispersion coefficient in Salem Sound varied between 0.1 and 20 m<sup>2</sup>/s. For this study, various values in a range between 1 and 10 m<sup>2</sup>/s were used, which lie in the observed range. Chlorine is in fact non-conservative since reaction with organic and inorganic compounds in water, volatilization, and photo-degradation contribute to its decay (Milne et al., 1993). Nonetheless, the environmental effects on TRC and the dominant decay mechanism in the seawater are not well known. We chose decay values between 0.1 and 100/d for the Sound.

Table 5-4 lists runs for the sensitivity study based on load type, amount of load, dispersion coefficient and decay rate. This study used the 2-D version of the model.

Table 5-4. Sensitivity study for load, dispersion and decay rate for 2-D model.

Run #	Load, mg/s and types of source	Dispersion coefficient, m <sup>2</sup> /s	Decay rate, 1/d	Comments
1	6000/(3×2000)	1	0.1	Figure 5-10
2	6000/(3×2000)	1	1	Figure 5-11 (top); Figure 5-12
3	6000/(3×2000)	1	10	
4	6000/(3×2000)	1	20	Scenario 1 in Table 4-4
5	6000/(3×2000)	1	100	
6	6000/(3×2000)	5	1	Figure 5-11 (bottom); Figure 5-12
7	6000/(3×2000)	10	1	
8	6000/(3×2000)	5	20	
9	6000/(3×2000)	10	20	
10	2000/(3×633)	1	20	Scenario 2 in Table 4-4
11	100/(3×33)	1	20	
12	60/(3×20)	1	20	Scenario 3 in Table 4-4

Results of the 2-D BFMAS sensitivity study indicated that BFMAS is insensitive to the type of source, as long as the distributed source cells are located close together. Figure 5-9 exhibits a comparison of simulations between single source vs. distributed source as time series of the TRC at the four monitoring stations located near the release site. The load used for the simulations was a continuous release at a rate of 6000 mg/s, and dispersion coefficient and decay rate used for the simulation were 1 m<sup>2</sup>/s and 0.1/day, respectively. A maximum differential concentration found between the two simulations over a 30-day period was about 6 µg/L, located east of the outfall. Although the time series location at the west site was about twice as far away from the release site as the north site, the two locations exhibited a similar difference of 2 µg/L. The difference at the south station was very small since the predicted concentrations were so low. Therefore, the TRC concentration was distributed relatively more in the east-west direction than in the north-south direction. This unilateral variation coincided with the tidal current direction, which is indicative of tidal current advection process affecting the movement of the contaminant.

Regardless of source type (single or distributed), a dispersion coefficient greater than 10 m<sup>2</sup>/s resulted in numerical instability. However, with a coefficient below 10 m<sup>2</sup>/s, the contaminant behaved in a way such that the larger the dispersion coefficient values resulted in greater contaminant spreading. Figure 5-10 shows the instantaneous TRC field for dispersion coefficients of 1 m<sup>2</sup>/s (Run#2) and 5 m<sup>2</sup>/s (Run#6). A larger spatial coverage in a more circular shape was found with the larger dispersion coefficient, but the contaminant value was smaller near the source, preserving mass conservation. Time series of TRC concentration in the near field (Figure 5-11) indicates that higher concentration is associated

Figure 5-9. Comparison of predicted TRC concentration with single load (blue) and distributed load (black) for Run#1.

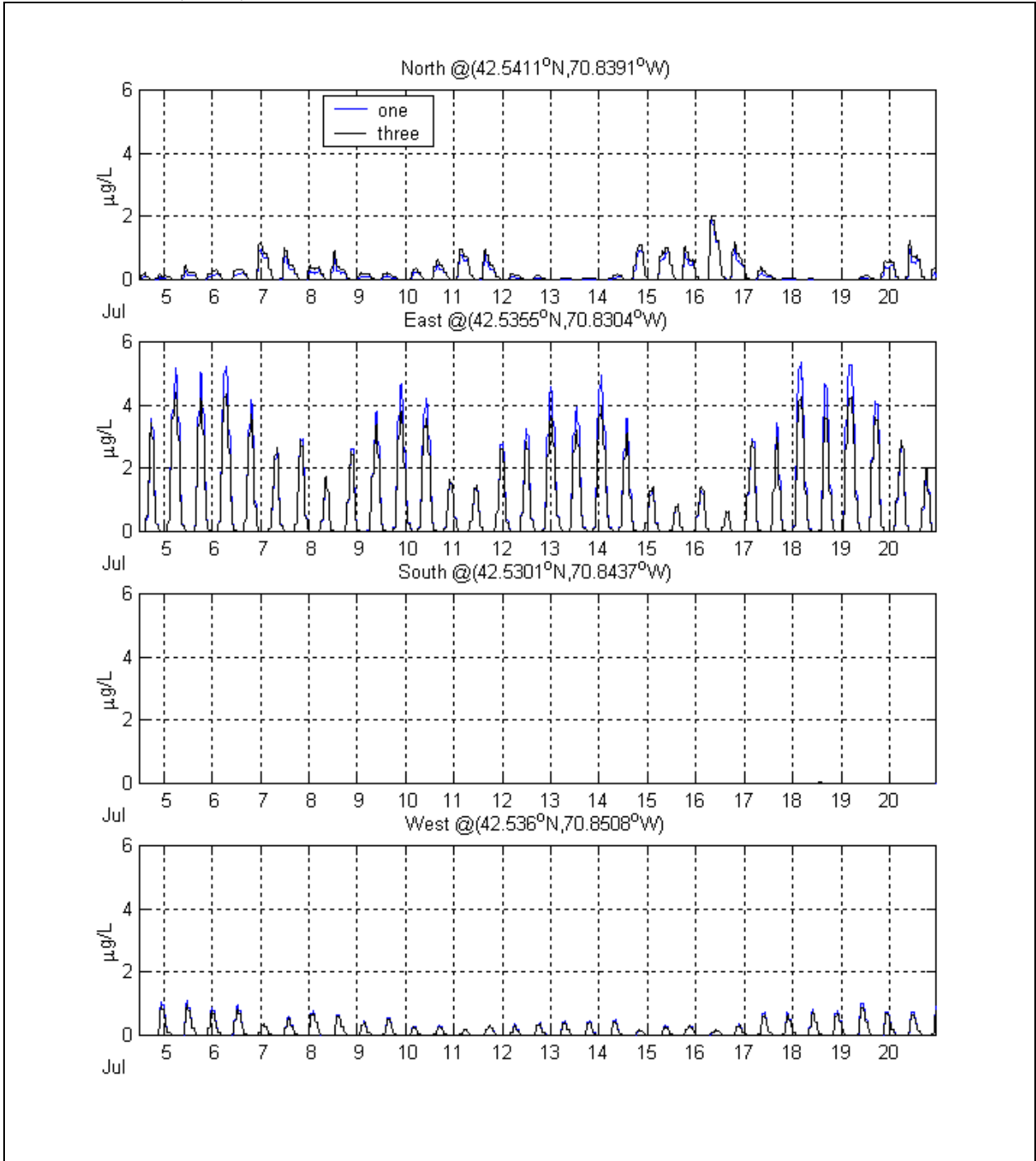


Figure 5-10. Comparison of the effluent contaminant field (mid-night July 14, 1985) between two different dispersion coefficients, top:  $1 \text{ m}^2/\text{s}$  (Run#2) and bottom:  $5 \text{ m}^2/\text{s}$  (Run#6).

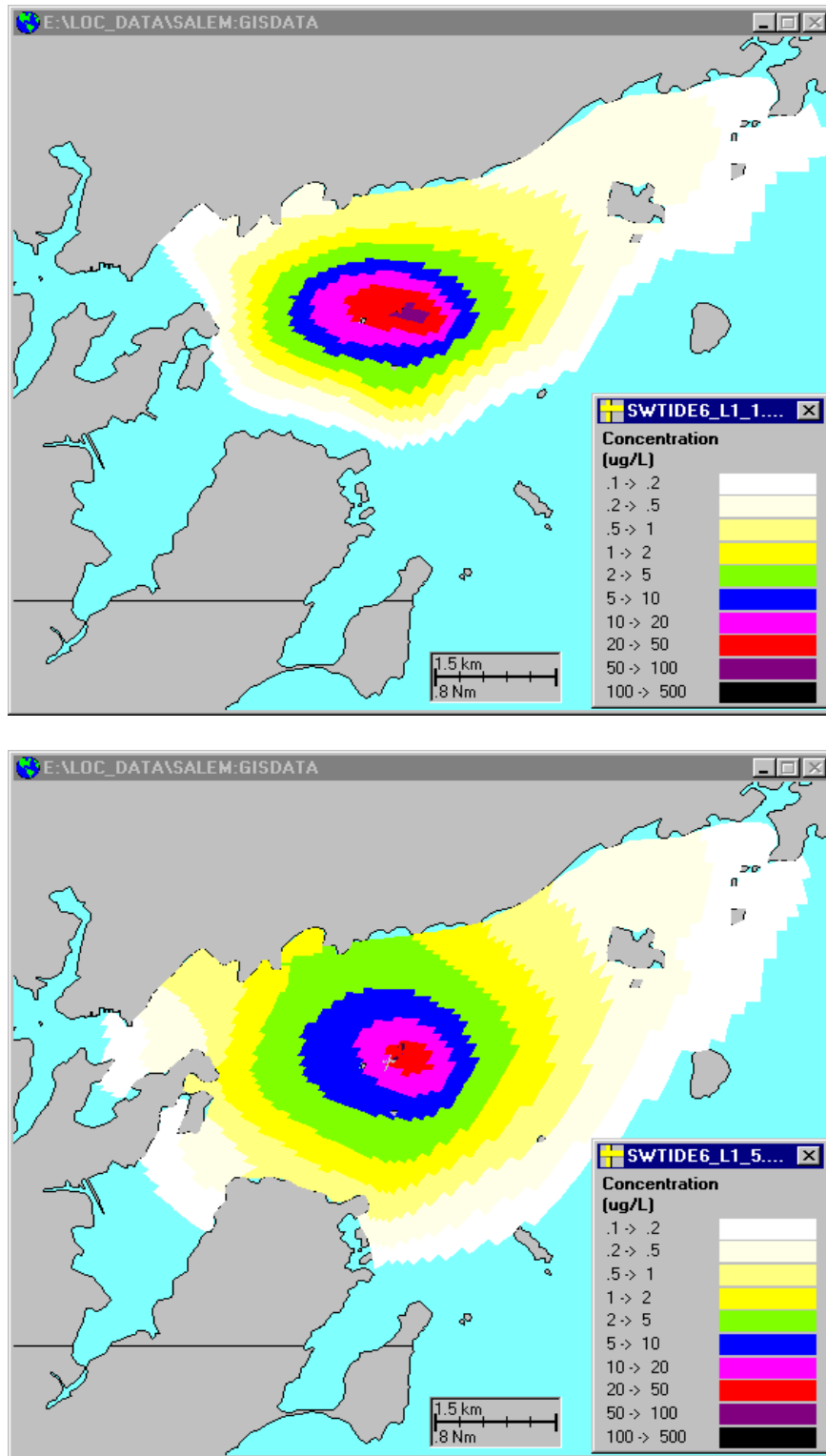
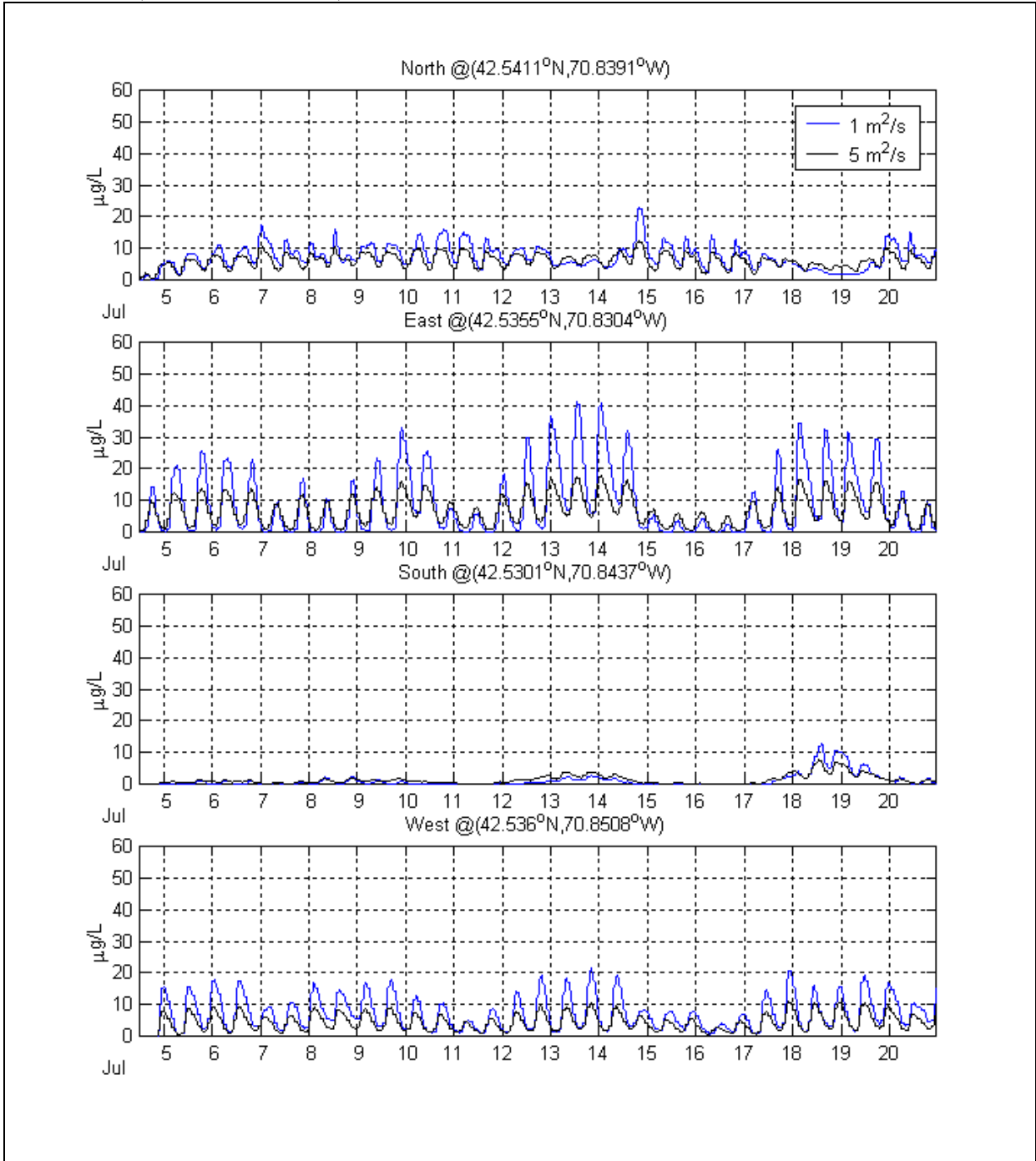


Figure 5-11. Time series of TRC concentration in the near field for different dispersion coefficients (Run#2 and Run#6).



with the lower dispersion coefficient value. This implies that a small dispersion value results in higher concentration but a smaller areal coverage than a larger value.

Simulations with different load levels showed that the predicted TRC concentration and transport responded linearly to the load. Thus the resulting concentrations of Run#11 (100

mg/s) that was a most recent condition at the SESD WWTP were 1.7% of the concentrations for Run#4 (6000 mg/s).

### 5.2.4 3-D Transport Simulations

The sensitivity study using the 3-D model varied the vertical diffusivity only. Other parameters were constant with one release site with a 6000 mg/s load, a dispersion coefficient of  $1 \text{ m}^2/\text{s}$  and a decay rate of 20/d. Table 5-5 lists the three different values of vertical diffusivity used.

Table 5-5. Sensitivity study for vertical diffusivity.

Scenario	Load, mg/s	Dispersion, $\text{m}^2/\text{s}$	Decay, 1/d	Vertical Diffusivity, $\text{m}^2/\text{s}$
1	6000	1	20	0.001
2	6000	1	20	0.005
3	6000	1	20	0.010

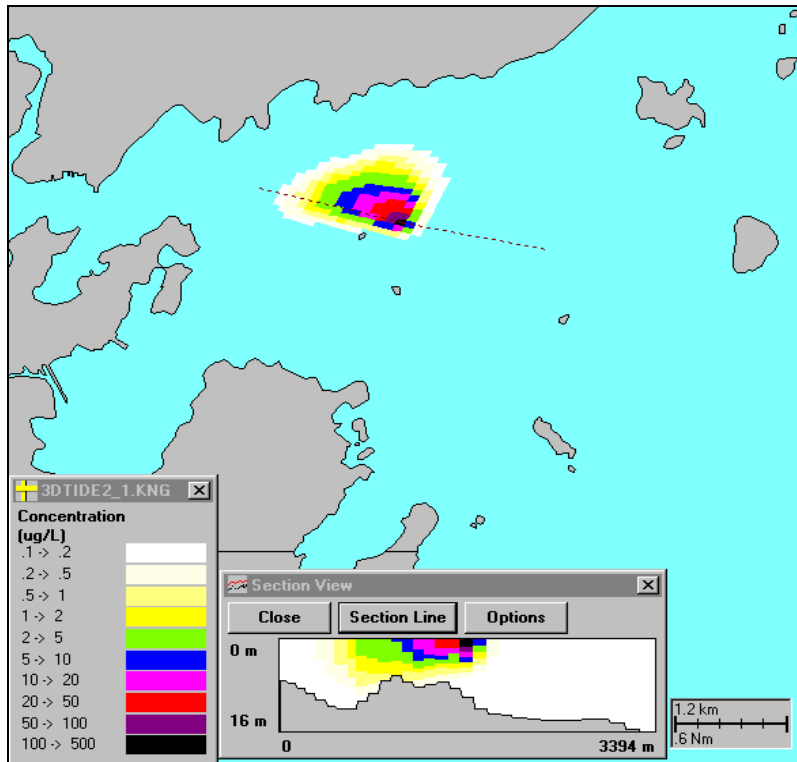
Higher vertical diffusivity resulted in greater transport in the vertical but less in the horizontal direction. Figures 5-12 to 5-15 presented simulated TRC concentration fields during maximum flood, maximum ebb and slack tides for the three scenarios. The inserted window shows a vertical section of TRC concentration along a line across the SESD discharge site (dashed line in the main figure).

Depending on tidal stage, the TRC spatial distribution is found at different locations relative to the release site. For instance, the larger TRC field is observed west of the release site during flood (Figure 5-12a, 5-13a and 5-14a), whereas it is found east of the release site during ebb (Figure 5-12b, 5-13b and 14-b). This is primarily due to advection by the ambient currents. When tide is in the slack condition, the plume is less skewed and appears to be distributed almost in symmetric, centered the release site. Regardless of tidal stages, however, the higher vertical diffusivity is applied, the less horizontal spatial coverage and the deeper penetration of the TRC are simulated. As vertical diffusivity is increased by an order of magnitude, the horizontal areal distribution (the concentration is greater than arbitrarily chosen concentration  $0.1 \text{ }\mu\text{g/L}$ ) is decreased by 23% during flood and 30% during ebb (Table 5-6). Similar decrease is observed with maximum TRC concentration at a release site, but higher rate of decrease than the areal coverage.

Among the tidal stages, the vertical penetration is the highest at the slack tide (Figure 5-15). Hence, there might be a greater impact possible on the ocean bottom at this tidal stage, compared to the other cycles.

Figure 5-12. Simulated TRC concentration distribution at maximum flood (a) and maximum ebb (b) for scenario 1. Inserted vertical section view is along the dashed line in the east-west direction.

(a)



(b)

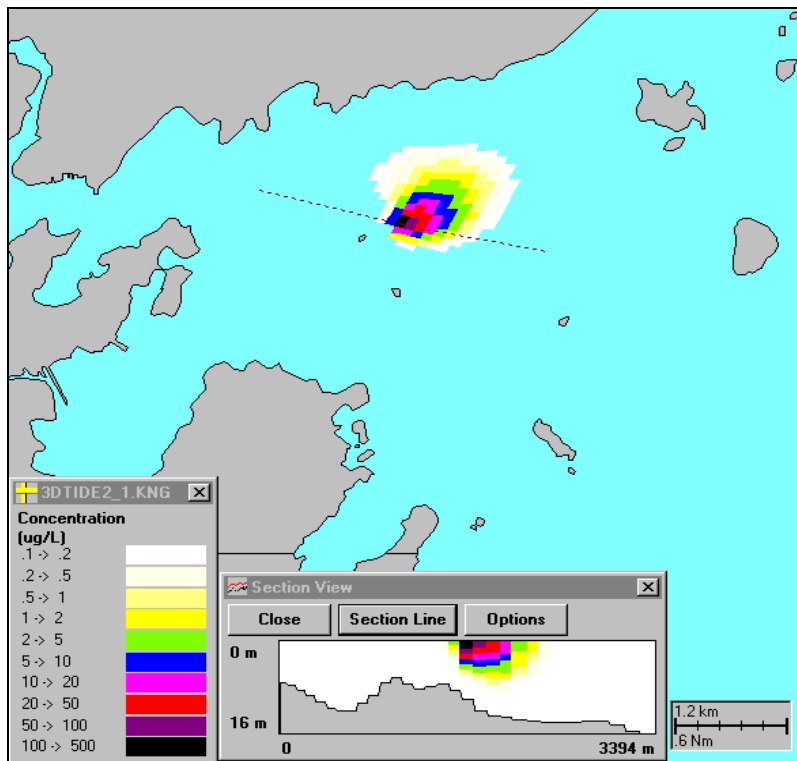
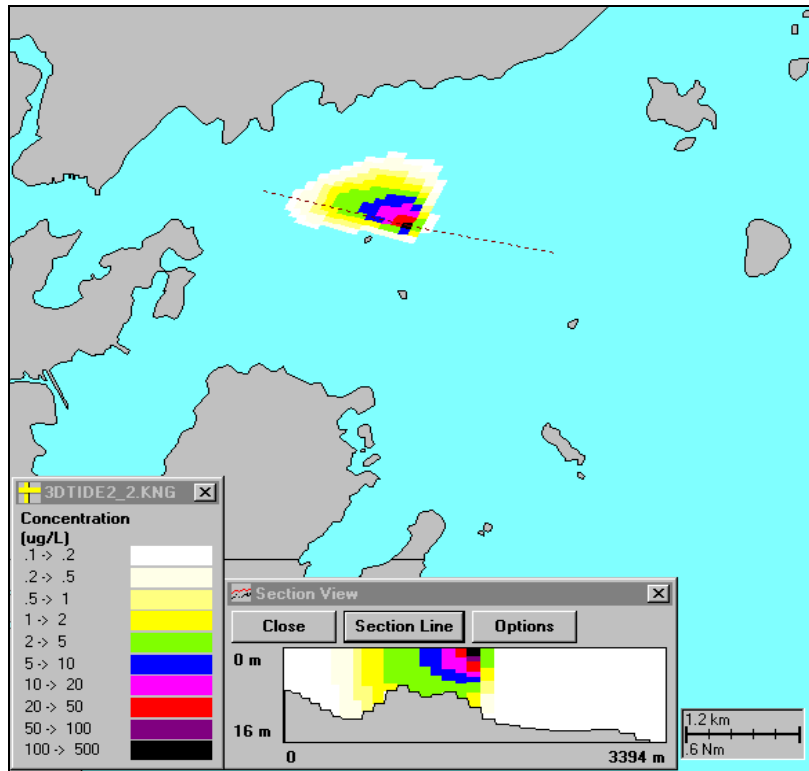


Figure 5-13. Simulated TRC concentration distribution at maximum flood (a) and maximum ebb (b) for scenario 2. Inserted vertical section view is along the dashed line in the east-west direction.

(a)



(b)

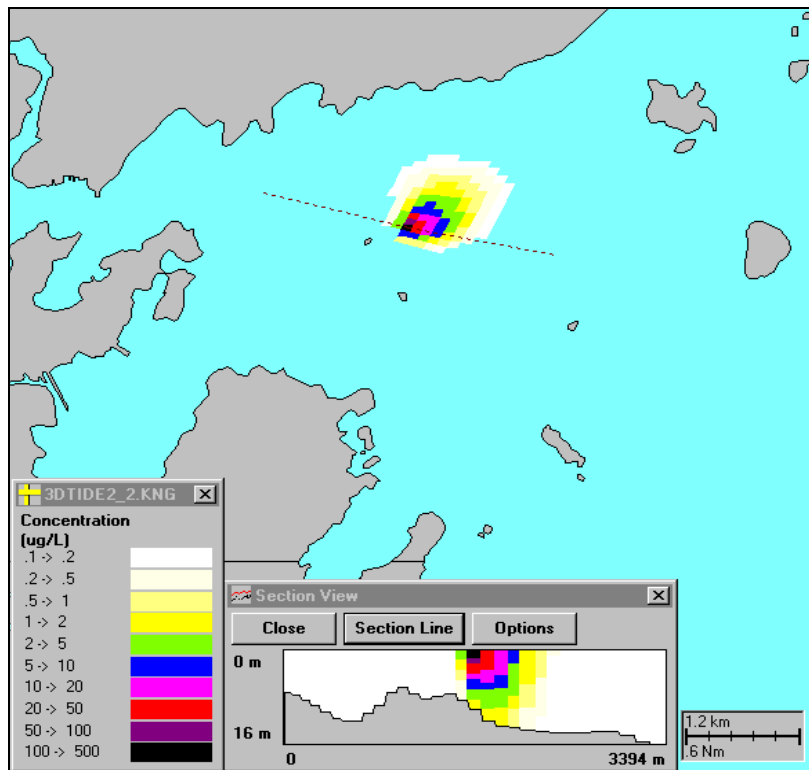
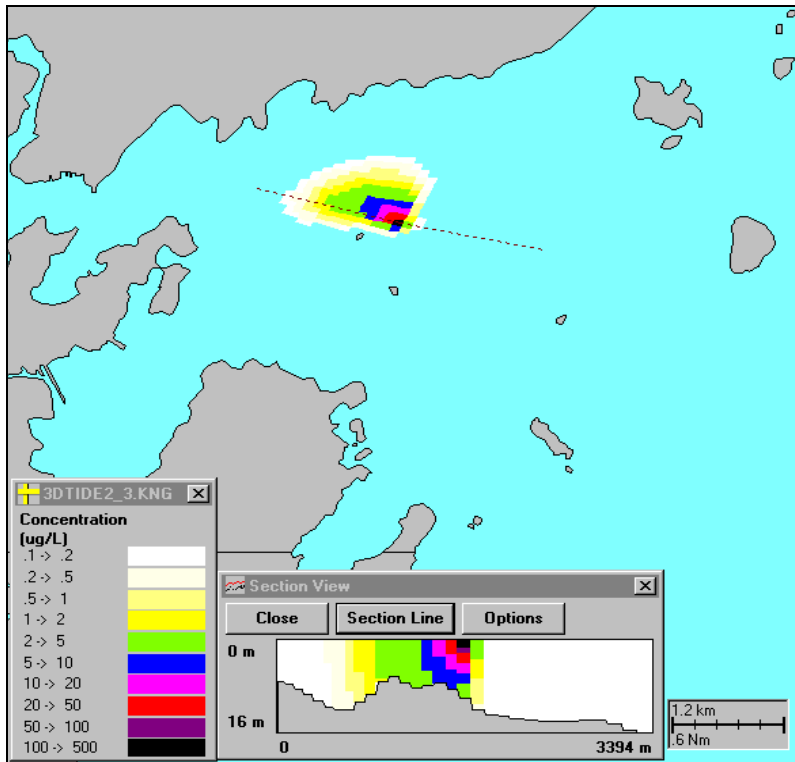


Figure 5-14. Simulated TRC concentration distribution at maximum flood (a) and maximum ebb (b) for scenario 3. Inserted vertical section view is along the dashed line in the east-west direction.

(a)



(b)

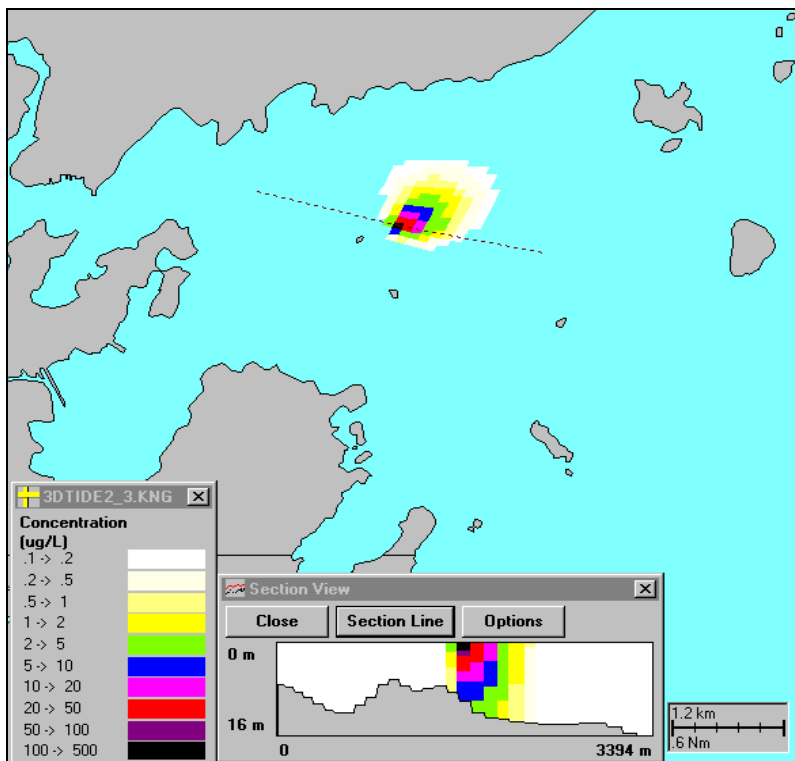
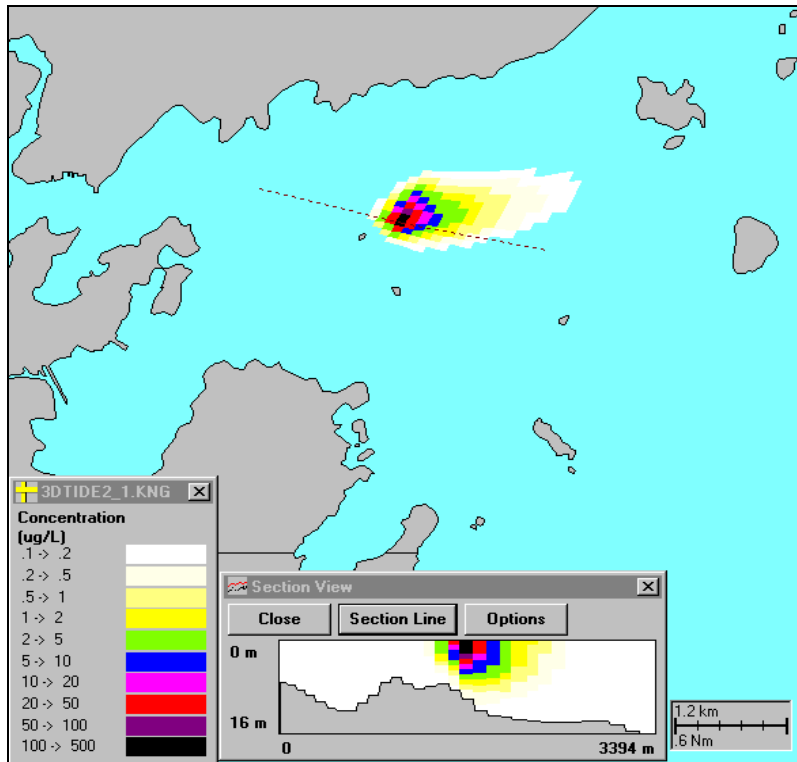
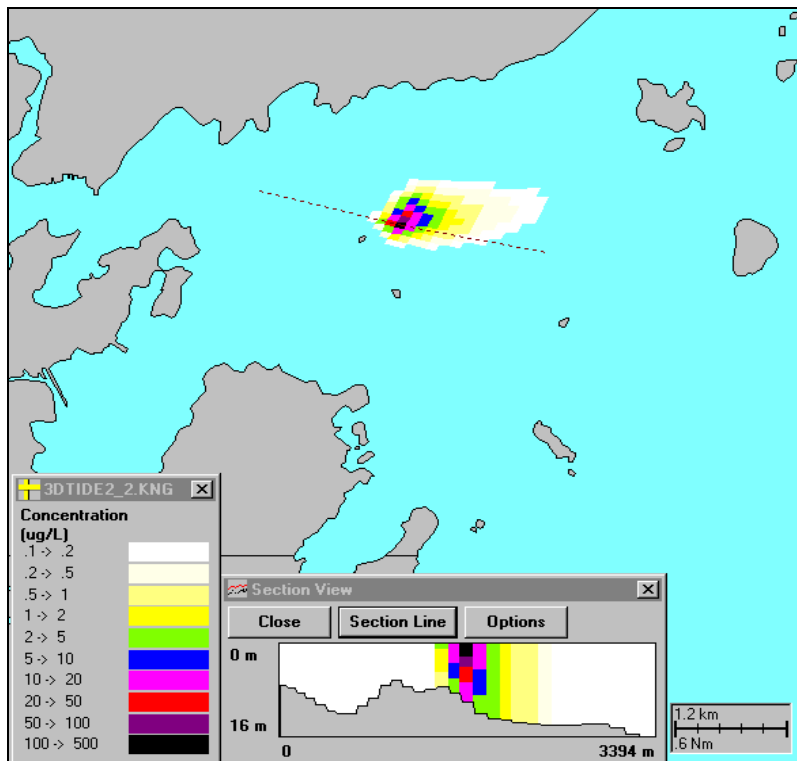


Figure 5-15. Simulated TRC concentration distribution during slack tide for Scenario 1 (a), Scenario 2 (b) and Scenario 3 (c). Inserted vertical section view is along the dashed line in the east-west direction.

(a)



(b)



(c)

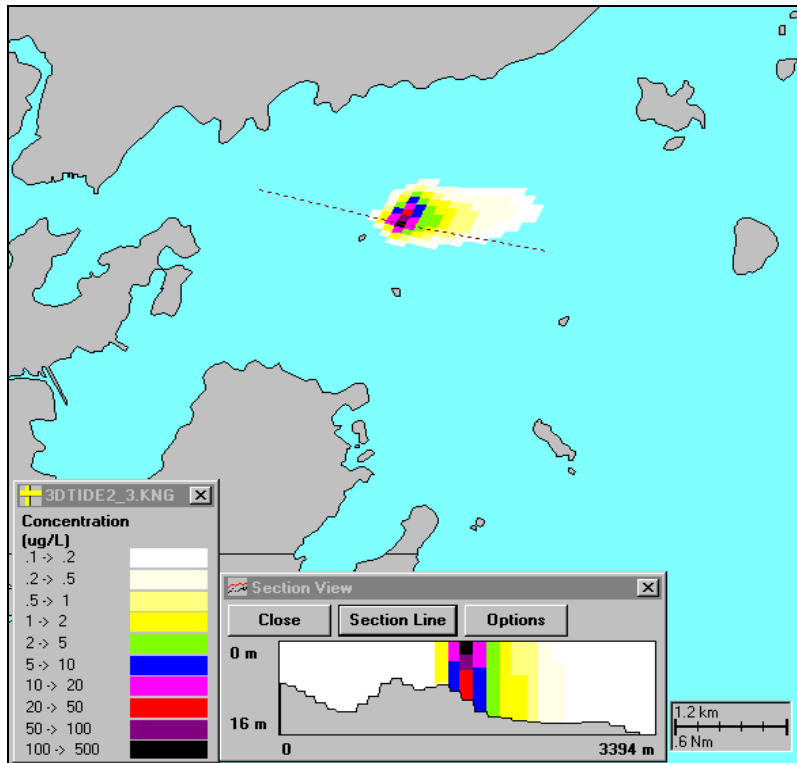


Table 5-6. Horizontal areal coverage of TRC (greater than 0.1 µg/L) and maximum TRC value during maximum flood and maximum ebb currents.

Run	Flood		Ebb	
	Area, km <sup>2</sup> (mi <sup>2</sup> )	Max. TRC, µg/L	Area, km <sup>2</sup> (mi <sup>2</sup> )	Max TRC, µg/L
1	1.61 (0.62)	230	1.67 (0.69)	270
2	1.30 (0.50)	160	1.23 (0.47)	180
3	1.24 (0.48)	130	1.15 (0.44)	150

## 5.2.5 Water Quality Comparisons

It is possible to compare the model results to federal water quality criteria that have been established for chlorine (USEPA, 1998). It should be emphasized, however, that the model predictions have not been calibrated to any actual measurements since there is no specific data on TRC concentrations in Salem Sound. The EPA chronic level criteria states that saltwater aquatic organisms should not be affected unacceptably if the 4-day average concentration of chlorine-produced oxidants does not exceed 7.5 µg/L (0.0075 mg/L) more than once every three years on average. The acute criteria states that saltwater aquatic organisms should not be affected unacceptably if the one-hour average concentration of chlorine-produced oxidants does not exceed 13 µg/L (0.013 mg/L) more than once every three years on the average. The source loads for the models are based on

reported maximum daily TRC concentrations at the plant over a month. These loads will tend to bias the modeling results toward higher values since the 4-day loads will typically be lower.

The results from CORMIX2, shown in Table 5-7, predicted that at the water surface right above the diffuser there were exceedances of both standards based on daily maximum flow rate and daily maximum load conditions (July and November 1998). By April 2000, however, there was no exceedance of either standard. Table 5-7 also shows the WQMAP predictions for maximum TRC concentrations. They are lower than the CORMIX2 results since WQMAP is a far field model and does not resolve any area finer than 9,000 m<sup>2</sup>. Again both the July and November 1998 results show exceedances but not the April 2000 results. The exceedances are local, however, with the largest area exceeding the chronic criteria occurring during flood tide conditions for July 1998. Other coverage areas with values of 9,000 m<sup>2</sup> indicate that the concentration is exceeded only in the discharge cell.

Table 5-7. CORMIX2 and WQMAP predictions of maximum TRC concentrations and coverage areas greater than water quality criteria for various plant operating conditions. The maximum WQMAP predicted TRC value is located at the discharge cell, whose area is 9,000 m<sup>2</sup>.

Load		July 1998	November 1998	April 2000	
CORMIX2 Water Surface Maximum Concentration, µg/L		85	41	1.4	
WQMAP Run		Run#4	Run#10	Run#12	
Flood Tide	Max TRC, µg/L	33	11	0.3	
	Area, m <sup>2</sup>	≥7.5 µg/L	80,000	9,000	0
		≥13.0 µg/L	42,000	0	0
Ebb Tide	Max TRC, µg/L	39	13	0.3	
	Area, m <sup>2</sup>	≥7.5 µg/L	65,000	9,000	0
		≥13.0 µg/L	54,000	9,000	0

This comparison indicates that the SESD plant does not contribute TRC at concentrations considered unacceptable under EPA criteria based on its monthly reported daily maximum operating conditions in April 2000. A full calibration of the BFMASS model may change this preliminary finding either up or down, however.

## 6. Field Monitoring Program Proposal

The experience of model development and application to Salem Sound and the SESD outfall residual chlorine problem has resulted in some recommendations for further monitoring. These recommendations fall into two general areas, physical and chemical measurements. Each area will be described in the following sections.

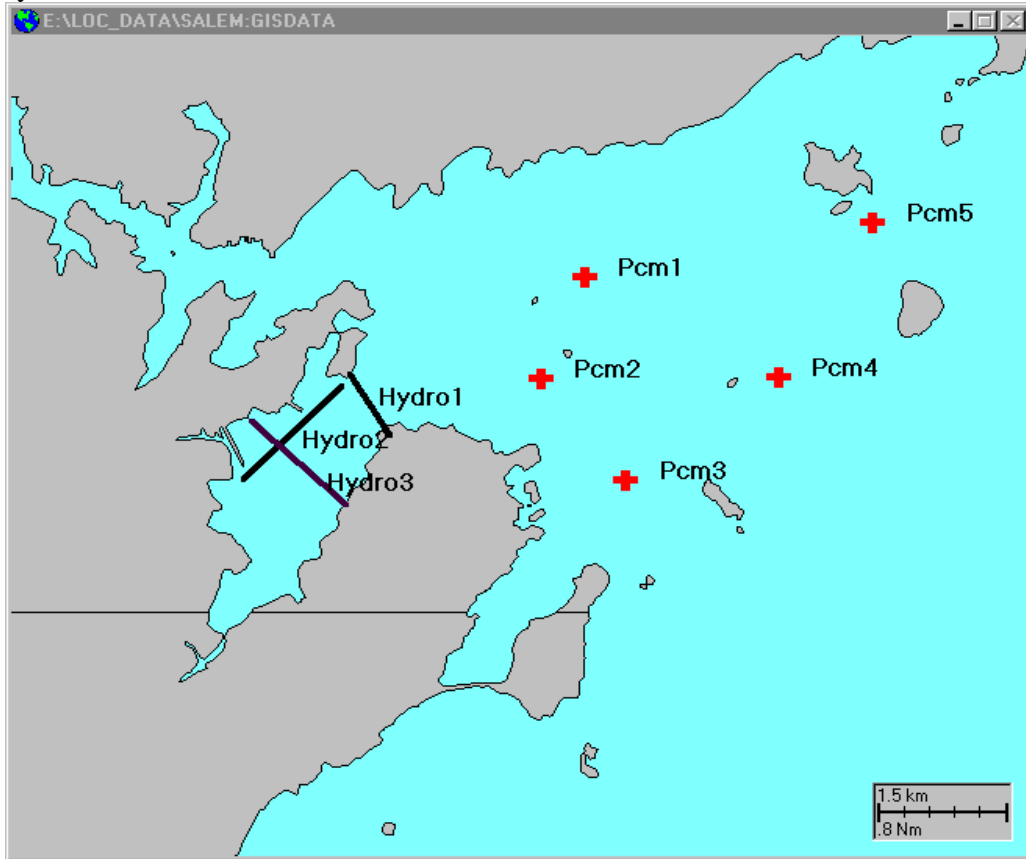
The most recently reported physical data set collected in the Sound occurred in 1985 as part of the SESD 301(h) waiver application. Figure 2-1b showed the location of current meters deployed in the fall of 1985. Some of the locations are not ideal for use in modeling of the Sound; three of them were located offshore in Massachusetts Bay and a fourth was at the offshore Sound boundary. Three of the instruments provided useful information, however, to characterize the circulation in the Sound. The model matched the observations well, except at CM2, in the southwest portion of the Sound. The inability to simulate these observations was also found by Zhang and Adams (1991) as part of the modeling of the Sound in support of the SESD 301(h) application. This suggests that the observations may be anomalous and perhaps not representative of the circulation in the area.

If further modeling studies are anticipated in Salem Sound it is recommended that additional velocity measurements be undertaken. Figure 6-1 shows a possible configuration of such a program. A total of five sites are proposed for current meter deployments (Pcm1 through Pcm5), two in the central portion of the Sound and three along the outer perimeter of the Sound. Fewer sites could be occupied if needed, based on the specific goals of the field program. Acoustic Doppler Current Profilers (ADCPs) are the suggested hardware because they can measure the vertical structure of the horizontal currents. It is suggested that a low energy summer period be monitored as well as a higher energy (late fall or early spring) period.

It is suggested that a series of ship mounted ADCPs also be employed to characterize the currents in the area. For instance, the model predicted a gyre structure in Salem Harbor under certain wind conditions. This type of circulation pattern can have a detrimental effect on flushing of pollutants and so may suggest a more detailed study of the area. Figure 6.1 also shows a set of tracks (Hydro 1, 2 and 3) in Salem Harbor that could be followed by the vessel with an ADCP. This intensive type of survey could be repeated over a tidal cycle to determine the strength and activity of this gyre circulation. Other areas could also be monitored with the same instrumentation again depending on the field program.

The issue of monitoring Total Residual Chlorine (TRC) in the marine environment is complex, in part due to chemical reactions with compounds in the water column, and interactions with biota. With a high decay and interaction rates TRC may be difficult to measure, particularly since its chronic criteria limit is only 0.0075 mg/L. An alternative approach may be to conduct a dye study of the SESD outfall that will provide estimates of dilution both near the outfall and further into the Sound. Here a known amount of dye is injected into the effluent. Monitoring equipment can then measure the three dimensional structure of the dye concentration from its fluorescence. A concurrent measurement of TRC from samples of effluent discharging from the outfall as well as further into the Sound can also be undertaken.

Figure 6-1. Proposed stations and transects for velocity, physical property and water quality measurements.



## 7. Conclusions and Summary

This report presents results of hydrodynamic simulations of Salem Sound. The presentation also includes preliminary assessments of total residual chlorine (TRC) levels, because the discharge of TRC from the South Essex Sewage District (SESD) Waste Water Treatment Plant (WWTP) was thought to potentially impact the natural resources in the Sound. The hydrodynamics and pollutant transport simulations were performed using the ASA WQMAP BFHYDRO and BFMASS models, respectively. Both of the models were based on boundary fitted grids that can conform complex coastlines and covered the area west of a line between Marblehead and Cape Ann. In addition the CORMIX2 model was applied to the SESD outfall diffuser.

The two-dimensional, vertically averaged hydrodynamic model was calibrated with the tidal ellipses and mean speed and direction of total currents for a period from July to September 1985 during which observations were available. The 11-layer 3-D model was also applied to the study domain. The results with the 3-D model was similar to that with 2-D model.

The hydrodynamic simulations indicated that the dynamics in the study area had two regimes in both space and time. In space, the currents inside the Sound were primarily governed by semi-diurnal  $M_2$  tides, and the speeds were 30 cm/s at maximum. Although there were local variations in currents due to bottom topography effects, especially conspicuous along the coastline, the flow was mainly in the direction of the Sound axis. The currents at the outer boundary of the Sound were driven by prevailing winds and the total current speed was generally large. In the time domain, the currents were differentiated to low and high frequency variations, where the former was controlled by the atmospheric forcing and the latter was governed by tides.

Atmospheric forcing in general pumps its energy into the ocean. As a result, it primarily alters the current direction which in turn aligns to the wind direction. During the simulation period, July-September 1985, the prevailing winds were oriented towards northeast at average speed of 4 m/s. Accordingly the circulation in the Sound formed a clockwise rotation, which was observed in the simulations.

The predicted tidal currents in most of the study area were of an elliptic shape whose major axis was in the same direction as the Sound axis. This prediction agreed with the observations, except at a location to the southwest (CM2). The observation suggested that the tides at that location were more circular and the tidal currents were the smallest among the three current meter sites. The simulation instead showed an elliptic rotation, being aligned to the northwest-southeast direction.

Hydrodynamic output from the 2-D and 3-D models were used in a simulation of the fate and transport of TRC that was discharged from the SESD outfall site which was located approximately in the middle of the study domain. TRC levels in the Sound were studied for four different loads (6000, 2000, 100 and 60 mg/s) continuously released at the diffuser. The different load values were derived from the 26 month-long record of flow-rate and TRC concentration at the SESD wastewater treatment plant. The model results showed the TRC distribution linearly responded to the load level. Sensitivity for source type (single or distributed) indicated that the fate and transport of TRC with a single source was no different from that with a distributed source. The maximum level near the diffuser for the distributed source was approximately one-third of the concentration for the single source, however. The TRC simulation was somewhat sensitive to dispersion and more sensitive to decay. The TRC distribution for the higher dispersion coefficient resulted in larger areal coverage than the lower value, whereas absolute concentration level in the near field was smaller for a higher value rather than a lower. The simulated TRC with a higher decay rate showed lower concentration and smaller areas than lower decay rate. The sensitivity study of vertical diffusivity suggested that the larger the diffusivity that was applied, the deeper the contaminant plume penetrated. However, the maximum concentration observed near the release site was smaller with large diffusivity.

From the sensitivity study analysis, relatively high TRC concentration exists near the release site and the TRC level rapidly decreases with distance from the release site. The TRC plume forms an elongated shape whose axis is in the direction of the current flow.

The near field simulation with CORMIX2 indicated that the TRC was quickly reached the surface as it was released at the diffuser ports. For some historical plant loads (July and November 2000), the water quality exceeded the USAEPA criteria based on maximum daily flow and load. Using later data (April 2000) the results of both CORMIX2 and WQMAP BFMASS suggested that the SESD plant does not contribute TRC at concentrations considered unacceptable under EPA criteria. The TRC predictions must be considered preliminary, however, since no actual model calibration was undertaken.

## 8. References

Ambrose, R.B. et al, 1993. The Water Quality Analysis Simulation Program, WASP5 Part A: Model Documentation, Part B: The WASP5 Input Data Set. U.S. Environmental Protection Agency, Athens, GA.

Bettors, W.J., 1990. Water circulation in channels at Salem Sound, Salem, Massachusetts. M.S. thesis, Boston College Department of Geology and Geophysics, Boston, MA.

CDM, 1986a. Section 301(h) revised application for modification of secondary treatment requirements for discharges into marine waters. Volume 2 Appendices, Prepared for the South Essex Sewerage District by Camp Dresser & McKee, Inc., Boston, MA, April.

CDM, 1986b. Section 301(h) revised application for modification of secondary treatment requirements for discharges into marine waters. Volume 3 – Biological field studies addendum, Prepared for the South Essex Sewerage District by Camp Dresser & McKee, Inc., Boston, MA, November.

CDM, 1991. Draft environmental impact report, Phase II, Facilities plan for wastewater treatment and disposal, Vol V, Appendix D, Effluent outfall. Prepared for the South Essex Sewerage District by Camp Dresser & McKee, Inc., Boston, MA, September.

CDM, 1991. Draft environmental impact report, Phase II, Facilities plan for wastewater treatment and disposal, Vol V, Appendix D: Effluent outfall, Attachments (1 Far field modeling results). Prepared for the South Essex Sewerage District by Camp Dresser & McKee, Inc., Boston, MA, September.

CDM, 1991. Draft environmental impact report, Phase II, Facilities plan for wastewater treatment and disposal, Vol V, Appendix D: Effluent outfall, Attachment 6 (Project technical memoranda). Prepared for the South Essex Sewerage District by Camp Dresser & McKee, Inc., Boston, MA, September.

CDM, 1992. Draft environmental impact report, Phase II, Facilities plan for wastewater treatment and disposal, Part II, Sections 10-16 (11 Effluent Outfall Evaluation). Prepared for the South Essex Sewerage District by Camp Dresser & McKee, Inc., Boston, MA, September.

CDM, 1994. Contract No. 93-2 wastewater treatment outfall diffuser. Prepared for the South Essex Sewerage District by Camp Dresser & McKee, Inc., Boston, MA, January.

Dallaire, T.R. and S.G. Halterman, 1991. Dissolved oxygen, temperature, and density profiles in Salem Sound and Massachusetts Bay, 1990. Massachusetts Department of Environmental Protection, Division of Water Pollution Control, Technical Services Branch, Westborough, MA, 42 p.

DMF, 2000. A study of the marine resources of Salem Sound, 1997. Massachusetts Division of Marine Fisheries.

Gardner, G.B., R.P. Eganhouse and G.T. Wallace, 1986. Baseline assessment of Salem Harbor – Salem Sound and adjacent waters. Final report submitted to the New England Aquarium by the University of Massachusetts, Boston, MA.

Huang, Hening, R.E. Ferger, J.P. Cooke and G.S. Fox, 1997. Effluent Total Residual Chlorine Decay in Outfall Pipe. *Journal of Environmental Engineering*, Vol. 123, No. 8, August 1997, p. 813-816.

Jirka, G.H., R.L. Doneker, and S.W. Hinton, 1996. User's manual for CORMIX: a hydrodynamic mixing zone model and decision support system for pollutant discharges into surface waters. DeFrees Hydraulics Laboratory, School of Civil and Environmental Engineering, Cornell University, Ithaca, NY; Cooperative Agreement No. CX 824847; Report to Office of Science and Technology, U.S. Environmental Protection Agency, Washington, DC, August.

Madala, R.V. and S.A. Piacsek, 1977. A semi-implicit numerical model for Baroclinic Oceans. *Journal of Computational Physics*, 23, 167-178.

Massachusetts Water Resources Authority (MWRA), 1988. Secondary treatment facilities plan, V. 5: Effluent outfall. Prepared by Camp Dresser & McKee, Inc., Boston, Mass.

Mendelsohn, D, T. Isaji and H. Rhines, 1995. Hydrodynamic and water quality modeling of Lake Champlain. *Report to Lake Champlain Management Conference*, Burlington, Vt, ASA Report 92-034.

MDWPC, 1985. Salem – Beverly Harbors tributaries, Water quality survey. Massachusetts Department of Environmental Quality Engineering, Division of Water Pollution Control, Technical Services Branch, Westborough, MA, 35 p.

Milne, G.D., S.J. Stanley and D.W. Smith, 1993. Residual chlorine decay in a broad, shallow river. *Wat. Res.* Vol. 27, No. 6, 993-1001.

Mitchell, D.F., N.J. Maciolek, K.M.Hopkins, and K.D.Wandland, 1998. Massachusetts Bay outfall monitoring program: Toxics issue report on biology of the lobster in Massachusetts Bay. MWRA Technical Report No. 98-13, Prepared for Massachusetts Water Resources Authority, Environmental Quality Department, Boston, MA by ENSR Consulting and Engineering, Woods Hole, MA.

Muin, M. 1993. A Three-Dimensional Boundary Fitted Circulation Model in Spherical Coordinates. *Ph. D. Dissertation*, Department of Ocean Engineering, University of Rhode Island, Kingston, RI.

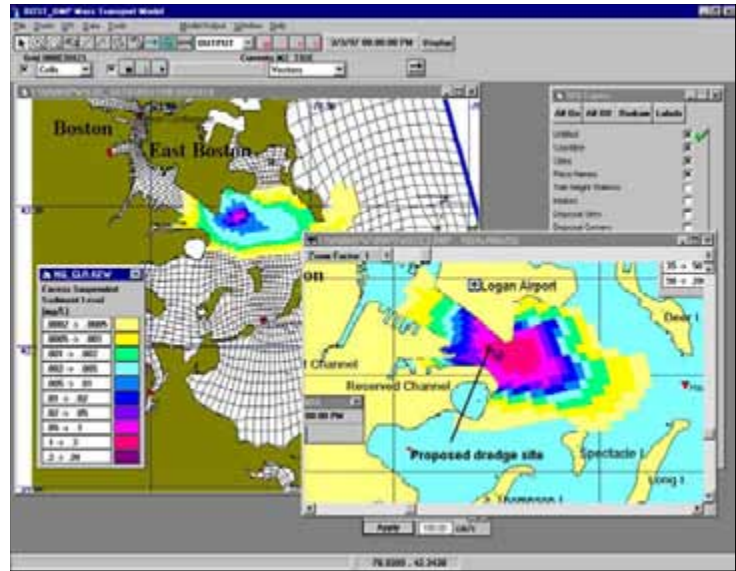
- Muin, M. and M. L. Spaulding, 1996. Two-dimensional boundary fitted circulation model in spherical coordinates. In: *Journal of Hydraulic Engineering*, Vol. 122, No. 9, September 1996, p. 512-521.
- Muin, M. and M. L. Spaulding, 1997a. Application of Three-dimensional boundary fitted circulation model to Providence River. *ASCE Journal of Hydraulic Engineering*. Vol. 123, No. 1.
- Muin, M. and M. L. Spaulding, 1997b. Three-dimensional boundary fitted circulation model. In: *Journal of Hydraulic Engineering*, Vol. 123, No. 1, January 1997, p. 2-12.
- Newman, K. A., S. L. Frankel, K. D. Stolzenbach, 1990. Flow cytometric detection and sizing of fluorescent particles deposited at a sewage outfall site. *Env. Sci. & Tech.* 24(4), 513-519.
- Ocean Surveys, 1986. Final report SESD / CDM oceanographic study Salem Sound / Massachusetts Bay. Prepared by Ocean Surveys, Inc., Old Saybrook, CT for Camp Dresser & McKee, Inc., Boston, MA as Appendix A of Section 301(h) Revised Application for modification of secondary treatment requirements for discharges into marine waters, Vol. 2 Appendices. Prepared for the South Essex Sewerage District by Camp Dresser & McKee, Inc., Boston, MA, April.
- Spaulding, M. L., and F. M. White, 1990. Circulation Dynamics in Mt. Hope Bay and the Lower Taunton River. *Coastal and Estuarine Studies*, Vol. 38, 494-510.
- Spaulding, M. L., D. Mendelsohn and J. C. Swanson, 1999. WQMAP: An integrated three-dimensional hydrodynamic and water quality model system for estuarine and coastal applications. *Marine Technology Society Journal*, Vol. 33, #3, Fall, 1999. 38-54.
- Swanson, J.C., D. Mendelsohn, 1993. Application of WQMAP to upper Narragansett Bay, Rhode Island. Estuarine and Coastal Modeling III. Proceedings of the 3<sup>rd</sup> International Conference, sponsored by the Waterway, Port, Coastal and Ocean Division of the ASCE, Oak Brook, IL, September 8-10, 1993.
- Swanson, J.C. and D. Mendelsohn, 1996. Water quality Impacts of dredging and disposal operations in Boston Harbor, ASCE North American Water and Environmental Congress '96 (NAWEC '96), Anaheim, CA, June 22-28, 1996.
- Zhang, X and E. Adams, 1991.. Validation studies of models TEA and ELA for the SESD outfall. Dept. of Civil Engineering, Massachusetts Institute of Technology, Cambridge, MA. Appearing as CDM, 1991, Draft environmental impact report, Phase II, Facilities plan for wastewater treatment and disposal, Vol V, Appendix D: Effluent outfall, Attachment 2. Prepared for the South Essex Sewerage District by Camp Dresser & McKee, Inc., Boston, MA, September.
- USEPA, 1999. National recommended water quality criteria – correction. EPA 822-Z-99-001. Office of Water, United States Environmental Protection Agency, April, 1999.

APPENDIX A  
WQMAP Product Description



Applied Science Associates, Inc.  
70 Dean Knauss Drive  
Narragansett, RI 02882-1143  
U.S.A.  
Tel: 401-789-6224  
Fax: 401-789-1932  
Email: [asa@appsci.com](mailto:asa@appsci.com)  
<http://www.appsci.com>

Applied Science Associates, Ltd.  
54 South Street  
St. Andrews, KY16 9JT  
Scotland  
Tel: 01334 478 354  
Fax: 01334 472 893  
Email: [asa@sol.co.uk](mailto:asa@sol.co.uk)  
<http://www.appsci.com>



## WQMAP

### Product Description

The ASA Water Quality Mapping and Analysis Package (WQMAP) is a set of hydrodynamic and water quality models integrated with a geographical information and environmental data system through an intuitive graphical user interface that runs under Microsoft Windows™. WQMAP is designed with modular elements. A customized suite of hydrodynamic and water quality models is incorporated into WQMAP, reflecting the needs of each user's application.

The WQMAP system is based on a state-of-the-art boundary-fitted coordinate modeling technique. Model types include two and three dimensional, time dependent numerical solutions to the basic conservation equations for water mass, momentum, constituent mass, energy, salt, sediment, and other conservative and non-conservative constituents. These models simulate a wide range of physical, chemical, and biological processes in various types of water bodies. They can help analyze system dynamics and predict the impacts of actual events or possible design or management alternatives. The models can be used to estimate currents and water surface elevations, assess water quality and eutrophication, identify pollutant sources, and perform environmental impact assessments.

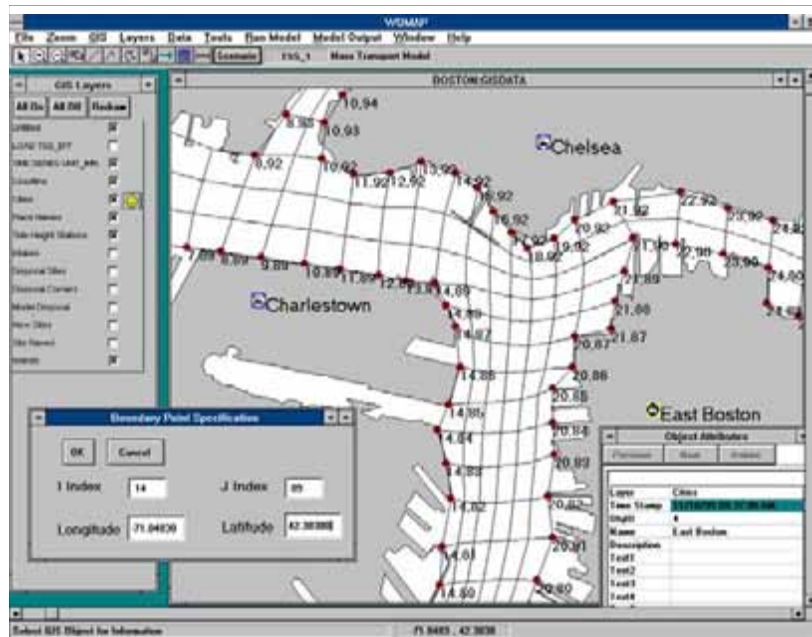
The basic WQMAP model structure consists of four components:

- **BFGRID: Boundary Fitted Coordinate Grid Generation**
- **BFHYDRO: Boundary Fitted Hydrodynamic Model**
- **BFMASS: Boundary Fitted Pollutant Transport Model**
- **BFWASP: Boundary Fitted Eutrophication Model**

## WQMAP COMPONENTS

### BFGRID: Boundary Fitted Coordinate Grid Generation

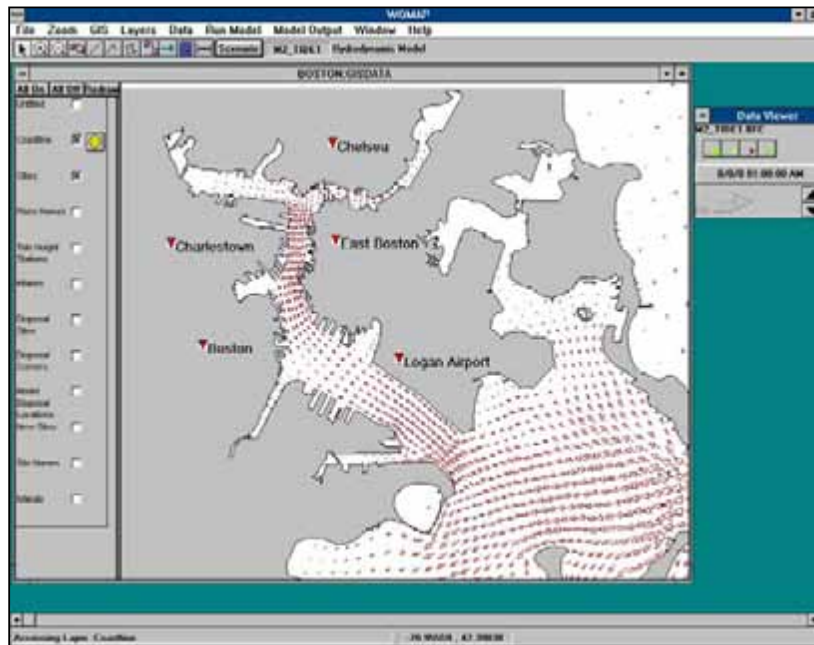
The grid generation software is a tool to build a grid, which segments the water body of interest. After the user specifies key grid nodes (grid corners) along the domain boundary, the model interpolates the remaining boundary node locations and then solves a Poisson equation to locate the interior nodes. Editing tools are included to add, delete, and move nodes. The resulting non-orthogonal grid contains quadrilateral areas of various sizes and orientation to resolve fine detail where needed, to cover large areas



at coarse resolution where detail is not needed and to map the grid boundaries to the geographical features of the water body being studied. The hydrodynamic and water quality models use this grid to numerically solve the appropriate conservation equations.

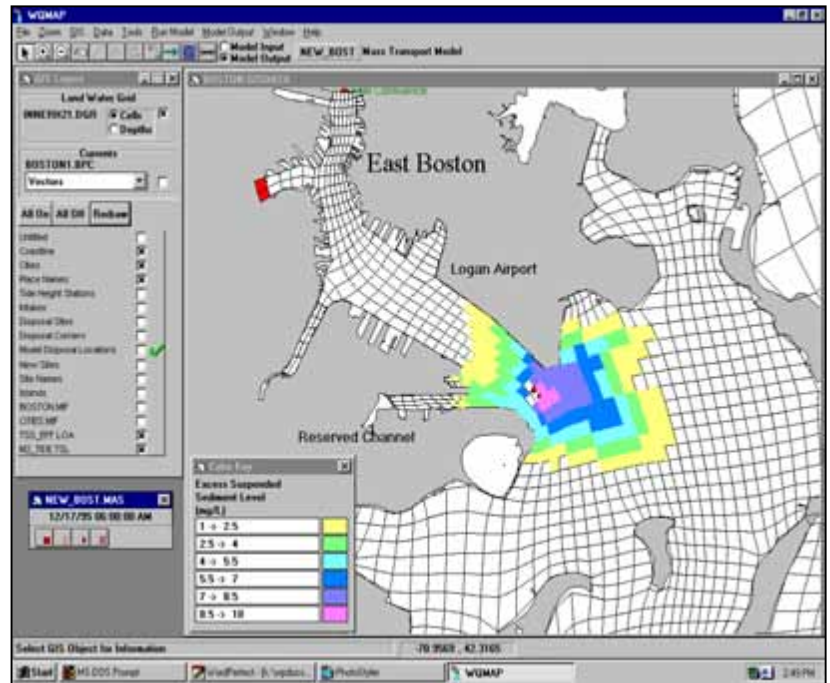
### BFHYDRO: Boundary Fitted Hydrodynamic Model

The hydrodynamic model solves the water mass and momentum equations on the boundary fitted grid to predict a time varying field of surface elevations and velocity vectors. Boundary forcing includes tides, winds, and river flows and density distributions. The standard model is configured to run in a vertically averaged mode, but can optionally run in a three dimensional mode with prognostic calculation of density induced flow, which also predicts a time varying field of salinity and temperature.



## BFMASS: Boundary Fitted Pollutant Transport Model System

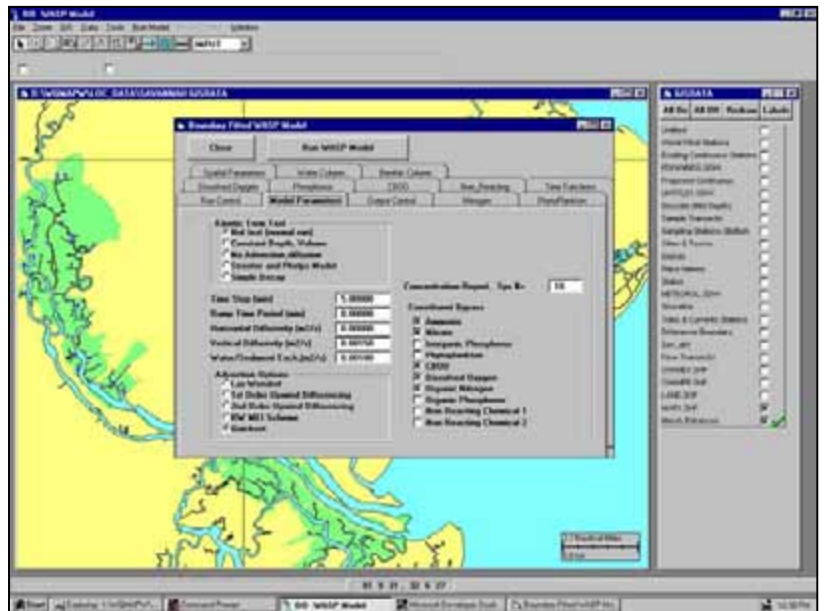
The pollutant transport model system solves the conservation of mass equation on the boundary fitted grid to predict time varying fields of constituent concentration. Single and multiple, constant and time varying loads can be applied. Constituents can include pathogens, excess temperature, metals, suspended sediment, nutrients, organics and conservative tracers. The standard model is configured to run in a vertically averaged mode but can optionally run in three dimensions. The constituent fates model consists of two possible configurations for single independent and multiple, linked or independent constituents incorporating increasingly complex reaction kinetics:



- Single constituent model including first order loss rate terms
- Multiple constituent model linked by a user defined reaction matrix

## BFWASP: Boundary Fitted Eutrophication Model System

BFWASP is a multiple constituent eutrophication model incorporating the full EPA WASP EUTRO model kinetic rate equations into the transport model system. The model solves the conservation of mass equations on the boundary fitted grid and the kinetic rate equations to predict the transport and transformation of up to either state variables. The state variables are components of four basic interacting systems simulating the phosphorus cycle, the nitrogen cycle, phytoplankton kinetics and the dissolved oxygen balance. The model is configured to run in three dimensions with sediment compartments. The formulation includes benthic interactions.



## Data Management

For most models, input data describing the study area (land-water grid, bathymetry, and topography), boundary conditions, discharge description, model parameters and output display parameters are required. In general, spatial information input to the model is handled through the gridding module or the WQMAP Geographical Information System, (GIS), time series data through the environmental data management tools and output display through a set of menu options or icon interrogation. Model parameters/options are managed through input forms or optionally through ASCII files.

While output varies with the model or problem of interest, the system supports plan and transect views of scalar and vector quantities. Typical displays include gridded bathymetry, concentration levels, and velocity vectors and particle distributions. In addition, models allow visualization of global mass or term balances of the constituent of concern. For predictions that are time dependent (e.g. velocity vectors, surface elevations, particle trajectories, constituent concentrations) the user interface allows single frame or animated views. In animations the user can use pause, stop, forward/reverse (fast/slow) and single step to assist in viewing the predictions.

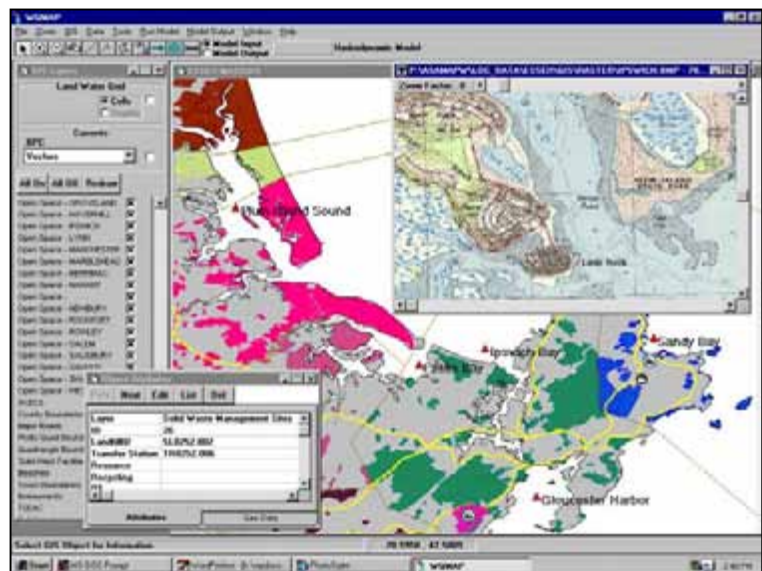
## Geographic Location

WQMAP is supplied with one base map, or location. Additional areas may be added as enhancements to the basic system. This base map serves as the largest domain over which the model will be employed. Application locations range from small rivers, lakes and estuarine systems with scales of kilometers to bays, seas and continental shelves, with scales of tens to hundreds of kilometers. For each location a geo-referenced shoreline and bathymetry is created from either charts or electronic data.

The user can have as many locations in the system as computer storage allows. Locations may be geographically distinct or may be embedded within an existing location at a higher resolution. The user can rapidly change from one location to another by simply pointing to the appropriate data set.

## Geographic Information System (GIS)

The embedded GIS allows the user to input, store, manipulate and display geographically referenced information. The simplified GIS has been designed to be user friendly, interactive, and fast. GIS data is often helpful in analyzing and interpreting model predictions. The GIS allows an unlimited number of geographic databases to be created each with multiple layers of data. Typical uses of the GIS include storing location names, natural resources (bird colonies, shell fishing areas, beaches, marshes, vegetation), pollutant sources, geographical reference



points such as buoys and channels, and environmental data (bathymetry, sediment type, rivers and flow data etc.). Through the use of linking procedures, additional information about geographically referenced data can be accessed. These link files include charts, graphics, tables, tutorials, bibliographies, text, scanned charts, photographs, or animations. Examples of data which might be stored in the GIS for a typical sewage outfall siting problem include: contaminant source strengths versus time for the discharge, details and photographs of outfall locations and configurations, water column and sediment quality information, distribution and abundance of biota including shellfish, fish, birds, and marine mammals.

## **Sample Applications**

The following are some examples of various configurations of WQMAP that have been assembled to respond to our client's needs:

### **Dredging Impacts**

A two-dimensional time dependent hydrodynamic and pollutant transport model application to predict the distribution of suspended sediments and pollutants as a result of dredging and disposal operations. Required inputs are tidal constituents at the open boundary and river flows for the hydrodynamic model. Inputs for the pollutant transport model are time varying loads simulating material release from dredging operations. Output includes contours of pollutant levels over time and maximum impacts.

### **Two Layer Channel Flow**

A three-dimensional time-dependent hydrodynamic model application to predict the occurrence of two layer flow in a channel connecting water bodies of different densities. Required inputs are system geometry and basin densities and elevations. Output is a time varying velocity structure through the channel.

### **Thermal Impacts**

A three-dimensional time dependent hydrodynamic model application to predict the extent of thermal plume from an electrical generating facility using once through cooling. Required inputs are open boundary tide height, temperature and salinity; river flow and temperature; and solar and atmospheric radiation. Outputs include the contours of temperature and temperature rise due to the plant over time.

### **Fecal Coliform Exceedance**

A three-dimensional hydrodynamic and pollutant transport model application to predict the distribution of fecal coliforms (FC). Required inputs are freshwater flows and tidal elevations for the hydrodynamic model and FC loads and decay rate for the pollutant transport model. Output is a time varying set of FC concentrations and area-time exceedances of water quality standards.

## **Causeway Removal Impacts**

A three-dimensional time-dependent hydrodynamic and pollutant transport model application to predict the changes in circulation and water quality from the removal of a highway causeway. Required inputs are system geometry, altered system geometry, river flow and load inputs. Outputs are, time varying velocity, numerical flushing estimates, sedimentation rates and phosphorus concentrations.

APPENDIX B  
Muin and Spaulding 1977

# THREE-DIMENSIONAL BOUNDARY-FITTED CIRCULATION MODEL

By Muslim Muin<sup>1</sup> and Malcolm Spaulding<sup>2</sup>

**ABSTRACT:** A spherical coordinate, three-dimensional, nonorthogonal, boundary-fitted circulation model (contravariant formulation) for application to estuarine, coastal sea, and continental shelf waters is presented. The model employs a split mode technique where the equations are decomposed into exterior and interior modes. The exterior mode (vertically averaged) described in an earlier paper (Muin and Spaulding 1996) is solved using a semiimplicit solution technique. The interior mode (vertical structure) is solved explicitly, except for the vertical diffusion terms that are solved implicitly. The temporally and spatially varying eddy viscosity and diffusivity are determined from a turbulent kinetic energy equation and an empirically specified length scale. A series of tests are presented to evaluate model performance where analytical solutions or other numerical solutions are available for comparison. The model's ability to predict the point vertical structure of tidal flow is tested against analytic solutions employing (1) constant viscosity; and (2) an eddy viscosity varying linearly with depth with a no-slip bottom boundary condition. The ability of the model to simulate three-dimensional tidal flow was tested against an exact solution for an annular section channel with quadratically varying bathymetry. The model was also tested against analytic solutions for steady residual flow generated by density gradient, wind, and river flow in a channel. The model predicted turbulent energy distributions generated from a bottom boundary were compared to those from a previous numerical study by Davies and Jones (1990). No-slip and bottom stress formulations at the sea bed, and their effect on the vertical structure of the flow are analyzed. The model was used to predict the salinity distribution in a simple rectangular channel identical to the Rotterdam Waterway. The computational method is very economical, stable, and accurate with the CFL stability condition up to 100.

## INTRODUCTION

Numerical modeling techniques are routinely used to study circulation and pollutant transport in estuarine and coastal waters. The majority of models employ finite-difference techniques on square grid systems. While this has proven useful in various applications, it becomes expensive when the study region is geometrically and bathymetrically complex. Such difficulties motivate the use of alternative solution approaches that allow flexibility in the grid specification, for example finite elements (Lynch and Werner 1987) and boundary-fitted coordinates (Johnson 1980; Spaulding 1984; Sheng 1986; Swanson 1986; Muin and Spaulding 1996).

This paper presents the extension of a two-dimensional (2D) vertically averaged, boundary fitted, spherical coordinate circulation model developed by Muin and Spaulding (1996) to three dimensions. The paper first presents the governing equations in spherical coordinates with appropriate assumptions and boundary conditions. The equations are further transformed to a  $\sigma$ -coordinate. This is followed by presentations of the governing equations in a generalized curvilinear coordinate system, turbulence parameterization, the solution methodology, and model testing for which analytic (linear problems) solutions or other numerical solutions are readily available. Testing emphasizes calculations of the vertical structure of the flow. Testing of the 2D vertically averaged version of the model for a series of horizontal flow problems (see Lynch and Gray 1978) was presented in Muin and Spaulding (1996).

## GOVERNING EQUATIONS

Using a spherical coordinate system, where  $\phi$  = longitude positive east;  $\theta$  = latitude positive north; and  $r$  = positive up,

<sup>1</sup>Jurusan Teknik Sipil, Institut Teknologi Bandung, Bandung, Indonesia.

<sup>2</sup>Prof. and Chair, Dept. of Oc. Engrg., Univ. of Rhode Island, Narragansett Bay Campus, Narragansett, RI 02882.

Note. Discussion open until June 1, 1997. Separate discussions should be submitted for the individual papers in this symposium. To extend the closing date one month, a written request must be filed with the ASCE Manager of Journals. The manuscript for this paper was submitted for review and possible publication on January 10, 1994. This paper is part of the *Journal of Hydraulic Engineering*, Vol. 123, No. 1, January, 1997. ©ASCE, ISSN 0733-9429/97/0001-0002-0012/\$4.00 + \$.50 per page. Paper No. 7655.

the equations of continuity, momentum, and conservation of substance can be written as

### Continuity

$$\frac{1}{r \cos \theta} \frac{\partial u}{\partial \phi} + \frac{1}{r} \frac{\partial v}{\partial \theta} - \frac{v}{r} \tan \theta + \frac{1}{r^2} \frac{\partial r^2 w}{\partial r} = 0 \quad (1)$$

### Momentum

$\phi$ -direction

$$\begin{aligned} \frac{\partial u}{\partial t} + \frac{u}{r \cos \theta} \frac{\partial u}{\partial \phi} + \frac{v}{r} \frac{\partial u}{\partial \theta} - \frac{uv}{r} \tan \theta + w \frac{\partial u}{\partial r} + \frac{uw}{r} - fv \\ = -\frac{1}{\rho_s r \cos \theta} \frac{\partial p}{\partial \phi} + \frac{\partial}{\partial r} \left( A_v \frac{\partial u}{\partial r} \right) \end{aligned} \quad (2)$$

$\theta$ -direction

$$\begin{aligned} \frac{\partial v}{\partial t} + \frac{u}{r \cos \theta} \frac{\partial v}{\partial \phi} + \frac{v}{r} \frac{\partial v}{\partial \theta} + \frac{uv}{r} \tan \theta + w \frac{\partial v}{\partial r} + \frac{vw}{r} + fu \\ = -\frac{1}{\rho_s r \cos \theta} \frac{\partial p}{\partial \theta} + \frac{\partial}{\partial r} \left( A_v \frac{\partial v}{\partial r} \right) \end{aligned} \quad (3)$$

$r$ -direction

$$\frac{\partial p}{\partial r} = -\rho g \quad (4)$$

### Conservation of Substance

$$\begin{aligned} \frac{\partial q}{\partial t} + \frac{u}{r \cos \theta} \frac{\partial q}{\partial \phi} + \frac{v}{r} \frac{\partial q}{\partial \theta} + w \frac{\partial q}{\partial r} = \frac{\partial}{\partial r} \left[ D_v \left( \frac{\partial q}{\partial r} \right) \right] \\ + \frac{D_v}{r^2} \left[ \frac{\partial^2 q}{\cos^2 \theta \partial \phi^2} + \frac{\partial^2 q}{\partial \theta^2} \right] \end{aligned} \quad (5)$$

### Equation of State of Sea Water

$$\rho = f(S, \theta) \quad (6)$$

where  $t$  = time;  $u$ ,  $v$  and  $w$  = velocity components in  $\phi$ ,  $\theta$ , and  $r$  directions, respectively;  $f$  = Coriolis parameter;  $p$  = pressure;  $g$  = gravity;  $\rho$  = water density;  $\rho_s$  = basin-averaged water density;  $A_v$  = vertical eddy viscosity;  $D_v$  = vertical eddy diffusivity.

ity;  $D_h$  = horizontal eddy diffusivity;  $\Theta$  = temperature °C;  $S$  = salinity (ppt); and  $q$  = concentration of a conservative substance such as  $\Theta$  or  $S$ .

The equations described previously assume the following: the flow is incompressible, density differences are neglected unless multiplied by gravity (Boussinesq approximation), the vertical acceleration is very small compared to gravity (hydrostatic assumption), and the horizontal stresses are neglected.

### Boundary Conditions

The land boundaries are assumed impermeable where the normal component of velocity is set to zero

$$\vec{V} \cdot \vec{n} = 0 \quad (7)$$

On river boundaries, the velocities are specified and the pressure gradient is set to zero. At open boundaries the water elevation or vertically varying velocity as a function of time is known from field observations or otherwise specified.

At closed boundaries the transport of substance is zero. At an open boundary the concentration must be specified during inflow. On outflow the substance is advected out of the model domain according to

$$\frac{\partial q}{\partial t} + \frac{u}{r \cos \theta} \frac{\partial q}{\partial \phi} = 0 \quad (8a)$$

$$\frac{\partial q}{\partial t} + \frac{v}{r} \frac{\partial q}{\partial \theta} = 0 \quad (8b)$$

At the surface, the wind stress is specified as

$$\tau_{\phi s} = \rho_a C_s W_{\phi} \sqrt{W_{\phi}^2 + W_{\theta}^2}, \quad \tau_{\theta s} = \rho_a C_s W_{\theta} \sqrt{W_{\phi}^2 + W_{\theta}^2} \quad (9)$$

where  $W_{\phi}$  and  $W_{\theta}$  = wind speeds in the  $\phi$  and  $\theta$  directions, respectively;  $\rho_a$  = density of air; and  $C_s$  = drag coefficient at the surface.

The kinematic free surface boundary condition is given as

$$w = \frac{\partial \zeta}{\partial t} + \frac{u}{r \cos \theta} \frac{\partial \zeta}{\partial \phi} + \frac{v}{r} \frac{\partial \zeta}{\partial \theta} \quad (10)$$

Two options are available to specify the bottom boundary condition

#### 1. Bottom stress condition

$$\tau_{\phi b} = \rho_b C_b u_b \sqrt{u_b^2 + v_b^2}, \quad \tau_{\theta b} = \rho_b C_b v_b \sqrt{u_b^2 + v_b^2} \quad (11)$$

where  $C_b$  = bottom drag coefficient; and  $u_b$  and  $v_b$  = velocity components at the bottom in the  $\phi$  and  $\theta$  directions, respectively.

#### 2. No-slip condition

$$u_b = 0 \quad \text{and} \quad v_b = 0 \quad (12)$$

At the bottom boundary, no momentum flux is allowed and the kinematic condition is specified

$$w = -u_b \frac{1}{r \cos \theta} \frac{\partial h}{\partial \phi} - v_b \frac{1}{r} \frac{\partial h}{\partial \theta} \quad (13)$$

The governing equations are transformed to a  $\sigma$ -coordinate system to resolve bathymetric variations with a constant number of grids. The transformation is defined as

$$\phi = \phi', \quad \theta = \theta', \quad r = R + \zeta + (\sigma - 1)(\zeta + h)/2, \quad t = t' \quad (14)$$

The governing equations now become (dropping the primes for convenience)

### Continuity

$$\frac{\partial \zeta}{\partial t} + \frac{1}{r \cos \theta} \frac{\partial uD}{\partial \phi} + \frac{1}{r} \frac{\partial vD}{\partial \theta} - \frac{vD}{r} \tan \theta + \frac{\partial \omega D}{\partial \sigma} = 0 \quad (15)$$

### Momentum

$\phi$ -direction

$$\begin{aligned} \frac{\partial uD}{\partial t} + \frac{1}{r \cos \theta} \frac{\partial uuD}{\partial \phi} + \frac{1}{r} \frac{\partial uvD}{\partial \theta} - \frac{2uvD}{r} \tan \theta + \frac{\partial u\omega D}{\partial \sigma} - fvD \\ = -\frac{gD}{2\rho_s r \cos \theta} \left\{ [\lambda + (\rho_s - 2\rho)(1 - \sigma)] \frac{\partial D}{\partial \phi} \right. \\ \left. + (4\rho - 2\rho_s) \frac{\partial \zeta}{\partial \phi} + D \frac{\partial \lambda}{\partial \phi} \right\} + \frac{4}{D} \frac{\partial}{\partial \sigma} \left( A_v \frac{\partial u}{\partial \sigma} \right) \end{aligned} \quad (16)$$

$\theta$ -direction

$$\begin{aligned} \frac{\partial vD}{\partial t} + \frac{1}{r \cos \theta} \frac{\partial uvD}{\partial \phi} + \frac{1}{r} \frac{\partial vvD}{\partial \theta} - \frac{uv - vv}{r} D \tan \theta \\ + \frac{\partial v\omega D}{\partial \sigma} + fvD = -\frac{gD}{2\rho_s r} \left\{ [\lambda + (\rho_s - 2\rho)(1 - \sigma)] \frac{\partial D}{\partial \theta} \right. \\ \left. + (4\rho - 2\rho_s) \frac{\partial \zeta}{\partial \theta} + D \frac{\partial \lambda}{\partial \theta} \right\} + \frac{4}{D} \frac{\partial}{\partial \sigma} \left( A_v \frac{\partial v}{\partial \sigma} \right) \end{aligned} \quad (17)$$

$\sigma$ -direction

$$\frac{2}{D} \frac{\partial p}{\partial \sigma} = -\rho g \quad (18)$$

### Conservation of Substance

$$\begin{aligned} \frac{\partial q}{\partial t} + \frac{u}{r \cos \theta} \frac{\partial q}{\partial \phi} + \frac{v}{r} \frac{\partial q}{\partial \theta} + \omega \frac{\partial q}{\partial \sigma} = \frac{4}{D^2} \frac{\partial}{\partial \sigma} \left[ D_v \left( \frac{\partial q}{\partial \sigma} \right) \right] \\ + \frac{D_v}{r^2} \left( \frac{\partial^2 q}{\cos^2 \theta \partial \phi^2} + \frac{\partial^2 q}{\partial \theta^2} \right) \end{aligned} \quad (19)$$

where

$$\lambda = \int_{\sigma}^1 \rho \, d\sigma \quad (20a)$$

$$\omega = -\frac{1}{D} (1 + \sigma) \frac{\partial \zeta}{\partial t} + \gamma_{\phi} u + \gamma_{\theta} v + \frac{2}{D} w \quad (20b)$$

$$\gamma_{\phi} = \frac{1}{D} \left[ \frac{1 - \sigma}{r \cos \theta} \frac{\partial h}{\partial \phi} - \frac{1 + \sigma}{r \cos \theta} \frac{\partial \zeta}{\partial \phi} \right] \quad (20c)$$

$$\gamma_{\theta} = \frac{1}{D} \left[ \frac{1 - \sigma}{r \cos \theta} \frac{\partial h}{\partial \theta} - \frac{1 + \sigma}{r \cos \theta} \frac{\partial \zeta}{\partial \theta} \right] \quad (20d)$$

where  $D = h + \zeta$  = total water depth.

The horizontal velocities and independent variables are next transformed to a curvilinear coordinate system. The equations of motion and continuity equation in a curvilinear coordinate system ( $\xi, \eta$ ), in terms of the contravariant velocity components, are as follows:

### Continuity

$$\begin{aligned} Jr \cos \theta \frac{\partial \zeta}{\partial t} + \frac{\partial}{\partial \xi} (\cos \theta Ju^c D) + \frac{\partial}{\partial \eta} (\cos \theta Jv^c D) \\ + Jr \cos \theta \frac{\partial (\omega D)}{\partial \sigma} = 0 \end{aligned} \quad (21)$$

## Momentum Equation

$\xi$ -direction

$$\begin{aligned} \frac{\partial u^r D}{\partial t} = & -\frac{\theta_z \theta_x + \cos^2 \theta \phi_x \phi_x}{J^2 \rho_x r \cos^2 \theta} \frac{Dg}{2} \left\{ [\lambda + (\rho_x - 2\rho)(1 - \sigma)] \frac{\partial D}{\partial \xi} \right. \\ & + (4\rho - 2\rho_x) \frac{\partial \xi}{\partial \xi} + D \frac{\partial \lambda}{\partial \xi} \left. \right\} + \frac{\theta_z \theta_x + \cos^2 \theta \phi_x \phi_x}{J^2 \rho_x r \cos^2 \theta} \frac{Dg}{2} \\ & \cdot \left\{ [\lambda + (\rho_x - 2\rho)(1 - \sigma)] \frac{\partial D}{\partial \eta} + (4\rho - 2\rho_x) \frac{\partial \xi}{\partial \eta} + D \frac{\partial \lambda}{\partial \eta} \right\} \\ & - \frac{\theta_x}{J^2 r \cos^2 \theta} \left[ \frac{\partial}{\partial \xi} (\phi_t \cos^2 \theta J u^r u^r D + \phi_x \cos^2 \theta J u^r v^r D) \right. \\ & \left. + \frac{\partial}{\partial \eta} (\phi_t \cos^2 \theta J u^r v^r D + \phi_x \cos^2 \theta J v^r v^r D) \right] \\ & + \frac{\phi_x}{J^2 r \cos^2 \theta} \left[ \frac{\partial}{\partial \xi} (\theta_t \cos^2 \theta J u^r u^r D + \theta_x \cos^2 \theta J u^r v^r D) \right. \\ & \left. + \frac{\partial}{\partial \eta} (\theta_t \cos^2 \theta J u^r v^r D + \theta_x \cos^2 \theta J v^r v^r D) \right] \\ & - \frac{\partial}{\partial \sigma} (\omega u^r D) + \frac{fD}{J \cos \theta} [(\theta_t \theta_x + \cos^2 \theta \phi_t \phi_x) u^r \\ & + (\theta_t \theta_x + \cos^2 \theta \phi_x \phi_x) v^r] + \frac{4}{D} \frac{\partial}{\partial \sigma} \left( A_v \frac{\partial u^r}{\partial \sigma} \right) \end{aligned} \quad (22)$$

$\eta$ -direction

$$\begin{aligned} \frac{\partial v^r D}{\partial t} = & \frac{\theta_z \theta_x + \cos^2 \theta \phi_x \phi_x}{J^2 \rho_x r \cos^2 \theta} \frac{Dg}{2} \left\{ [\lambda + (\rho_x - 2\rho)(1 - \sigma)] \frac{\partial D}{\partial \xi} \right. \\ & + (4\rho - 2\rho_x) \frac{\partial \xi}{\partial \xi} + D \frac{\partial \lambda}{\partial \xi} \left. \right\} - \frac{\theta_z \theta_x + \cos^2 \theta \phi_x \phi_x}{J^2 \rho_x r \cos^2 \theta} \frac{Dg}{2} \\ & \cdot \left\{ [\lambda + (\rho_x - 2\rho)(1 - \sigma)] \frac{\partial D}{\partial \eta} + (4\rho - 2\rho_x) \frac{\partial \xi}{\partial \eta} + D \frac{\partial \lambda}{\partial \eta} \right\} \\ & + \frac{\theta_x}{J^2 r \cos^2 \theta} \left[ \frac{\partial}{\partial \xi} (\phi_t \cos^2 \theta J u^r u^r D + \phi_x \cos^2 \theta J u^r v^r D) \right. \\ & \left. + \frac{\partial}{\partial \eta} (\phi_t \cos^2 \theta J u^r v^r D + \phi_x \cos^2 \theta J v^r v^r D) \right] \\ & - \frac{\phi_t}{J^2 r \cos^2 \theta} \left[ \frac{\partial}{\partial \xi} (\theta_t \cos^2 \theta J u^r u^r D + \theta_x \cos^2 \theta J u^r v^r D) \right. \\ & \left. + \frac{\partial}{\partial \eta} (\theta_t \cos^2 \theta J u^r v^r D + \theta_x \cos^2 \theta J v^r v^r D) \right] \\ & - \frac{\partial}{\partial \sigma} (\omega v^r D) - \frac{fD}{J \cos \theta} [(\theta_t \theta_x + \cos^2 \theta \phi_t \phi_x) u^r \\ & + (\theta_t \theta_x + \cos^2 \theta \phi_x \phi_x) v^r] + \frac{4}{D} \frac{\partial}{\partial \sigma} \left( A_v \frac{\partial v^r}{\partial \sigma} \right) \end{aligned} \quad (23)$$

## Conservation of Substance

$$\begin{aligned} \frac{\partial q}{\partial t} + \frac{u^r}{r} \frac{\partial q}{\partial \xi} + \frac{v^r}{r} \frac{\partial q}{\partial \eta} + \omega \frac{\partial q}{\partial \sigma} = & \frac{4}{D^2} \frac{\partial}{\partial \sigma} \left( D_v \frac{\partial q}{\partial \sigma} \right) + \frac{D_v}{r^2 J^2} \\ & \cdot \left[ \left( \frac{\theta_z \theta_x}{\cos^2 \theta} + \phi_x \phi_x \right) \frac{\partial^2 q}{\partial \xi^2} - 2 \left( \frac{\theta_z \theta_x}{\cos^2 \theta} + \phi_t \phi_x \right) \frac{\partial^2 q}{\partial \xi \partial \eta} \right. \\ & \left. + \left( \frac{\theta_t \theta_x}{\cos^2 \theta} + \phi_t \phi_t \right) \frac{\partial^2 q}{\partial \eta^2} \right] \end{aligned} \quad (24)$$

where  $u^r$  and  $v^r$  = contravariant velocities in the  $(\xi, \eta)$  directions, respectively;  $\xi$  = water elevation;  $D$  =  $\xi$  + depth; and

the Jacobian,  $J = \phi_x \theta_x - \phi_x \theta_x$ . The relationship between the contravariant velocities ( $u^r, v^r$ ) and velocities in spherical coordinates ( $u, v$ ) is given by

$$u = \cos \theta \phi_x u^r + \cos \theta \phi_x v^r \quad (25a)$$

$$v = \theta_x u^r + \theta_x v^r \quad (25b)$$

## TURBULENCE PARAMETERIZATION

The turbulence parameterization is a key model component for predicting flow and mixing processes in stratified fluids. There is, however, no universally accepted procedure to represent turbulence (ASCE 1988; Cheng and Smith 1990). In this study, we employ a one equation turbulent kinetic energy model to calculate the vertical eddy viscosity and diffusivity. The length scale is specified using the approach suggested by Blackadar (1962) that has been successfully used in modeling turbulence for tidal problems (Davies and Jones 1990). The effect of stratification is accounted for by using an empirical relationship similar to the ones employed for the mixing length approach. This model accounts for the convection, diffusion, and time history of turbulent kinetic energy in unsteady flows.

### Turbulent Energy

The turbulence kinetic energy equation in spherical and  $\sigma$ -coordinates is given as follows:

$$\begin{aligned} \frac{\partial b}{\partial t} + \frac{u}{r \cos \theta} \frac{\partial b}{\partial \xi} + \frac{v}{r} \frac{\partial b}{\partial \eta} + \omega \frac{\partial b}{\partial \sigma} = & \frac{4}{D^2} \frac{\partial}{\partial \sigma} \left( A_v \frac{\partial b}{\partial \sigma} \right) \\ & + A_v \left[ \left( \frac{2}{D} \frac{\partial u}{\partial \sigma} \right)^2 + \left( \frac{2}{D} \frac{\partial v}{\partial \sigma} \right)^2 \right] + \beta g \frac{2A_v}{D\sigma} \frac{\partial \Phi}{\partial \sigma} - \epsilon \end{aligned} \quad (26)$$

where  $b$  = kinetic energy.

After transformation to curvilinear coordinates  $(\xi, \eta)$ , the preceding equation can be written as

$$\begin{aligned} \frac{\partial b}{\partial t} + \frac{u^r}{r} \frac{\partial b}{\partial \xi} + \frac{v^r}{r} \frac{\partial b}{\partial \eta} + \omega \frac{\partial b}{\partial \sigma} = & \frac{4}{D^2} \frac{\partial}{\partial \sigma} \left( A_v \frac{\partial b}{\partial \sigma} \right) \\ & + A_v \left[ \left( \frac{2}{D} \frac{\partial u}{\partial \sigma} \right)^2 + \left( \frac{2}{D} \frac{\partial v}{\partial \sigma} \right)^2 \right] + \beta g \frac{2A_v}{D\sigma} \frac{\partial \Phi}{\partial \sigma} - \epsilon \end{aligned} \quad (27)$$

where  $\beta$  = volumetric expansion coefficient;  $\sigma_v$  = empirical diffusion constant;  $\sigma$  = Schmidt number;  $\Phi$  = mean scalar quantity; and  $\epsilon$  = dissipation. In this study the interchange between turbulent kinetic energy and potential energy or production/dissipation by buoyant forces is neglected. It is assumed that the turbulent kinetic energy is advected and diffused in a homogeneous fluid while the effect of stratification is accounted for by an empirical formula using a Richardson number (damping function). As argued by Abraham (1988), the reproduction of internal mixing at tidal slack is beyond the capability of present turbulence models and, hence, they should not be used where this aspect is important.

### Eddy Viscosity and Diffusivity Relationships

Based on dimensional reasoning the eddy viscosity is related to the kinetic energy  $b$  and mixing length  $L_m$  by

$$A_v = C_v L_m \sqrt{b} \quad (28)$$

where  $C_v$  = empirical constant.

In homogeneous water, the vertical eddy viscosity and diffusivity are considered to be equal,  $A_v = D_v$ . In the presence of a stable vertical density gradient, both  $A_v$  and  $D_v$  are lower than their homogeneous values. The magnitude of  $A_v$  is always greater than the corresponding value of  $D_v$ .

The general form for the eddy viscosity and diffusivity are given as

$$A_e = f(R_i) C_v L_m \sqrt{b} \quad (29a)$$

$$D_e = g(R_i) C_v L_m \sqrt{b} \quad (29b)$$

Several semiempirical relations for  $f(R_i)$  and  $g(R_i)$  have been proposed by Munk and Anderson (1948) and Officer (1976).

#### Munk and Anderson (1948)

$$f(R_i) = (1 + 10.0R_i)^{-0.75} \quad (30a)$$

$$g(R_i) = (1 + 3.33R_i)^{-0.75} \quad (30b)$$

#### Officer (1976)

$$f(R_i) = (1 + R_i)^{-1} \quad (31a)$$

$$g(R_i) = (1 + R_i)^{-1} \quad (31b)$$

where the Richardson number,  $R_i$ , is defined by

$$R_i = -\frac{2g}{\rho D} \frac{\frac{\partial \rho}{\partial \sigma}}{\left[ \frac{\partial(u)}{\partial \sigma} \right]^2 + \left[ \frac{\partial(v)}{\partial \sigma} \right]^2} \quad (32)$$

#### Dissipation

From dimensional analysis the expression for dissipation, in terms of the turbulent kinetic energy and mixing length, is given by

$$\varepsilon = C_\varepsilon (b^{3/2}/L_m) \quad (33)$$

where  $C_\varepsilon$  = empirical constant.

#### Mixing Length

The mixing length formulation proposed by Blackadar (1962) is

$$L_m = \frac{KD[1 + (\sigma - 1/2)]}{1 + \frac{KD[1 + (\sigma - 1/2)]}{L_m}} \quad (34)$$

where  $K$  = Von Karman's constant;  $D$  = total water depth and in which the mixing length,  $L_m$ , increases from the sea bottom to the surface and the value of  $L_m$  is determined by the vertical distribution of the turbulent energy as follows:

$$L_m = \gamma D \frac{\int_{-1}^1 b^{3/2} [1 + (\sigma - 1/2)] d\sigma}{\int_{-1}^1 b^{3/2} d\sigma} \quad (35)$$

The constant  $\gamma$  determines the vertical extent of the boundary layer and vertical eddy viscosity, and is adjusted to match field observations. The viscosity increases rapidly with increasing  $\gamma$  in both amplitude and vertical extent (Mofjeld and Lavelle 1983). The constant  $\gamma$  typically ranges from 0.05 to 0.3. The coefficients in (28), (34), and (35) have values  $C_v = 0.463$ ;  $C_\varepsilon = 0.1$ ;  $\sigma_b = 1.37$ ; and  $K = 0.4$  (Davies and Jones 1990).

#### Boundary Conditions

The boundary condition at the surface is specified as

$$\frac{2\alpha_s A_e}{D} \frac{\partial b}{\partial \sigma} = \alpha_s U_*^2 \quad (36)$$

where  $U_*$  = friction velocity due to the wind stress and  $\alpha_s$ ,  $\alpha_b$  are coefficients. A similar boundary condition is used by Davies and Jones (1988) in which  $\alpha_s = 0.73$ , and  $\alpha_b = 2.6$ . In the absence of wind forcing the flux of turbulence at the surface disappears.

For a no-slip bottom boundary condition, the turbulent kinetic energy flux into the sea bed is zero (Davies and Jones 1988) and, therefore

$$\frac{\partial b}{\partial \sigma} = 0 \quad (37)$$

For the bottom stress boundary condition, the bottom boundary layer is not resolved in detail. The turbulent kinetic energy,  $b$ , at the first grid point near the wall (where the turbulence is assumed in equilibrium and the velocity follows the log-law) is given as follows:

$$b = U_*^2 / \sqrt{C_v C_\varepsilon} \quad (38)$$

where  $U_*$  = friction velocity associated with the bottom stress. While this boundary condition is not always rigorously satisfied under unsteady conditions (Celik and Rodi 1985), it is used as a first-order approximation.

#### SOLUTION TECHNIQUE

The basic approach is to transform the dependent, as well as independent, variables in spherical coordinates to a curvilinear coordinate system. The equation of motion is split into exterior and interior modes to increase the allowable time step and, hence, reduce the computational time.

The velocity is decomposed into

$$u = U^* + u'' \quad (39a)$$

$$v = V^* + v'' \quad (39b)$$

where  $(U^*, V^*)$  and  $(u'', v'')$  = vertically averaged velocities and deviation velocity (from the vertically averaged velocity) in  $(\xi, \eta)$  directions, respectively. Solution of the exterior mode using a semiimplicit (space staggered grid) solution, methodology, and presentations of the approach used to generate the boundary conforming grid are presented by Muin and Spaulding (1996). The focus here is on three-dimensional (3D) aspects, including the deviation velocity and the turbulence equation.

Subtracting the vertically averaged momentum equations from the 3D momentum equations gives the vertical deviation velocity equations of motion

$$\frac{\partial u'' D}{\partial t} = \frac{4}{D} \frac{\partial}{\partial \sigma} \left( A_e \frac{\partial u''}{\partial \sigma} \right) + A \quad (40a)$$

$$\frac{\partial v'' D}{\partial t} = \frac{4}{D} \frac{\partial}{\partial \sigma} \left( A_e \frac{\partial v''}{\partial \sigma} \right) + B \quad (40b)$$

where  $A$  and  $B$  = nonbarotropic terms in the equations of motion. These terms are solved explicitly. The diffusion term in (40) is solved implicitly using a three-level scheme to damp out spurious oscillations (Fletcher 1988). The algorithm is second-order accurate both in time and space. A tridiagonal set of equations in the unknown velocity deviation is solved using a Thomas algorithm. Both the exterior and interior modes are solved at the same time step.

The finite difference procedure used to solve the turbulent kinetic energy equations has been described by Davies and Jones (1990). In the present study, a three-level time discretization (Fletcher 1988) is used instead of the Crank-Nicholson method of Davies and Jones (1990). A nonstaggered grid is used in the vertical. The  $C$  form of Davies and Jones' (1990) numerical scheme is employed to calculate the dissipation term

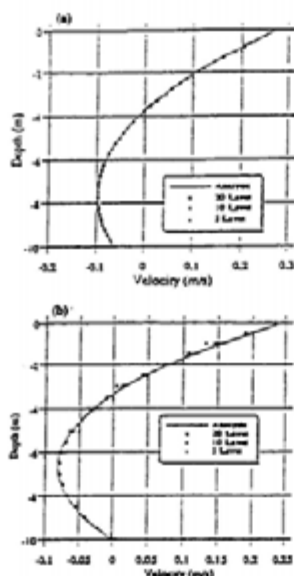


FIG. 2. Comparison of Model Predicted Vertical Structure of Velocity with Analytic Solution for Wind Driven Flow ( $A_w = 10 \text{ cm}^2/\text{s}$ ,  $\tau_w = 0.1 \text{ N/m}^2$  (1 dyne/cm<sup>2</sup>),  $k = 0.05 \text{ cm/s}$ ) for: (a) Bottom Stress; and (b) No-Slip Bottom Boundary Condition (Model Results Are Presented for 5, 10, and 20 Vertical Levels)

shown in Fig. 2(a). It can be seen that as the resolution increases the model predictions approach the analytic solution, especially near the bottom. The model represents the vertical velocity structure more accurately than for the density induced flow problem. The maximum errors are about 2% for five levels, 0.6% for 10 levels, and 0.2% for 20 levels. A similar problem, as in the density-induced flow, was found for the no-slip condition at the bottom and the boundary condition at the surface was modified to first order. The results are shown in Fig. 2(b). Again model prediction for this case is more accurate than in the baroclinic forcing problem.

#### Density Gradient Wind and River Forcing

The last test case considered flow driven by a combination of density gradient, wind, and river flow. The model was run using 20 levels. The results, not shown here, were simulated for bottom stress and no-slip bottom specifications, respectively. The agreement is excellent (<0.5%) for the bottom stress bottom boundary condition. The model underpredicts the velocity by about 5% in the mid-depth region for the no-slip bottom boundary condition.

#### Tidal Driven Flow

Two tests were employed to check the model's ability to simulate the vertical structure of tidal flow. The first test case is a point model in which the bottom boundary is specified using a no-slip condition, and the water slope is assumed known. The model was tested against constant and linearly varying vertical eddy viscosities. In the second test a bottom stress condition was employed at the sea bed. The bottom friction was linearized and related to the vertically averaged velocity.

#### Point Model Test

##### Constant Viscosity

The analytic solution for this problem was given in article 347 in Lamb (1945). The following data are used in model

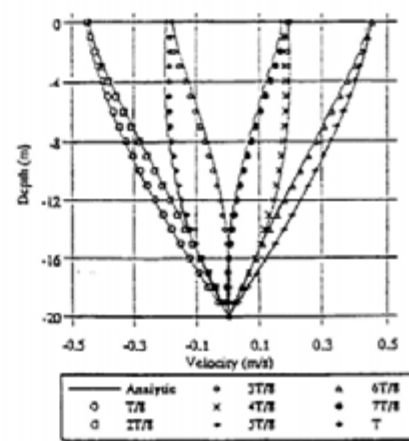


FIG. 3. Comparison of Model Predicted Velocity Structure with Analytic Solution for Tidally Driven Flow (Imposed Pressure Gradient of  $0.058 \text{ N/m}^2$ ) with Constant Vertical Viscosity,  $A_v = 0.011 \text{ m}^2/\text{s}$  at 1/8 Time Intervals Through One Tidal Cycle (Time Step,  $\Delta t = 279.45 \text{ s}$ )

testing. The imposed pressure gradient was  $0.058 \text{ N/m}^2$ ; period  $T = 12.42 \text{ h}$ ; depth  $h = 20 \text{ m}$ ; vertical viscosity  $A_v = 0.011 \text{ m}^2/\text{s}$ ; and time step  $\Delta t = 279.45 \text{ s}$  (160 steps per cycle). The test was performed using 20 levels. The model was started with zero velocities. The water slope was applied gradually (linear ramp over 4 cycles) until a steady state was achieved. Comparison between the analytic solution and the model prediction is shown in Fig. 3. The agreement is excellent throughout the water column.

#### Viscosity Varying Linearly with Height

Two simulations were studied with viscosity; one increasing and one decreasing linearly from the sea bed to the sea surface. The analytic solution is presented in Prandle (1982). Simulations were performed using the same depth, grid size, period, time step, sea surface slope, and initial condition as the constant viscosity test case.

In the case of viscosity increasing linearly from the bottom (sea surface), the viscosity at the sea bed (surface) is set at  $A_w = 0.001 \text{ m}^2/\text{s}$ ; and the viscosity at the sea surface (bed)  $A_w = 0.021 \text{ m}^2/\text{s}$ . The results of these simulations are in excellent agreement with the analytic solutions. The boundary layer in the linearly increasing case is (referenced from the sea bed) thinner than the constant viscosity case due to the lower viscosity near the bottom. The boundary layer for the linearly decreasing case is thicker than for the constant viscosity case and occupies the whole water column due to the fact that the vertical viscosity at the bottom is higher than in the two previous cases.

#### 3D Testing

Lynch and Officer (1985) derived an analytic solution for the 3D flow driven by periodic forcing, with linearized bottom stress ( $ku_b$ ,  $kv_b$ ) and linked to the vertically averaged solution for an annular channel. The solutions were assembled from one-dimensional (1D) vertical diffusion and 2D vertically averaged solutions of the governing equations.

Consider the quarter-circle geometry with quadratically varying bathymetry  $h = h_0 r^2$ . Note  $r$  refers to the radius of the annular channel. The sketch of geometry, bathymetry, and grid configuration are shown in Fig. 4. The viscosity is constant throughout the depth. The analytic solution, however, requires that  $A_v/(\Omega h^2)$  and  $kh/A_v$  be constant, and hence  $A_v$  and  $k$  must

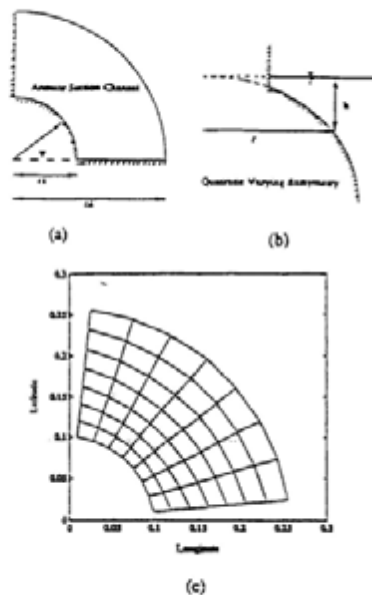


FIG. 4. Three-Dimensional Tidally Driven Model Test for: (a) Geometry; (b) Bathymetry; and (c) Grid Configuration ( $r_1 = 9,950$  m;  $r_2 = 31,250$  m;  $h = 5 (r/r_1)^2$ )

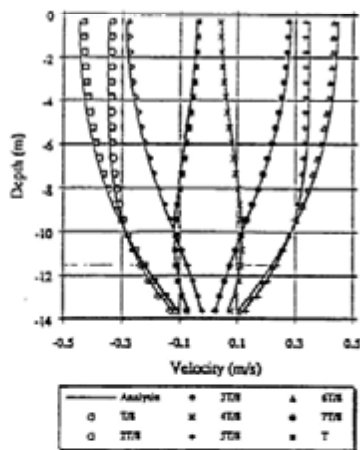


FIG. 5. Vertical Structure of Velocity at Increments of  $1/8$  of  $M_2$  Tidal Period at  $r = 16,660$  m and  $\Psi = 39.4^\circ$  for Three-Dimensional Model Test in Annular Section Channel,  $r_1 = 9,950$  m;  $r_2 = 31,250$  m;  $A_w/(\Omega h^2) = 0.1$ ;  $kh/A_w = 10$ ;  $\Delta t = 558.9$  s

vary horizontally. Model tests were performed using a coarse, slightly nonorthogonal  $7 \times 7$  grid system. The following parameters were used: inner radius  $r_1 = 9,950$  m; outer radius  $r_2 = 31,250$  m;  $\Omega = 1.4 \times 10^{-4} \text{ s}^{-1}$ ;  $kh/A_w = 10$ ;  $A_w/(\Omega h^2) = 0.1$ ; and  $h_s = 5/r_1^2 \text{ m}^{-1}$ . The open boundary was specified by varying the tidal amplitude  $\zeta_o = 0.1 \cos(2\psi)$  m, where  $\psi$  = rotation angle. The model was run using eight and 20 levels in the vertical and time steps of 279.45, 558.9, and 1117.3 s.

Comparison of the model and analytical solution at point (5, 5) or at radius 16,660 m and  $\psi = 39.375^\circ$  for 20 levels with a time step of 558.9 s at one-eighth period increment is

shown in Fig. 5. The agreement is very good. The largest errors ( $<10\%$ ) are near the surface area.

Sensitivity of the model predicted near surface currents (at 778, 774, 3778, 772) to grid resolution and time step in the near surface region is shown in Table 1. The maximum errors occur at slack tide (at 772). The model predicted errors decrease with decreasing time step. Model errors using eight vertical levels are approximately the same as those using 20 vertical levels.

A vector plot of the velocity field at the surface at 774 (not presented) shows that the agreement between model predictions and analytic solution is excellent, even though the grid was relatively coarse and slightly nonorthogonal. The errors are less than 5%, except at the corner point of the inner radius  $r = r_1$ . Here they are about 10% due to the fact that the velocity is very small at this location. The errors become much smaller ( $<0.6\%$ ) at the outer radius near the open boundary. Comparison of the model-predicted velocity time series at a radius of 16,660 m,  $\psi = 39.375^\circ$ , and for 0.35 m and 13.65 m below the sea surface with the analytic solution are shown in Fig. 6. The bottom velocity leads the surface velocity by 0.85 h. Predictions are again in excellent agreement with the analytic solution.

#### Turbulence Model Simulations

A simulation was performed in an open-closed, rectangular channel driven with tidal forcing, and a water depth of 10 m. The channel length is 51.34 km, and is represented by 20 horizontal grids. The tidal amplitude was 1.2 m, with a period of 12.42 h.  $\gamma = 0.4$ . A point 5.55 km from the open channel, where the pressure gradient has a magnitude that would give a current with amplitude 1.0 m/s in an inviscid calculation, was chosen to study the vertical structure of the velocity, eddy viscosity, and turbulent energy. The simulation assumed a bo-

TABLE 1. Model Prediction Errors (%) of Surface Velocity at  $r = 16,660$  m and  $\Psi = 39.4^\circ$  for Annular Section Channel with Quadratic Bathymetry Using 8 and 20 Vertical Levels with Time Steps of 279.45, 558.9, and 1117.3 s

t	8 Level			20 Level		
	279.45 s	558.9 s	1117.3 s	279.45 s	558.9 s	1117.3 s
	(CFL = 0.5)	(CFL = 1.0)	(CFL = 2.0)	(CFL = 3.1)	(CFL = 6.2)	(CFL = 12.4)
(1)	(2)	(3)	(4)	(5)	(6)	(7)
778	4.1	4.2	4.8	3.9	4.0	4.6
774	3.7	3.7	4.0	3.5	3.5	3.9
3778	3.1	3.0	3.0	3.1	3.0	3.0
772	8.7	10.0	12.6	7.6	8.8	11.6

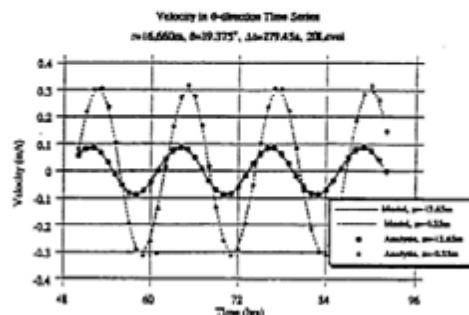


FIG. 6. Comparison of Model Predicted Velocity Time Series with Analytical Solution at  $r = 16,660$  m and  $\Psi = 39.4^\circ$  for Three-Dimensional Model Test in Annular Section Channel Driven by  $M_2$  Tide at Open Boundary with Varying Amplitude of  $\zeta_o = 0.1 \cos(2\psi)$  m;  $r_1 = 9,950$  m;  $r_2 = 31,250$  m;  $A_w/(\Omega h^2) = 0.1$ ;  $kh/A_w = 10$ ;  $\Delta t = 279.45$  s; and 20 Vertical Levels

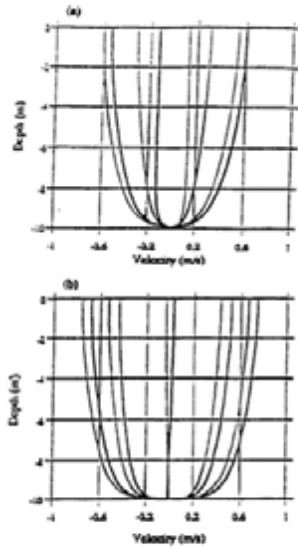


FIG. 7. Comparison of (a) Model Predicted Vertical Structure of Velocity with (b) Numerical Simulations of Davies and Jones (1990) for One-Dimensional Turbulence Model Test Driven by  $M_2$  Tide with Imposed Pressure Gradient of  $0.14 \text{ N/m}^2$ ; No-Slip Bottom Boundary Condition;  $\gamma = 0.4$ ;  $\Delta t = 558.9 \text{ s}$ ; and 40 Vertical Levels

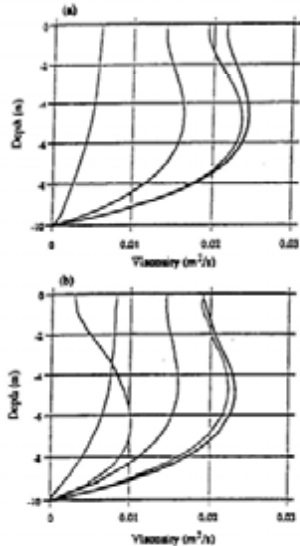


FIG. 8. Comparison of (a) Model Predicted Vertical Structure of Viscosity with (b) Numerical Simulations of Davies and Jones (1990) for One-Dimensional Turbulence Model Test Driven by  $M_2$  Tide with Imposed Pressure Gradient of  $0.14 \text{ N/m}^2$ ; No-Slip Bottom Boundary Condition;  $\gamma = 0.4$ ;  $\Delta t = 558.9 \text{ s}$ ; and 40 Vertical Levels

homogeneous fluid. The Coriolis, baroclinic, and advective terms were neglected to compare the present results with the circulation and turbulence model developed by Davies and Jones (1990).

For a no-slip condition at the bottom boundary, simulations

were conducted using 40 levels with a time step of  $558.9 \text{ s}$ . A comparison between the results of the present model (40 levels) and Davies and Jones' (1990) with 100 levels and a logarithmic transformation is shown in Figs. 7–10. Results are given at one-eighth intervals during the tidal cycle. The maximum surface velocity of the present model is about 20%

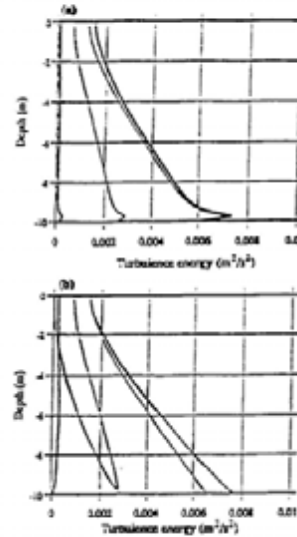


FIG. 9. Comparison of (a) Model Predicted Vertical Structure of Turbulence Energy with (b) Numerical Simulations of Davies and Jones (1990) for One-Dimensional Turbulence Model Test Driven by  $M_2$  Tide with Imposed Pressure Gradient of  $0.14 \text{ N/m}^2$ ; No-Slip Bottom Boundary Condition;  $\gamma = 0.4$ ;  $\Delta t = 558.9 \text{ s}$ ; and 40 Vertical Levels

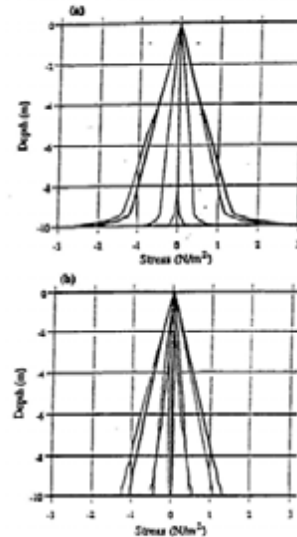


FIG. 10. Comparison of (a) Model Predicted Vertical Structure of Shear Stress with (b) Numerical Simulations of Davies and Jones (1990) for One-Dimensional Turbulence Model Test Driven by  $M_2$  Tide with Imposed Pressure Gradient of  $0.14 \text{ N/m}^2$ ; No-Slip Bottom Boundary Condition;  $\gamma = 0.4$ ;  $\Delta t = 558.9 \text{ s}$ ; and 40 Vertical Levels

lower than their results. The structure of the eddy viscosity, turbulent energy, and shear stress are similar. However, the bottom shear stresses are twice as high in Davies and Jones (1990) than in the present simulation because the present grid structure does not provide sufficient resolution in the near-bed region. This problem is more severe at low grid resolution.

For the bottom stress specification, simulations were performed using 10 and 40 levels with a time step of 279.45 s. In these simulations the bottom drag coefficient was set at 0.0025, and  $\gamma = 0.4$ . A comparison between simulations using high (40 levels) and low vertical resolution (10 level) is shown in Fig. 11 for the velocity profile. The maximum viscosity, shear stress, and energy (not shown) computed using the low resolution grid are approximately 25% higher than simulations using the high resolution grid. The velocity structure (Fig. 11), however, is not significantly affected. Further tests showed that a stable and accurate velocity prediction can be obtained using

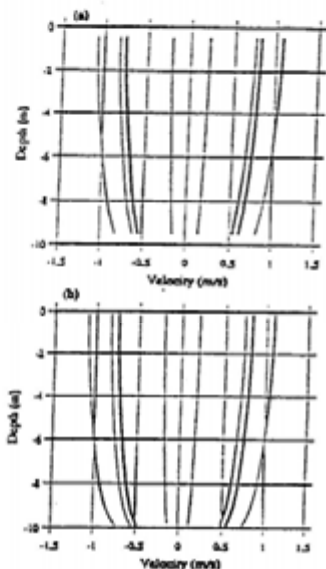


FIG. 11. Comparison of Model Predicted Vertical Structure of Velocity Using (a) 10 and (b) 40 Vertical Levels at Location 5.55 km from Open Boundary for Turbulence Model Test Driven by  $M_2$  Tide; Bottom Stress Condition;  $\gamma = 0.4$ ;  $C_b = 0.0025$ ;  $\Delta t = 558.9$  s

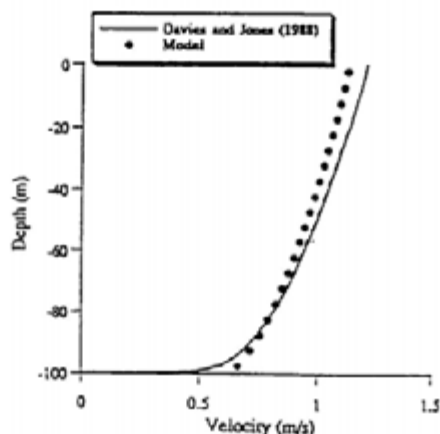


FIG. 12. Comparison of Model (Bottom Stress Condition) Predicted Vertical Structure of Velocity with Numerical Simulations of Davies and Jones (1988) Driven by Wind Stress;  $\tau_s = 1.0$  N/m<sup>2</sup>;  $C_b = 0.0025$ ; and  $\gamma = 0.2$

a time step of 1117.8 s (550 CFL, based on the diffusive time scale for 40 levels).

The model was also tested against steady wind-induced flow with a depth of 100 m, a wind stress of 1 N/m<sup>2</sup>, a bottom stress specification; 20 levels, with a friction coefficient of  $C_b = 0.0025$ , and  $\gamma = 0.2$ . A comparison of the velocity computed using the present model and similar results by Davies and Jones (1988) with 100 levels and a logarithmic transformation is presented in Fig. 12. The agreement is very good. A maximum difference of 5% is predicted near the surface and the sea bed. The model-predicted vertical structure of viscosity gives excellent agreement at middepth and near the surface, but slightly overpredicts at the bottom. The turbulent energy simulated by the present model is higher than Davies and Jones' (1988) model both at the surface and bottom. Differences that occur near the bottom are due to differences in the bottom boundary condition specification. The present simulations employ a bottom stress condition where the turbulent energy at the sea bed is specified while Davies and Jones (1988) use a no-slip bottom condition and specify no energy flux at the sea bed. In general the agreement is excellent although the present work uses relatively low grid resolution compared to Davies and Jones (1988).

#### Salinity Intrusion Simulations

Ippen and Harleman (1961) derived an analytical solution for salinity intrusion under the assumption that the salinity distribution can be represented by the equilibrium of the 1D convective-diffusion processes where the time and cross-sectionally averaged fresh water (seaward) flux of salt is balanced by the horizontal diffusive flux of salt (landward). The effect of gravitational convection by density differences (density included) is neglected. Consider a rectangular channel with a length of 105.5 km, a river flow velocity of 0.000714 m/s, and horizontal diffusion coefficients of 4, 6, 8, and 10 m<sup>2</sup>/s. The advective term in the salt transport equation is solved by the Lax-Wendroff method. The open boundary is specified by a constant salinity of 30 ppt. Comparison between model predictions and the analytic solution for various values of the horizontal diffusion coefficient  $D_x$  is shown in Fig. 13. The agreement between the model and analytical solution is excellent.

Finally the model was used to predict the salinity intrusion in Rotterdam Waterway using identical conditions to those employed by Smith and Takhar (1981). The simulation was intended to evaluate the ability of the model to predict salinity intrusion. The waterway was represented by a rectangular channel with a length of 99 km. The width and depth were

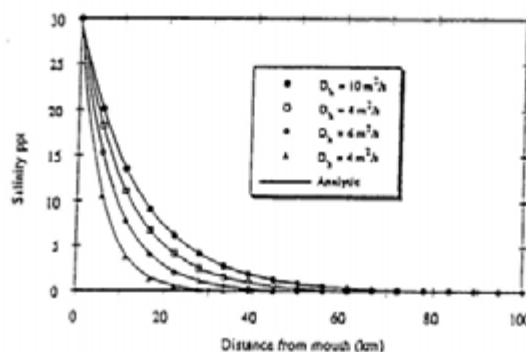


FIG. 13. Comparison of Model Predicted Salinity Distribution with Analytic Solution for One-Dimensional Salinity Intrusion Test (Transport Equation is Solved by Lax-Wendroff Method; River Flow Velocity is 0.000714 m/s; and Horizontal Diffusion Coefficients of 4, 6, 8, and 10 m<sup>2</sup>/s Are Used)

kept constant with values of 400 and 13 m, respectively. The river inflow was 1,000 m<sup>3</sup>/s. The model was run using 40 grids along the channel and 20 levels in the vertical. The initial conditions for velocity, elevation, and salinity were set to zero. Along the open boundary (mouth) the salinity distribution is assumed to vary from 30 ppt at the bottom to 20 ppt at the surface on inflow. The model was run with an  $M_2$  tide. The time step was 558.9 s with a tidal amplitude at the open boundary of 0.9 m. The advective term in the salt transport equation was solved using the upwind method. The Lax-Wendroff method was not used because it required a large horizontal diffusivity ( $\sim 5000$  m<sup>2</sup>/s) to maintain stability. The model was run for 66 d to achieve steady state.

A simulation was performed in which the vertical viscosity and diffusivity were calculated by the turbulence model. The bottom friction,  $C_b$ , was 0.0010. It was found that the model was very sensitive to the value of  $\gamma$  in the mixing length specification. Since the turbulent energy source is from the bottom boundary, the bottom drag coefficient,  $C_b$ , is also important in determining the vertical velocity structure. Fig. 14 shows the salinity distribution along the channel for  $C_b = 0.0005$  and  $\gamma = 0.03$  with the empirical formulation of (30), which was taken from Officer (1976), implemented to represent stratification effects. Smith and Takhar's (1981) model predictions and field observations are also shown [Fig. 14(a)]. The results show that the model-predicted high tide salinity distribution is in reasonable agreement with and an improvement over Smith and Tak-

har's results. Both the present and Smith and Takhar (1981) models do not accurately predict the low tide salinity distribution. As analyzed by Smith and Takhar (1981), the poor model performance for the low water salinity distribution is caused by the dock system in the waterway acting as a source and sink of salt on the ebb and flood tide, respectively.

## CONCLUSION

A detailed description of the 3D boundary-fitted circulation model in spherical coordinates for coastal waters is presented. Both the dependent and independent horizontal variables are transformed to a boundary-fitted coordinate system. The equations are also transformed to  $\sigma$ -coordinates to resolve the variation in bathymetry. Both the exterior and interior mode are solved using the same time step. The numerical scheme is second order in time and space. The time step is not restricted by the shallow water gravity wave and vertical diffusion CFL criteria. The eddy viscosity/diffusivity can be specified or obtained from a one equation turbulence energy model.

A series of model tests to linear problems shows that the present model is fully capable of predicting the vertical structure of the flow in response to tidal, wind, river, and density forcing. The 3D model test in an annular section channel with quadratic bathymetry under tidal forcing has shown the model's ability to resolve a more complicated geometry and bathymetry.

The model, with a bottom stress condition, gives good predictions of the vertical structure of the velocity, shear stress, turbulence energy, and eddy viscosity even at modest vertical grid resolutions. No iteration or filtering is employed. The no-slip bottom boundary condition version of the present model fails to accurately predict the shear stress and energy distributions at the sea bed for 40 vertical levels because of the lack of vertical resolution near the sea bed.

Agreement between the model and analytic solution is excellent for the 1D salinity intrusion problem where the density gradient induced flow is neglected. The model accurately predicted the salinity distribution at high tide in the Rotterdam Waterway where the viscosity/diffusivity were obtained from a turbulence model. The poor results at low tide were probably caused by the lack of consideration of the effect of the dock system on the salinity field (Smith and Takhar 1981).

The CPU time of the internal mode with turbulence model for each water cell per computational step is  $3.1 \times 10^{-6}$  min on a 486/50 MHz personal computer system using a Lahey F7732 Version 5.1 Fortran compiler. The CPU time of the external mode is  $2.9 \times 10^{-6}$  min using the same machine and compiler.

## APPENDIX I. REFERENCES

- Abraham, G. (1988). "Turbulence and mixing in stratified tidal flows." *Physical processes in estuaries*, P. Dronkers and R. Leussen, eds., Springer-Verlag KG, Berlin, Germany.
- ASCE Task Committee on Turbulence Models in Hydraulic Computations. (1988). "Turbulence modeling of surface water flow and transport: Part I." *J. Hydr. Engrg.*, ASCE, 114(9), 970-991.
- Blackadar, A. K. (1962). "The vertical distribution of wind and turbulent exchange in a neutral atmosphere." *J. Geophys. Res.*, 67, 3095-3120.
- Celik, I., and Rodi, W. (1985). "Calculation of wave-induced turbulent flows in estuaries." *Oc. Engrg.*, 12(6), 531-542.
- Cheng, R. T., and Smith, P. E. (1990). "A survey of three-dimensional numerical estuarine models." *Estuarine and coastal modeling*, M. L. Spaulding, ed., ASCE, New York, N.Y., 1-15.
- Davies, A. M., and Jones, J. E. (1988). "Modelling turbulence in shallow sea regions." *Small-scale turbulence and mixing in the ocean, Proc. 19 Liege Colloquium on Oc. Hydrodyn.*, J. C. Nihoul and B. M. Jamart, eds., Univ. of Liege, Liege, Belgium.
- Davies, A. M., and Jones, J. E. (1990). "On the numerical solution of the turbulence energy equations for wave and tidal flows." *Int. J. for Numer. Meth. in Fluids*, 11, 1-25.

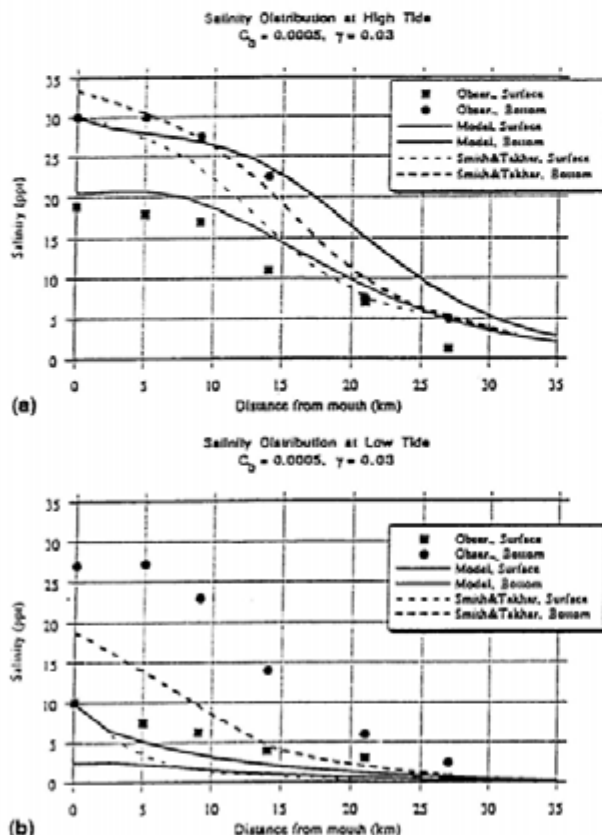


FIG. 14. Comparison of Model Predicted Salinity Distribution along Channel with Observations and Numerical Simulation of Smith and Takhar (1981) for Rotterdam Waterway at: (a) High Tide; and (b) Low Tide (Vertical Viscosity and Diffusivity Are Obtained from Turbulence Model Using Bottom Friction;  $C_b = 0.0005$ ; and  $\gamma = 0.3$ )

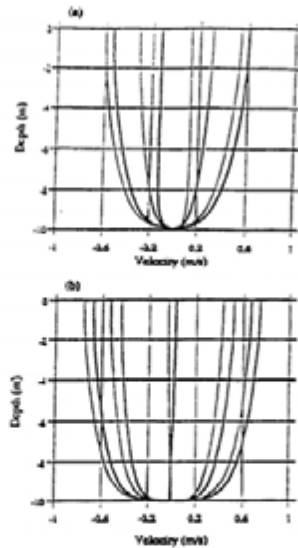


FIG. 7. Comparison of (a) Model Predicted Vertical Structure of Velocity with (b) Numerical Simulations of Davies and Jones (1990) for One-Dimensional Turbulence Model Test Driven by  $M_2$  Tide with Imposed Pressure Gradient of  $0.14 \text{ N/m}^2$ ; No-Slip Bottom Boundary Condition;  $\gamma = 0.4$ ;  $\Delta t = 558.9 \text{ s}$ ; and 40 Vertical Levels

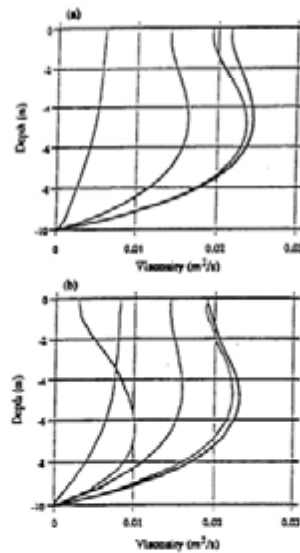


FIG. 8. Comparison of (a) Model Predicted Vertical Structure of Viscosity with (b) Numerical Simulations of Davies and Jones (1990) for One-Dimensional Turbulence Model Test Driven by  $M_2$  Tide with Imposed Pressure Gradient of  $0.14 \text{ N/m}^2$ ; No-Slip Bottom Boundary Condition;  $\gamma = 0.4$ ;  $\Delta t = 558.9 \text{ s}$ ; and 40 Vertical Levels

mogeneous fluid. The Coriolis, baroclinic, and advective terms were neglected to compare the present results with the circulation and turbulence model developed by Davies and Jones (1990).

For a no-slip condition at the bottom boundary, simulations

were conducted using 40 levels with a time step of 558.9 s. A comparison between the results of the present model (40 levels) and Davies and Jones' (1990) with 100 levels and a logarithmic transformation is shown in Figs. 7–10. Results are given at one-eighth intervals during the tidal cycle. The maximum surface velocity of the present model is about 20%

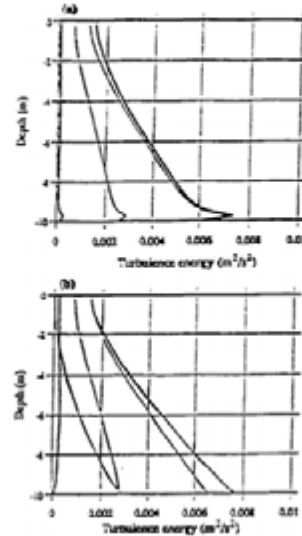


FIG. 9. Comparison of (a) Model Predicted Vertical Structure of Turbulence Energy with (b) Numerical Simulations of Davies and Jones (1990) for One-Dimensional Turbulence Model Test Driven by  $M_2$  Tide with Imposed Pressure Gradient of  $0.14 \text{ N/m}^2$ ; No-Slip Bottom Boundary Condition;  $\gamma = 0.4$ ;  $\Delta t = 558.9 \text{ s}$ ; and 40 Vertical Levels

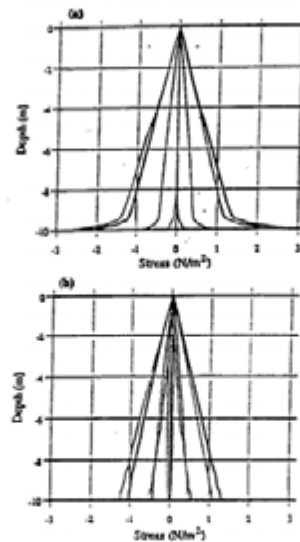


FIG. 10. Comparison of (a) Model Predicted Vertical Structure of Shear Stress with (b) Numerical Simulations of Davies and Jones (1990) for One-Dimensional Turbulence Model Test Driven by  $M_2$  Tide with Imposed Pressure Gradient of  $0.14 \text{ N/m}^2$ ; No-Slip Bottom Boundary Condition;  $\gamma = 0.4$ ;  $\Delta t = 558.9 \text{ s}$ ; and 40 Vertical Levels

- Fletcher, C. A. J. (1988). *Computational techniques for fluid dynamics, volume I, fundamental and general techniques*. Springer-Verlag New York, Inc., New York, N.Y.
- Ippen, A. T., and Hartleman, D. R. F. (1961). "One-dimensional analysis of salinity intrusion in estuaries." *Tech. Bull. No. 5*, Com. on Tidal Hydr., U.S. Army Corps of Engrs., Fort Belvoir, Va.
- Johnson, B. H. (1980). "VAHM-A vertically averaged hydrodynamic model using boundary-fitted coordinates." *MP HL-80-3*, U.S. Army Corps of Engrs. Wtrwy. Experiment Station, Vicksburg, Miss.
- Lamb, H. (1945). *Hydrodynamics*. Dover Publications, Inc., New York, N.Y.
- Lynch, D. R., and Gray, W. G. (1978). "Analytic solutions for computer flow model testing." *J. Hydr. Div., ASCE*, 104(00), 1409-1428.
- Lynch, D. R., and Officer, C. B. (1985). "Analytic solutions for three-dimensional hydrodynamic model testing." *Int. J. for Numer. Meth. in Fluids*, 5, 529-543.
- Lynch, D. R., and Werner, F. E. (1987). "Three-dimensional hydrodynamics on finite-element. Part I: Linearized harmonic model." *Int. J. for Numer. Meth. in Fluids*, 7, 871-909.
- Mofjeld, H. O., and Lavelle, J. W. (1984). "Setting the length scale in a second-order closure model of the unstratified bottom boundary layer." *J. Phys. Oceanography*, 14, 833-839.
- Muin, M. (1993). "A three-dimensional boundary-fitted circulation model in spherical coordinates." PhD dissertation, Univ. of Rhode Island, Narragansett Bay Campus, Narragansett, R.I.
- Muin, M., and Spaulding, M. L. (1996). "Two-dimensional boundary-fitted circulation model in spherical coordinates." *J. Hydr. Engrg., ASCE*, 122(9), 512-521.
- Munk, W. H., and Anderson, E. R. (1948). "Notes on theory of thermocline." *J. Marine Res.*, 7, 276.
- Officer, C. B. (1976). *Physical oceanography of estuaries*. John Wiley & Sons, Inc., New York, N.Y., 120.
- Prandle, D. (1982). "The vertical structure of tidal currents." *Geophys. Astrophys. Fluid Dyn.*, 22, 29-49.
- Sheng, Y. P. (1986). "A three-dimensional mathematical model of coastal, estuarine and lake currents using boundary-fitted grid." *Tech. Rep. No. 585*, Aeronautical Research Associates of Princeton, Princeton, N.J.
- Smith, T. J., and Takhar, H. S. (1981). "A mathematical model for partially mixed estuaries using the turbulence energy equation." *Estuarine, Coast., and Shelf Sci.*, 13, 27-45.
- Spaulding, M. L. (1984). "A vertically averaged circulation model using boundary-fitted coordinates." *J. Phys. Oceanography*, 14, 973-982.
- Swanson, J. C. (1986). "A three-dimensional numerical model system of coastal circulation and water quality." PhD dissertation, Univ. of Rhode Island, Kingston, R.I.

## APPENDIX II. NOTATION

The following symbols are used in this paper:

- $A_v$  = vertical eddy viscosity;  
 $a$  = tidal wave amplitude;  
 $b$  = turbulence kinetic energy;  
 $C_b$  = empirical constant in eddy viscosity relationship;  
 $C_s$  = drag coefficient at surface;  
 $C_b$  = drag coefficient at bottom;  
 $C_e$  = empirical constant in energy dissipation relationship;  
 $D$  = elevation + water depth;
- $D_h$  = horizontal eddy diffusivity;  
 $D_v$  = vertical eddy diffusivity;  
 $g$  = gravitation;  
 $h$  = water depth;  
 $J$  = Jacobian of curvilinear coordinate;  
 $K$  = Von Karman constant;  
 $k$  = linearized bottom friction;  
 $L$  = wave length;  
 $L_m$  = mixing length;  
 $l$  = length of channel;  
 $n$  = node number;  
 $p$  = pressure;  
 $q$  = concentration of substance;  
 $R$  = radius of earth;  
 $RI$  = Richardson number;  
 $S$  = salinity;  
 $T$  = wave period;  
 $t$  = time;  
 $u_r$  = river flow;  
 $U_{*w}$  = friction velocity due to wind stress;  
 $U_{*b}$  = friction velocity due to bottom stress;  
 $U, V$  = vertically averaged velocity in  $\phi$  and  $\theta$  direction;  
 $U^r, V^r$  = vertically averaged velocity in curvilinear coordinate;  
 $u, v, w$  = water velocity in  $\phi, \theta, r$  direction;  
 $u^r, v^r$  = water velocity in curvilinear coordinate;  
 $u_b$  = bottom velocity in  $\phi$  direction;  
 $v_b$  = bottom velocity in  $\theta$  direction;  
 $W_\phi$  = wind speed in  $\phi$  direction;  
 $W_\theta$  = wind speed in  $\theta$  direction;  
 $\beta$  = volumetric expansion coefficient;  
 $\gamma$  = constant parameter in mixing length formulation;  
 $\epsilon$  = dissipation rate of energy;  
 $\zeta$  = water elevation;  
 $\zeta_o$  = water elevation amplitude at open boundary;  
 $\Theta$  = temperature °C;  
 $\nu$  = water surface slope;  
 $\kappa$  = wave number;  
 $\Lambda$  = horizontal density gradient;  
 $\xi, \eta$  = generalized curvilinear coordinate system;  
 $\rho$  = water density;  
 $\rho_a$  = air density;  
 $\rho_w$  = water density average;  
 $\bar{\rho}$  = vertically averaged of water density;  
 $\rho'$  = vertically density difference;  
 $\sigma$  = vertical coordinate transformation;  
 $\sigma_b$  = empirical diffusion constant;  
 $\sigma_s$  = Schmidt number;  
 $\tau_b$  = bottom shear stress;  
 $\tau_s$  = wind shear stress;  
 $\Phi$  = mean scalar quantity;  
 $\phi, \theta, r$  = spherical coordinate system;  
 $\Omega$  = wave frequency; and  
 $\omega$  = vertical velocity in  $\sigma$  transform coordinate.

## APPENDIX C

### CORMIX Output





0.00	0.00	1.73	1.0	0.140E+01	0.05	0.05
0.00	0.00	1.73	1.0	0.140E+01	0.05	0.05
0.00	0.00	2.03	1.4	0.102E+01	0.09	0.09
0.00	0.00	2.34	2.0	0.717E+00	0.12	0.12
0.01	0.00	2.64	2.6	0.546E+00	0.15	0.15
0.01	0.00	2.95	3.2	0.434E+00	0.19	0.19
0.02	0.00	3.25	3.9	0.355E+00	0.22	0.22
0.02	0.00	3.55	4.7	0.298E+00	0.25	0.25
0.03	0.00	3.86	5.5	0.253E+00	0.28	0.28
0.04	0.00	4.17	6.4	0.219E+00	0.31	0.31
0.05	0.00	4.47	7.3	0.191E+00	0.34	0.34
0.06	0.00	4.77	8.3	0.169E+00	0.38	0.38
0.06	0.00	5.08	9.3	0.150E+00	0.41	0.41
0.07	0.00	5.38	10.4	0.134E+00	0.44	0.44
0.08	0.00	5.69	11.5	0.121E+00	0.47	0.47
0.10	0.00	5.99	12.7	0.110E+00	0.50	0.50
0.11	0.00	6.29	13.9	0.100E+00	0.53	0.53
0.12	0.00	6.60	15.2	0.918E-01	0.56	0.56
0.13	0.00	6.90	16.6	0.844E-01	0.59	0.59
0.14	0.00	7.21	17.9	0.780E-01	0.62	0.62
0.15	0.00	7.51	19.3	0.722E-01	0.65	0.65
0.17	0.00	7.82	20.8	0.672E-01	0.68	0.68

Cumulative travel time = 9. sec

Merging of individual jet/plumes not found in this module, but interaction

will occur in following module. Overall jet/plume interaction dimensions:

0.17	0.00	7.82	20.8	0.672E-01	0.68	99.05
------	------	------	------	-----------	------	-------

END OF CORJET (MOD110): JET/PLUME NEAR-FIELD MIXING REGION

BEGIN MOD232: LAYER BOUNDARY IMPINGEMENT/UPSTREAM SPREADING

Vertical angle of layer/boundary impingement = 87.61 deg  
Horizontal angle of layer/boundary impingement = 0.00 deg

Because of VERY SMALL ambient velocity, BUOYANT SPREADING REGION becomes

EXCESSIVELY LARGE, greatly exceeding the region of interest.  
NO STEADY-STATE BEHAVIOR likely for this case. PROGRAM STOPS!

END OF MOD232: LAYER BOUNDARY IMPINGEMENT/UPSTREAM SPREADING

\*\* End of NEAR-FIELD REGION (NFR) \*\*

At the end of the NFR, the plume POSITION EXCEEDS SPECIFIED LIMITS for the regulatory mixing zone (RMZ) and/or the region of interest (ROI).

Specifications may be overly restrictive.

Use larger ROI values in subsequent iteration!

SIMULATION ENDS.







0.00	0.00	1.73	1.0	0.140E+01	0.05	0.05
0.00	0.00	1.73	1.0	0.140E+01	0.05	0.05
0.00	0.00	2.15	1.6	0.876E+00	0.10	0.10
0.01	0.00	2.57	2.4	0.577E+00	0.15	0.15
0.01	0.00	3.00	3.3	0.418E+00	0.19	0.19
0.02	0.00	3.42	4.4	0.321E+00	0.24	0.24
0.03	0.00	3.84	5.5	0.256E+00	0.28	0.28
0.04	0.00	4.27	6.7	0.209E+00	0.32	0.32
0.05	0.00	4.69	8.0	0.175E+00	0.37	0.37
0.07	0.00	5.11	9.4	0.148E+00	0.41	0.41
0.08	0.00	5.53	11.0	0.128E+00	0.45	0.45
0.09	0.00	5.95	12.6	0.111E+00	0.50	0.50
0.11	0.00	6.38	14.3	0.977E-01	0.54	0.54
0.13	0.00	6.80	16.1	0.868E-01	0.58	0.58
0.14	0.00	7.22	18.0	0.777E-01	0.62	0.62
0.16	0.00	7.64	20.0	0.699E-01	0.67	0.67
0.18	0.00	8.07	22.1	0.634E-01	0.71	0.71
0.19	0.00	8.49	24.2	0.577E-01	0.75	0.75
0.21	0.00	8.91	26.4	0.528E-01	0.80	0.80
0.23	0.00	9.33	28.8	0.485E-01	0.84	0.84
0.25	0.00	9.76	31.2	0.448E-01	0.88	0.88
0.27	0.00	10.18	33.6	0.415E-01	0.92	0.92

Cumulative travel time = 14. sec

Merging of individual jet/plumes not found in this module, but interaction

will occur in following module. Overall jet/plume interaction dimensions:

0.27	0.00	10.18	33.6	0.415E-01	0.92	99.05
------	------	-------	------	-----------	------	-------

END OF CORJET (MOD110): JET/PLUME NEAR-FIELD MIXING REGION

BEGIN MOD232: LAYER BOUNDARY IMPINGEMENT/UPSTREAM SPREADING

Vertical angle of layer/boundary impingement = 87.29 deg  
Horizontal angle of layer/boundary impingement = 0.00 deg

Because of VERY SMALL ambient velocity, BUOYANT SPREADING REGION becomes

EXCESSIVELY LARGE, greatly exceeding the region of interest.  
NO STEADY-STATE BEHAVIOR likely for this case. PROGRAM STOPS!

END OF MOD232: LAYER BOUNDARY IMPINGEMENT/UPSTREAM SPREADING

\*\* End of NEAR-FIELD REGION (NFR) \*\*

At the end of the NFR, the plume POSITION EXCEEDS SPECIFIED LIMITS for the regulatory mixing zone (RMZ) and/or the region of interest (ROI).

Specifications may be overly restrictive.

Use larger ROI values in subsequent iteration!

SIMULATION ENDS.







Individual jet/plumes before merging:

0.00	0.00	1.70	1.0	0.140E+01	0.05	0.05
0.00	0.00	1.70	1.0	0.140E+01	0.05	0.05
0.01	0.00	2.07	1.5	0.934E+00	0.09	0.09
0.03	0.00	2.44	2.2	0.630E+00	0.13	0.13
0.06	0.00	2.80	3.0	0.464E+00	0.18	0.18
0.09	0.00	3.17	3.9	0.359E+00	0.22	0.22
0.14	0.00	3.54	4.9	0.287E+00	0.26	0.26
0.19	0.00	3.90	6.0	0.235E+00	0.30	0.30
0.25	0.00	4.27	7.1	0.196E+00	0.34	0.34
0.31	0.00	4.63	8.4	0.166E+00	0.38	0.38
0.38	0.00	4.99	9.8	0.142E+00	0.42	0.42
0.45	0.00	5.35	11.3	0.124E+00	0.46	0.46
0.53	0.00	5.71	12.9	0.108E+00	0.51	0.51
0.61	0.00	6.07	14.6	0.955E-01	0.55	0.55
0.70	0.00	6.43	16.5	0.849E-01	0.59	0.59
0.79	0.00	6.79	18.4	0.761E-01	0.64	0.64
0.88	0.00	7.14	20.3	0.688E-01	0.68	0.68
0.98	0.00	7.50	22.3	0.625E-01	0.72	0.72
1.08	0.00	7.85	24.5	0.571E-01	0.76	0.76
1.19	0.00	8.21	26.6	0.524E-01	0.80	0.80
1.29	0.00	8.56	28.9	0.483E-01	0.85	0.85
1.40	0.00	8.91	31.2	0.447E-01	0.89	0.89

Cumulative travel time = 12. sec

Merging of individual jet/plumes not found in this module, but interaction

will occur in following module. Overall jet/plume interaction dimensions:

1.40	0.00	8.91	31.2	0.447E-01	0.89	99.05
------	------	------	------	-----------	------	-------

END OF CORJET (MOD110): JET/PLUME NEAR-FIELD MIXING REGION

BEGIN MOD232: LAYER BOUNDARY IMPINGEMENT/UPSTREAM SPREADING

Vertical angle of layer/boundary impingement	=	72.38 deg
Horizontal angle of layer/boundary impingement	=	0.00 deg

UPSTREAM INTRUSION PROPERTIES:

Upstream intrusion length	=	887.43 m
X-position of upstream stagnation point	=	-886.02 m
Thickness in intrusion region	=	0.45 m
Half-width at downstream end	=	1169.36 m
Thickness at downstream end	=	0.57 m

In this case, the upstream INTRUSION IS VERY LARGE, exceeding 10 times the local water depth.

This may be caused by a very small ambient velocity, perhaps in combination with large discharge buoyancy.

If the ambient conditions are strongly transient (e.g. tidal), then the

CORMIX steady-state predictions of upstream intrusion are probably unrealistic.

The plume predictions prior to boundary impingement and wedge formation

will be acceptable, however.

Control volume inflow:

X	Y	Z	S	C	BV	BH
1.40	0.00	8.91	31.2	0.447E-01	0.89	99.05

\*\* CMC HAS BEEN FOUND \*\*

The pollutant concentration in the plume falls below CMC value of 0.130E-01

due to mixing in this control volume.

The actual extent of the TOXIC DILUTION ZONE will be smaller than control

volume outflow values predicted below.

Profile definitions:

BV = top-hat thickness, measured vertically

BH = top-hat half-width, measured horizontally in y-direction

ZU = upper plume boundary (Z-coordinate)

ZL = lower plume boundary (Z-coordinate)

S = hydrodynamic average (bulk) dilution

C = average (bulk) concentration (includes reaction effects, if any)

	X	Y	Z	S	C	BV	BH	ZU
ZL								
	-886.02	0.00	9.80	9999.9	0.000E+00	0.00	0.00	9.80
9.80								
	-856.58	0.00	9.80	136.9	0.102E-01	0.10	165.37	9.80
9.70								
	-712.31	0.00	9.80	56.8	0.246E-01	0.24	401.69	9.80
9.56								
	-568.05	0.00	9.80	42.8	0.326E-01	0.33	543.47	9.80
9.47								
	-423.78	0.00	9.80	36.6	0.382E-01	0.38	655.26	9.80
9.42								
	-279.52	0.00	9.80	33.3	0.419E-01	0.42	750.58	9.80
9.38								
	-135.25	0.00	9.80	31.7	0.440E-01	0.44	835.09	9.80
9.36								
	9.02	0.00	9.80	31.3	0.432E-01	0.45	911.80	9.80
9.35								
	153.28	0.00	9.80	35.9	0.193E-01	0.48	982.54	9.80
9.32								
	297.55	0.00	9.80	43.8	0.809E-02	0.53	1048.52	9.80
9.27								

\*\* WATER QUALITY STANDARD OR CCC HAS BEEN FOUND \*\*

The pollutant concentration in the plume falls below water quality standard

or CCC value of 0.750E-02 in the current prediction interval.

This is the spatial extent of concentrations exceeding the water quality

standard or CCC value.

	441.82	0.00	9.80	48.8	0.372E-02	0.56	1110.59	9.80
9.24								
	586.08	0.00	9.80	50.9	0.183E-02	0.57	1169.36	9.80
9.23								

Cumulative travel time = 11706. sec

END OF MOD232: LAYER BOUNDARY IMPINGEMENT/UPSTREAM SPREADING

-----

\*\* End of NEAR-FIELD REGION (NFR) \*\*

In this design case, the diffuser is located CLOSE TO BANK/SHORE.  
Some boundary interaction occurs at end of near-field.

This may be related to a design case with a VERY LOW AMBIENT VELOCITY.

The dilution values in one or more of the preceding zones may be too high.

Carefully evaluate results in near-field and check degree of interaction.

Consider locating outfall further away from bank or shore.

In the next prediction module, the plume centerline will be set to follow the bank/shore.

-----

BEGIN MOD241: BUOYANT AMBIENT SPREADING

Plume is ATTACHED to RIGHT bank/shore.

Plume width is now determined from RIGHT bank/shore.

Profile definitions:

BV = top-hat thickness, measured vertically

BH = top-hat half-width, measured horizontally in y-direction

ZU = upper plume boundary (Z-coordinate)

ZL = lower plume boundary (Z-coordinate)

S = hydrodynamic average (bulk) dilution

C = average (bulk) concentration (includes reaction effects, if any)

Plume Stage 2 (bank attached):

	X	Y	Z	S	C	BV	BH	ZU
ZL	586.08	-1093.00	9.80	50.9	0.183E-02	0.59	2262.36	9.80
9.21	606.78	-1093.00	9.80	51.0	0.166E-02	0.59	2271.29	9.80
9.21	627.47	-1093.00	9.80	51.2	0.150E-02	0.59	2280.19	9.80
9.21	648.17	-1093.00	9.80	51.3	0.136E-02	0.59	2289.05	9.80
9.21	668.87	-1093.00	9.80	51.4	0.123E-02	0.59	2297.87	9.80
9.21	689.56	-1093.00	9.80	51.6	0.112E-02	0.59	2306.67	9.80
9.21	710.26	-1093.00	9.80	51.7	0.101E-02	0.59	2315.43	9.80
9.21	730.95	-1093.00	9.80	51.9	0.919E-03	0.59	2324.16	9.80
9.21	751.65	-1093.00	9.80	52.0	0.832E-03	0.59	2332.86	9.80
9.21	772.35	-1093.00	9.80	52.1	0.754E-03	0.59	2341.53	9.80
9.21								







0.00	0.00	1.70	1.0	0.140E+01	0.05	0.05
0.00	0.00	1.70	1.0	0.140E+01	0.05	0.05
0.01	0.00	2.07	1.5	0.934E+00	0.09	0.09
0.03	0.00	2.44	2.2	0.630E+00	0.13	0.13
0.06	0.00	2.80	3.0	0.464E+00	0.18	0.18
0.09	0.00	3.17	3.9	0.359E+00	0.22	0.22
0.14	0.00	3.54	4.9	0.287E+00	0.26	0.26
0.19	0.00	3.90	6.0	0.235E+00	0.30	0.30
0.24	0.00	4.26	7.1	0.196E+00	0.34	0.34
0.31	0.00	4.63	8.4	0.166E+00	0.38	0.38
0.38	0.00	4.99	9.8	0.142E+00	0.42	0.42
0.45	0.00	5.35	11.3	0.124E+00	0.46	0.46
0.53	0.00	5.71	12.9	0.108E+00	0.51	0.51
0.61	0.00	6.07	14.6	0.956E-01	0.55	0.55
0.70	0.00	6.43	16.4	0.850E-01	0.59	0.59
0.79	0.00	6.79	18.3	0.763E-01	0.64	0.64
0.88	0.00	7.14	20.3	0.689E-01	0.68	0.68
0.98	0.00	7.50	22.3	0.626E-01	0.72	0.72
1.08	0.00	7.85	24.4	0.572E-01	0.76	0.76
1.18	0.00	8.21	26.6	0.525E-01	0.80	0.80
1.28	0.00	8.56	28.9	0.483E-01	0.85	0.85
1.39	0.00	8.91	31.2	0.447E-01	0.89	0.89

Cumulative travel time = 12. sec

Merging of individual jet/plumes not found in this module, but interaction

will occur in following module. Overall jet/plume interaction dimensions:

1.39	0.00	8.91	31.2	0.447E-01	0.89	99.05
------	------	------	------	-----------	------	-------

END OF CORJET (MOD110): JET/PLUME NEAR-FIELD MIXING REGION

BEGIN MOD232: LAYER BOUNDARY IMPINGEMENT/UPSTREAM SPREADING

Vertical angle of layer/boundary impingement = 72.53 deg  
Horizontal angle of layer/boundary impingement = 0.00 deg

UPSTREAM INTRUSION PROPERTIES:

Upstream intrusion length = 808.94 m  
X-position of upstream stagnation point = -807.54 m  
Thickness in intrusion region = 0.44 m  
Half-width at downstream end = 1114.88 m  
Thickness at downstream end = 0.59 m

In this case, the upstream INTRUSION IS VERY LARGE, exceeding 10 times the local water depth.

This may be caused by a very small ambient velocity, perhaps in combination with large discharge buoyancy.

If the ambient conditions are strongly transient (e.g. tidal), then the

CORMIX steady-state predictions of upstream intrusion are probably unrealistic.

The plume predictions prior to boundary impingement and wedge formation

will be acceptable, however.

Control volume inflow:

X	Y	Z	S	C	BV	BH
1.39	0.00	8.91	31.2	0.447E-01	0.89	99.05

\*\* CMC HAS BEEN FOUND \*\*

The pollutant concentration in the plume falls below CMC value of 0.130E-01

due to mixing in this control volume.

The actual extent of the TOXIC DILUTION ZONE will be smaller than control

volume outflow values predicted below.

Profile definitions:

BV = top-hat thickness, measured vertically

BH = top-hat half-width, measured horizontally in y-direction

ZU = upper plume boundary (Z-coordinate)

ZL = lower plume boundary (Z-coordinate)

S = hydrodynamic average (bulk) dilution

C = average (bulk) concentration (includes reaction effects, if any)

	X	Y	Z	S	C	BV	BH	ZU
ZL								
	-807.54	0.00	9.80	9999.9	0.000E+00	0.00	0.00	9.80
9.80								
	-780.22	0.00	9.80	135.6	0.103E-01	0.10	157.67	9.80
9.70								
	-646.31	0.00	9.80	56.3	0.248E-01	0.24	382.97	9.80
9.56								
	-512.41	0.00	9.80	42.4	0.329E-01	0.32	518.15	9.80
9.48								
	-378.50	0.00	9.80	36.3	0.385E-01	0.37	624.73	9.80
9.43								
	-244.60	0.00	9.80	33.1	0.421E-01	0.41	715.61	9.80
9.39								
	-110.69	0.00	9.80	31.6	0.442E-01	0.43	796.18	9.80
9.37								
	23.21	0.00	9.80	31.3	0.403E-01	0.44	869.32	9.80
9.36								
	157.12	0.00	9.80	36.2	0.188E-01	0.48	936.76	9.80
9.32								
	291.02	0.00	9.80	43.5	0.841E-02	0.54	999.67	9.80
9.26								

\*\* WATER QUALITY STANDARD OR CCC HAS BEEN FOUND \*\*

The pollutant concentration in the plume falls below water quality standard

or CCC value of 0.750E-02 in the current prediction interval.

This is the spatial extent of concentrations exceeding the water quality

standard or CCC value.

	424.93	0.00	9.80	47.9	0.410E-02	0.57	1058.84	9.80
9.23								
	558.83	0.00	9.80	49.8	0.212E-02	0.59	1114.88	9.80

9.21

Cumulative travel time = 11161. sec

END OF MOD232: LAYER BOUNDARY IMPINGEMENT/UPSTREAM SPREADING

-----

\*\* End of NEAR-FIELD REGION (NFR) \*\*

In this design case, the diffuser is located CLOSE TO BANK/SHORE.  
Some boundary interaction occurs at end of near-field.

This may be related to a design case with a VERY LOW AMBIENT VELOCITY.

The dilution values in one or more of the preceding zones may be too high.

Carefully evaluate results in near-field and check degree of interaction.

Consider locating outfall further away from bank or shore.

In the next prediction module, the plume centerline will be set to follow the bank/shore.

-----

BEGIN MOD241: BUOYANT AMBIENT SPREADING

Plume is ATTACHED to RIGHT bank/shore.

Plume width is now determined from RIGHT bank/shore.

Profile definitions:

BV = top-hat thickness, measured vertically

BH = top-hat half-width, measured horizontally in y-direction

ZU = upper plume boundary (Z-coordinate)

ZL = lower plume boundary (Z-coordinate)

S = hydrodynamic average (bulk) dilution

C = average (bulk) concentration (includes reaction effects, if any)

Plume Stage 2 (bank attached):

	X	Y	Z	S	C	BV	BH	ZU
ZL	558.83	-1089.50	9.80	49.8	0.212E-02	0.59	2204.38	9.80
9.21	580.89	-1089.50	9.80	49.9	0.191E-02	0.59	2214.12	9.80
9.21	602.95	-1089.50	9.80	50.0	0.172E-02	0.59	2223.82	9.80
9.21	625.01	-1089.50	9.80	50.2	0.155E-02	0.59	2233.47	9.80
9.21	647.06	-1089.50	9.80	50.3	0.140E-02	0.59	2243.09	9.80
9.21	669.12	-1089.50	9.80	50.5	0.126E-02	0.59	2252.67	9.80
9.21	691.18	-1089.50	9.80	50.6	0.113E-02	0.59	2262.21	9.80
9.21	713.24	-1089.50	9.80	50.8	0.102E-02	0.59	2271.71	9.80
9.21	735.30	-1089.50	9.80	50.9	0.917E-03	0.59	2281.17	9.80
9.21	757.36	-1089.50	9.80	51.1	0.825E-03	0.59	2290.59	9.80

